SHORT TERM STATISTICS OF ATMOSPHERIC TURBULENCE AND OPTICAL PROPAGATION

by

Philip A. Pincus

Submitted in partial fulfillment of the requirements for the degree of
Doctor of Philosophy

At

The Oregon Graduate Center

January 1976

Approvals:

J. Fred Holmes
Associate Professor
Chairman
Department of Applied Physics

C. M. McIntyre
Assistant Professor
Department of Applied Physics

R. A. Elliott
Assistant Professor
Department of Applied Physics

J. R. Kerr
Professor
Department of Applied Physics

TABLE OF CONTENTS

Acknowledgements

I would like to gratefully acknowledge the guidance and support of my advisor Dr. J. Richard Kerr. From the suggestion of the problem to the completion of this work, he has been a source of inspirational ideas and encouragement.

The aid of Dr. Richard A. Elliott and Dr. James R. Dunphy throughout this work and the technical support of Carl Miller and Gordon Frost are also greatly appreciated.

I would like also to thank members of my advisory and thesis committees Drs. Michael A. Gray, George P. O'Leary, Thomas M. Loehr, Gail A. Massey, J. Fred Holmes and Charles M. McIntyre, who have seen me through the many years of my graduate studies at the Oregon Graduate Center.

This work was supported by the Defense Advanced Research Projects Agency and monitored through the Rome Air Development Center.

Abstract

This thesis is concerned with the statistical properties of the random processes describing optical wave propagation through the turbulent atmosphere. Of specific interest are the effects of short time averaging, necessitated by various circumstances, on the statistical measures of the random processes, most significantly the variances C_n^2, the atmospheric structure constant, and σ_χ^2, the normalized variance of the log optical amplitude fluctuations. Details of the statistical properties, including probability distribution functions, power spectra and correlation functions are presented. These include the following results. Small scale atmospheric fluctuations, in the present work differential temperature fluctuations, are seen to be highly non-Gaussian, with flatness factors as high as 14. The square of the temperature difference fluctuations, related to C_n^2, are nearly lognormally distributed in well developed turbulence, over a range of short averaging times. The fluctuations in the logarithm of the optical irradiance after propagation through turbulence were similarly analyzed. These fluctuations are normally distributed over a wide range of turbulence conditions. Measurements of the two point conditional distributions show that the log irradiance fluctuations may be multidimensional Gaussian only when the turbulence level is low enough that σ_χ^2 is much less than the saturation value.

The averaging time dependence of the mean square error in the above variance measurements due to finite averaging time is described analytically as a simple $1/\tau$ relationship. The magnitude of this 'error', the data spread, depends on characteristics of the unaveraged random process, the flatness factor and the integral scale of the correlation function. A number of characteristics of the data spread of C_n^2 and σ_χ^2 are presented including the dependence on turbulence level, mean wind speed and averaging time. The relationship between the data spreads in measured C_n^2 and σ_χ^2 is investigated. This relationship involves a measure of the large scale structure of the C_n^2 field along the propagation path. Measurements of the various data spreads and the spatial correlation function of C_n^2 support the analytically derived relationships.

Finally the effects of intermittent turbulence conditions on the various statistical measurements are discussed. These results include increased

relative data spread in short time averaged C_n^2 measurements and deviation from lognormality of the probability distribution function of the temperature differential squared. The effects of intermittency on the propagation problem appear to be limited to the resultant increased data spread of the σ_χ^2 measurements.

List of Figures

CHAPTER I. INTRODUCTION

The possibility of extremely high rates of information transmission over optical electromagnetic waves and the recent development of lasers and associated hardware have stimulated a strong interest in the field of optical communications. The earth's atmosphere, as one of the possible communication channels, has been the object of intense study with regard to its effect on optical propagation. One of the fundamental problems encountered in the propagation of an optical wave through the atmosphere involves fluctuations in the optical field at a remote receiver induced by the small local fluctuations in the index of refraction associated with atmospheric turbulence. A great number of theoretical and experimental investigations concerning optical scintillation and turbulence have been undertaken in the past decade. It is through these efforts that this phenomena has become understood to the point that general techniques in transmitter and receiver design have been developed for cancelling and correcting for the effects of the turbulent atmosphere on the propagating laser beam.

Throughout the brief recent history of the propagation problem, the assumptions of isotropy, homogeneity and stationarity of the atmosphere have been invoked, explicitly in the theoretical work to allow solutions of the complex equations encountered and implicitly in the experiments to allow comparison with the theoretical models. It is to the practical aspects of the temporal and spatial behavior of the atmospheric turbulence and the consequent effects on optical propagation that the present work is addressed. Before proceeding with these problems, however, a brief introduction to the propagation problem and the required turbulence parameters is presented.

The basic propagation scheme of interest here is best described in terms of the simple block diagram of Fig. I.1. The first block is the transmitter consisting of a stable laser and necessary optical components to form a beam of given geometric characteristics (e.g. plane wave, spherical wave, or focused beam). The second block is the communications channel

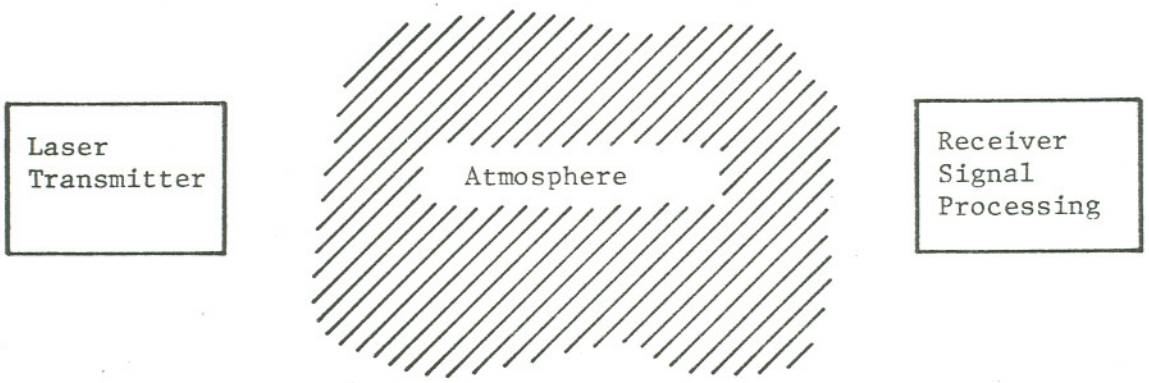

Figure I.1. Block diagram of basic propagation experiment.

which in this work consists of a horizontal path through the lower boundary layer of the atmosphere.* The final block is the receiver which detects the fluctuating optical signal. The receiver block also includes all necessary processing equipment to measure the desired parameters describing the received optical signal.

The solution of the optical propagation problem involves solving the wave equation, in this case the scalar wave equation in a charge-free region

$$\nabla^2 E(r,t) + k^2 n^2(r,t) E(r,t) = 0 \qquad (I.1)$$

Here $n(r,t)$, the index of refraction, is a randomly fluctuating function of position and time. A successful approach to the solution of this equation over a range of conditions has been a perturbation method developed by Rytov, in which the optical field $E(r,t)$ is transformed according to the transformation $E(r,t) = \exp(\psi(r,t)) = \exp(\chi + iS)$. χ is the logarithm of the amplitude (log amplitude) and S is the phase of the wave. Following this transformation, both $n(r,t)$ and $\psi(r,t)$ are expanded in perturbation series. This results in a hierarchy of coupled equations to which spectral analysis has been applied to calculate the spatial power spectra and structure functions (Tatarskii, 1971) of the log amplitude and phase of the optical signal after propagation through the turbulent atmosphere. The general propagation case results in a solution for the spatial power spectral density $F(\kappa,k,L)$ of the form

$$F(\kappa,k,L) = G(\kappa,k,L)\, \Phi_n(\kappa) \qquad (I.2)$$

where $\Phi_n(\kappa)$ is the power spectral density associated with the fluctuating index of refraction, $G(\kappa,k,L)$ is a filter function which describes how the distribution of energy in the different turbulence scales is transformed into the distribution of energy in the received optical signal, κ is the spatial wavenumber, k is 2π divided by the optical wavelength, and L is the propagation distance. The form of $G(\kappa,k,L)$ of course depends

---

*It should be noted that propagation in the vertical direction such as for earth to satellite communications is also an area of active interest.

on the geometry of the optical wave being propagated. Integration of the power spectral density over all spatial wavenumbers yields the corresponding variance. In the case of a point source producing a spherical wave propagating through the turbulence, the variance of the log amplitude is given as

$$\sigma_\chi^2 = 2\pi^2 k^2 L^2 \int_0^\infty \left\{ 1 - \left(\frac{2\pi k}{\kappa^2 L}\right)^{1/2} \left[\cos\left(\frac{\kappa^2 L}{4k}\right) C\left(\left(\frac{\kappa^2 L}{2\pi k}\right)^{1/2}\right) + \sin\left(\frac{\kappa^2 L}{4k}\right) S\left(\left(\frac{\kappa^2 L}{2\pi k}\right)^{1/2}\right)\right]\right\} \phi_n(\kappa)\kappa d\kappa \qquad (I.3)$$

where $C(\chi) = \int_0^\chi \cos\left(\frac{\chi t^2}{2}\right) dt$ and $S(\chi) = \int_0^\chi \sin\left(\frac{\chi t^2}{2}\right) dt$. Finally then, to calculate the log amplitude variance, an expression for $\phi_n(\kappa)$ is needed.

One form of the spectrum, $\phi_n(\kappa)$, which is commonly employed and will be further discussed in a later chapter is

$$\phi_n(\kappa) = 0.033\, C_n^2\, \kappa^{-11/3} \exp\left(-\frac{\kappa^2}{\kappa_m^2}\right) \qquad (I.4)$$

where C_n^2 is the index of refraction structure parameter, a measure of the intensity of the fluctuation in the refractive index, and κ_m is given by $5.92/\ell_o$ where ℓ_o is the inner scale of the turbulence, a small scale limit at which viscosity effects begin to effect the transfer of turbulent energy. We note that in Eq. (I.4) C_n^2 is implicitly an ensemble averaged quantity. Substituting Eq. (I.4) into Eq. (I.3), allowing for $L >> \frac{\ell_o^2}{\lambda}$ which will be true for wavelengths in the visible over a path length of 1 kilometer or more, results in the following relationship between the ensemble variables $\langle\sigma_\chi^2\rangle$ and $\langle C_n^2\rangle$

$$\langle\sigma_\chi^2\rangle = 0.124\, \langle C_n^2\rangle\, k^{7/6} L^{11/6} \qquad (I.5)$$

If C_n^2 is allowed to be a function of the position along the path, which allows for propagation through inhomogeneous turbulence such as in the vertical direction, Eq. (I.5) becomes (for spherical wave propagation)

$$\langle\sigma_\chi^2\rangle = 0.14\, k^{7/6} \int_o^L d\eta \langle C_n^2(\eta)\rangle \left(\frac{\eta}{L}\right)^{5/6} (L-\eta)^{5/6} \quad . \quad (I.6)$$

Eqs. (I.5) and (I.6) being the results of a perturbation analysis are in fact found to be valid over a limited range. As the path integrated turbulence increases, that is, as $\langle C_n^2\rangle$, L or k increase, the measured value of $\langle\sigma_\chi^2\rangle$ increases as in Eq. (I.5), until approximately $\langle\sigma_\chi^2\rangle = 0.3$, when the intensity of the fluctuations saturate, and the measured $\langle\sigma_\chi^2\rangle$ becomes nearly independent of that predicted on the basis of Eq. (I.5). Recent experimental and theoretical investigations have led to some understanding of the saturation phenomena, and final confirmation of the saturation models is awaiting results of experiments currently being performed in the range of very large path integrated turbulence levels. The present work is confined primarily to the low turbulence regime in which Eq. (I.5) is valid.

Eqs. (I.5) and (I.6) form the fundamental relationships between the ensemble measures of the turbulent field and the measures describing the observed effects on the optical signal. In practice, however, it is finite and in some cases very short time averages which are of practical interest and which are readily measurable. In attempting to understand the short time averaging effects, we will present models which have been developed of the turbulence and propagation problems, and experiments which we have designed and carried out to verify and extend these models. In addition, we have compiled results of atmospheric turbulence observations and optical propagation results over a very wide range of atmospheric conditions. These results are primarily in the form of statistical properties such as probability distribution functions, central moments, correlation functions, and power spectral densities of the random processes which characterize the atmospheric fluctuations and the optical field's fluctuations.

In Chapters II and III, we present results of these characterizations for the index of refraction or temperature fluctuations and the log irradiance fluctuations respectively. In the time averaged measurements of quantities such as the variance of these random processes, a large spread in the data is often observed even under homogeneous atmospheric conditions. Chapter IV presents a detailed inquiry into the data spread in short time averaged variance measurements of the turbulence and optical fluctuations. We shall see the dependence of the observed data spread in the turbulence measurements on such parameters as turbulence level, wind velocity and averaging time under a number of atmospheric conditions. The relationship between the observed data spreads in the optical and the turbulence measurements will be shown to be dependent on large scale structures of the turbulent intensity (C_n^2), and models describing this relationship will be presented. A number of measurements of the large scale correlation function of the turbulent intensity will be described and related to the phenomenological models presented.

Finally, in Chapter V, we focus on one particularly identifiable, frequently observed characteristic of atmospheric turbulence, its intermittent nature. Of specific interest are the relationships of intermittency of turbulence to the observed large data spread in the measurements and to the statistical characteristics of turbulent fluctuations described in Chapter II. We present a number of experimental results aimed at quantifying turbulence intermittency and relating it to statistical measures of the atmospheric turbulence fluctuations in addition to some observations of the causes of such intermittency.

CHAPTER II. Atmospheric Turbulence Fluctuations

II.1. Introduction

In this chapter we begin a description of the statistical properties of the fluctuations in the local index of refraction of the atmosphere due to clear air turbulence. The first section presents the basic physical models generally used to describe the observed fluctuations in atmospheric turbulence parameters and their associated statistical properties, power spectral densities and probability distribution functions. We proceed with a description of the experimental equipment used to observe these fluctuations and to measure the relevant statistical properties. Finally, examples of observations of the fluctuations and measurements of the statistical functions are presented. This data provides quantitative evidence in support of our phenomenological understanding of the randomly fluctuating index of refraction.

II.2. Models of Small Scale Atmospheric Turbulence

As the direct measurement of the fluctuating index of refraction over the small scales of interest in the atmosphere (several millimeters up to a meter) would be an extremely difficult problem, we first express these fluctuations in terms of more readily measurable quantities. At the optical wavelengths of interest here, the index of refraction is best described by the use of the refractivity, $N = (n - 1) \times 10^6$ where n is the actual index of refraction of the atmosphere. N is simply related to thermodynamic quantities via the relation

$$N \propto P/T \qquad \text{(II.1)}$$

where P is the pressure and T the absolute temperature. The contribution of humidity fluctuations is neglected throughout this work, although recent investigations (Friehe & LaRue 1972, 1973, 1974) have shown that under certain conditions, both direct humidity fluctuations and correlations between humidity and temperature fluctuations may significantly influence the intensity of index of refraction fluctuations. Neglecting also pressure fluctuations which are small and short-lived (Lawrence, Ochs, & Clifford 1970) compared to fluctuations in the temperature, the fluctua-

tions in the index of refraction are given by

$$\Delta N \propto \frac{P}{T^2} \Delta T \qquad \text{(II.2)}$$

Thus, under atmospheric conditions, measurements of the local temperature fluctuations can be directly related to the fluctuations in the index of refraction. As presented in the introduction, it is the spatial spectrum $\phi_n(\kappa)$, its transform, the structure function $D_n(r)$, (Strohbehn 1968) and the related structure parameter C_n^2 which relate to the problem at hand. Translating to the temperature domain, the atmospheric variables of interest are the following:

ΔT	Temperature fluctuations at a point
$\Delta T_{12} = T(\underline{r}_1) - T(\underline{r}_2)$	Two point temperature difference fluctuations
$D_T(r) = \langle [T(\underline{r}_1)-T(\underline{r}_1+\underline{r})]^2 \rangle$	Temperature structure function

(II,3)

The mechanisms of production of temperature fluctuations under atmospheric conditions are very difficult to describe in that they depend on such inhomogeneous processes as large scale wind patterns, solar heating, and surface characteristics. It is the dependence of the fluctuating optical field parameters of interest on the relatively small scale sizes of the turbulence that makes the problem tractable. Through the use of dimensional analysis and similarity arguments, simple models of the turbulence over the scales of interest have been developed which are in general agreement with experimental observations. In the following we briefly review some of the arguments and results of the models of atmospheric turbulence.

The most successful model of atmospheric turbulence was developed primarily by Kolmogorov (see Hinze 1959). It is assumed that the range of scale sizes of eddies can, under certain conditions, be broken into three distinct regimes. In the range of the largest scales, energy is put into the turbulent flow field through the nonisotropic, large scale processes mentioned above. This large scale, low wavenumber range, in which there is no universal form for the energy spectral density, extends from the largest scale sizes in the flow down to what is called the outer

scale of the turbulence, L_o, below which it is assumed that there are no mechanisms of energy input into the turbulent field. In the lower boundary layer of the atmosphere it is generally agreed that the outer scale is some fraction of the order of one half of the height above the ground. In the upper atmosphere, outer scale measurements are surely non-isotropic, possibly being hundreds of meters in the horizontal direction while on the order of meters in the vertical direction due to layering of the atmosphere. The second regime lies between the outer scale and a small scale limit referred to as the inner scale of the turbulence, ℓ_o. In this regime, the energy input at the larger scales is assumed to be transferred without dissipation from the largest scales to the smaller through an energy cascade process. Eddies of the size of the outer scale, because of instabilities, continually break down into eddies of smaller and smaller sizes. This range of intermediate scale sizes is known as the inertial subrange, and the spatial spectrum is predicted to be universal to all flows and independent of the particular conditions influencing the production of the turbulence. Finally in the third regime, that is for scale sizes less than the inner scale, the energy in the turbulent field is dissipated through viscous processes, and the spectral density falls off quickly with increasing wavenumber, or decreasing eddy size. We note that this general model of isotropic turbulence and its spectral distribution as developed originally applied to turbulent velocity fluctuations (a vector field), but it has been shown (Tatarskii 1961) that it is applicable to temperature fluctuations and other "passive additives" that are mixed by the velocity field.

It is the inertial subrange region of the spectrum that is of particular importance here, because as seen in equation (I.3), the spectral filter function for optical amplitude fluctuations goes to zero at small wavenumbers, and thus the large scale temperature fluctuations are "filtered out" in this problem. We note, however, that for optical phase effects, the large scale temperature fluctuations may play a significant role.

In the inertial subrange, it is postulated that the structure function of the temperature fluctuations, $D_T(\underline{r})$ is isotropic, and depends only on the separation r and the amount of energy input into the turbulence at scales larger than the outer scale. As the energy put into the turbu-

lence flow beyond the outer scale is equal to the energy dissipated in eddies smaller than the inner scale (the cascade process conserves energy in the inertial subrange) the structure function can be expressed as some function of the dissipation rate of thermal fluctuations due to diffusion N, the rate of energy dissipation of the mechanical turbulence ε, and the separation r. Thus

$$D_T(r) = \text{constant } r^{\alpha} N^{\beta} \varepsilon^{\gamma} \qquad \text{(II.4)}$$

Using dimensional analysis, $D_T(r)$ can be shown to be given by

$$D_T(r) = \text{constant } N\varepsilon^{-1/3} r^{2/3}$$

$$= C_T^2 r^{2/3} \qquad \text{(II.5)}$$

where C_T^2 the temperature structure parameter is effectively defined by this relation. The index of refraction structure parameter is related directly to C_T^2 by

$$C_n^2 = [79 \times 10^{-6} P/T^2]^2 C_T^2 \qquad \text{(II.6)}$$

where P is the pressure in millibars, and T is the temperature in Kelvins. Transforming the structure function yields the three dimensional spatial power spectrum of the temperature fluctuations (Strohbehn 1968)

$$\phi_T(\kappa) \propto \kappa^{-11/3} \qquad \text{(II.7)}$$

known as the Kolmogorov spectrum of turbulence. Eq.(I.4) of the introduction included an additional factor $\exp(-\kappa^2/\kappa_m^2)$ to describe the fast decay of the power spectral density for scale sizes less than the inner scale due to viscous dissipation. Transforming Eq. (II.4) for isotropic turbulence to the one dimensional spectral density which is most amenable to measurement we find in the inertial subrange,

$$\phi_T(\kappa) \propto \kappa^{-5/3} \qquad \text{(II.8)}$$

One further assumption is often made concerning the turbulent flow which allows for comparison of the theoretically derived results with relatively easily measured parameters. This involves a transformation of the spatial parameters to temporal parameters through the relationship $\bar{x} = t \cdot \bar{u}$ where $\bar{u}$ is the mean wind velocity and is referred to commonly as Taylor's hypothesis (Taylor 1938, Hinze 1959). The substitution of $t\bar{u}$ for $\bar{x}$ may be valid only if the mean wind velocity $\bar{u}$ is much greater than the fluctuating part of the velocity and is generally applied only to turbulent scale sizes less than the outer scale. The physical interpretation of this hypothesis, also referred to as the frozen flow hypothesis, is that the turbulent field observed at a fixed point in space as a function of time may be assumed to be the result of a 'frozen in' turbulence field that is swept by the observation point with the mean wind velocity $\bar{u}$. Thus a temporal trace of the turbulent field is equivalent to the instantaneous distribution of the turbulent fluctuations along some spatial axis parallel to $\bar{u}$. We shall employ this assumption throughout our discussion of small scale turbulent fluctuations, and in a later chapter we shall see explicit limits to its applicability.

Soon after the work of Kolmogorov in developing the above model of turbulent fluctuations and their spectral properties, it was pointed out by Landau (1959) that the energy dissipation rates ε and N were themselves random functions of time. Not until 1961 however, was the turbulent model reformulated taking these fluctuations into account (Kolmogorov 1961, Obukov 1961). This work has led to a number of important results concerning the probability distributions of certain small scale fluctuation parameters. The basic agruments which again were formulated in terms of velocity fluctuations proceed from the consideration of some non-negative measure of the turbulence ϕ_r averaged over some small volume of dimension r (Gurvich and Yaglom 1967). The similarity hypothesis of turbulence then implies that the probability distribution of the ratio of $\phi_{r'}/\phi_{r''}$ where both r' and r'' are within the 'inertial subrange', i.e., $\ell_o < r', r'' < L_o$ is dependent only on the ratio r'/r''. ϕ_r is then expressed as

$$\phi_r = \frac{\phi_r}{\phi_N}\,\frac{\phi_N}{\phi_{N-1}} \cdots\cdots \frac{\phi_{N-k+1}}{\phi_{N-k}}\,\phi_{N-k} \qquad \text{(II.9)}$$

where the decreasing subscripts on the ϕ's indicate averaging of ϕ over volumes of decreasing size, and ϕ_{N-k} indicates ϕ averaged over such a small volume that the fluctuations can be neglected. Letting $a_N = \frac{\phi_N}{\phi_{N-1}}$ yields

$$\phi_r = \phi_{N-k} \prod_{i=N-k+1}^{r} a_i \qquad \text{(II.10)}$$

Taking the logarithm of Eq. (II.10) produces finally

$$\log \phi_r = \log \phi_{N-k} + \sum_i a_i \quad . \qquad \text{(II.11)}$$

As the a_i are independent random variables with the same distribution function by the similarity argument, the Central Limit theorem implies that the distribution function of $\log \phi_r$ will approach a normal distribution for a large enough number of elements in the sum of Eq. (II.11). Thus ϕ_r and in the case of interest here (ΔT_{12}^2) averaged over some range of volumes whose scales are less than the outer scale should have a lognormal distribution. Further arguments suggest the form of the variance of the distribution of $\log \phi_r$ as

$$\sigma^2_{\phi_r} = A + \mu \log \frac{L_o}{r} \qquad \text{(II.12)}$$

where L_o is the outer scale, A a non-universal function of the large scale flow, and μ a universal constant referred to as Kolmogorov's constant and observed to be approximately 0.5 for velocity derivative fluctuations.

Extensions of this theory of fluctuations in the dissipation rates for temperature fluctuations have also led to predictions of modifications of the '2/3' power law behavior of the structure function and consequent modification of the '5/3' law for the power spectrum. Van Atta (1971) calculates the exponent of r in the structure function for a scalar characteristic of turbulence such as the temperature, allowing for fluctuations

in the dissipation rates as described above. The calculations are dependent on the correlation between the dissipation rate of the kinetic energy ε and the scalar dissipation rate N. For the correlation coefficient ρ, independent of the scale size within the inertial range, the variations predicted in the power law spectrum range from $k^{-1.39}$ to $k^{-1.72}$ depending on the actual value of the correlation coefficient. Variations of this order are often within experimental error, and as such are difficult to verify but have been reported (see for example Kerr 1972, Kruspe 1974).

II.3. Experimental

The observations of the temperature fluctuations of interest here and the accurate measurement of C_T^2 or C_n^2 require a thermal sensor able to resolve fluctuations of the temperature of the order of several millidegrees, over scale sizes of the order of millimeters. A microthermal amplifier capable of performing these measurements is built by Contel (Model No. MT-2), and a number of these sensors, each capable of operating in either a single probe mode or a two probe differential mode, were available for this work.

The temperature sensitive element of the MT-2 microthermal amplifier is a length of Wollaston processed platinum wire etched to a diameter of 1.5 microns and approximately 2,5 millimeters in length soldered to the end of an extended probe assembly mounted on the amplifier itself. Two of these probes make up two legs of an AC bridge through which a small current is run. The current through the probe wires themselves is kept to less than 100 microamps to prevent the probes from heating above the ambient temperature level. This ensures that they are relatively insensitive to fluctuations in the local wind velocity. Temperature fluctuations at the probe wires then induce small resistance changes in the wire resulting in a fluctuating current through the bridge proportional to the fluctuating temperature difference between the two probes. This current is converted to a fluctuating voltage and amplified and filtered as indicated in the block schematic diagram of the amplifier in Fig. II.1. The slow feedback loop to the bridge acts as a high pass filter and as a stabilizer for the system to allow continuous operation over long periods with drifts in the ambient temperature level. The outputs of the unit consist of voltages proportional to the fluctuations in the temperature at

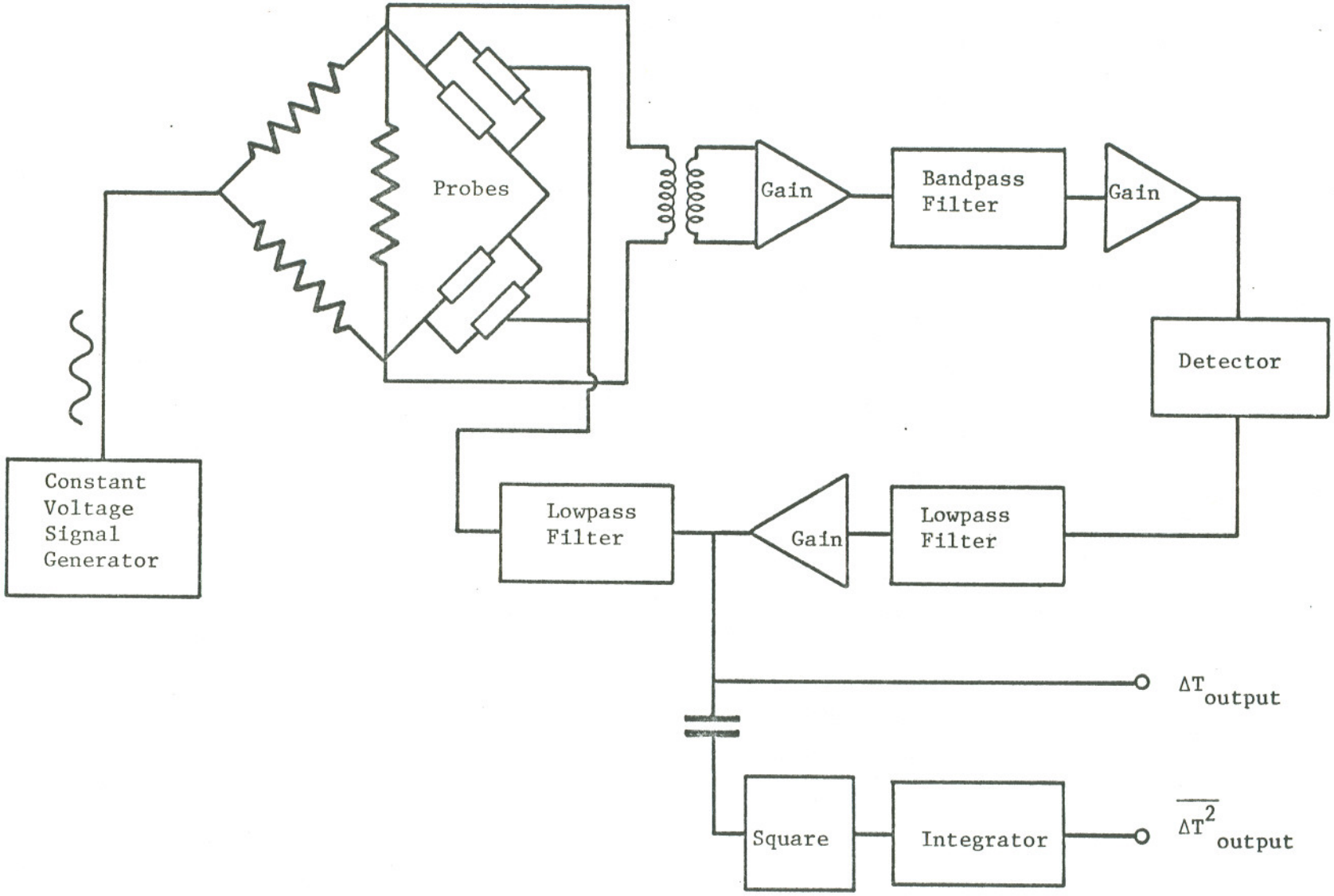

Figure II,1. Schematic block diagram of microthermal amplifier.

a single probe or the difference temperature between two probes, and a variable time constant, low pass filtered voltage proportional to the mean square temperature fluctuation between the two probes.

As the thermal coefficient of the probe wire is known, calibration of the system is simply accomplished by adding a known small resistance into one of the legs of the bridge. This simulates a calculable temperature change at the probe, and results in a calibration voltage at the output of the unit. This calibration procedure is further simplified by having each unit equipped with an internal calibration circuit.

These amplifiers require a careful setup and balancing procedure, but will operate essentially unattended continuously if the atmospheric conditions do not change drastically. The probes themselves being of the order of microns in diameter, are quite fragile and an attempt to keep them from the path of raindrops, large dust particles, and insects must be made. Finally, to facilitate measurements at the height of interest, 2 meters above the ground, each amplifier was mounted on a portable tripod which permitted orientation of the probes relative to the wind.

Data from the microthermal amplifier, which consists of single or double probe temperature fluctuations and mean square values of the temperature fluctuations from up to five of the sensors, were recorded on an FM tape recorder (HP 3960A) with a bandwidth of 1.25 kilohertz. These field recordings were then returned to the lab where they were digitized, fed into a PDP-11 digital computer, and recorded on 9 track digital magnetic tapes for further analysis on the computer. The computer processing is outlined in Appendix 1.

The field site at which all experimental measurements were made is located approximately 35 miles south of Portland, Oregon amid the farmland of the Willamette valley. The site used for the turbulence measurements themselves is situated about 300 meters east of a road and a small cluster of large trees. The prevailing winds at the site are generally either northerly or southerly. The only obstacle to the atmospheric flow is a small building which houses the recording and other electronic instruments for the experiments. As the microthermal sensors are portable, they are placed such that the building is downwind of them.

II.4. Experimental Results

II.4a. Spectral Properties and Correlation Functions

Figure II.2 shows a typical trace of temperature fluctuations observed with a single thermal probe when the average wind speed was 1.5 meters per second. The vertical scale indicates maximum peak-to-peak fluctuations of the order of $0.4^{o}K$. We note the nearly continuous appearance of rapid fluctuations in the temperature in addition to significant slower trends. The power spectrum associated with the single probe fluctuations is seen in Figure II.3. The solid line indicates the predicted 5/3 power law dependence over the inertial subrange. Note that this spectrum is plotted versus the temporal frequency as measured although in the inertial subrange we could use Taylor's hypothesis to transform to the spatial frequency. This spectrum shows rather clearly a break at the high frequency end of the inertial subrange indicating the onset of the dissipation regime. From the frequency of the breakpoint and the wind velocity, we can calculate the inner scale, in this case $\sim$ 1 cm.

Figure II.4 shows a trace of two probe differential temperature fluctuations. In this case, the low frequencies, as expected are not seen as in the single probe case. The probes were separated approximately 10 cm which should filter out all fluctuations whose scale is appreciably larger than that separation. The 'spikiness' of these traces, indicating fluctuations over a wide range of magnitudes, is often referred to as small scale intermittency, a characteristic common to small scale atmospheric turbulence variables in general.

The power spectrum of the two probe differential measurements shown in Figure II.4 is seen in Figure II.5. Also shown for later reference is the power spectrum of the square of these two probe fluctuations which shows enhanced low frequency components. Figure II.6 shows the autocorrelation functions calculated from the low frequency spectrum of this same data for the temperature difference fluctuations and their square. The use of the log scale on the abscissa is to allow the correlation function to be displayed over a wide range of its argument. This graph illustrates a number of important points with regard to the correlation function $\rho(\tau)$ and the integral scale (which will be seen below to be important in predicting errors in short time averaged measurements of certain sta-

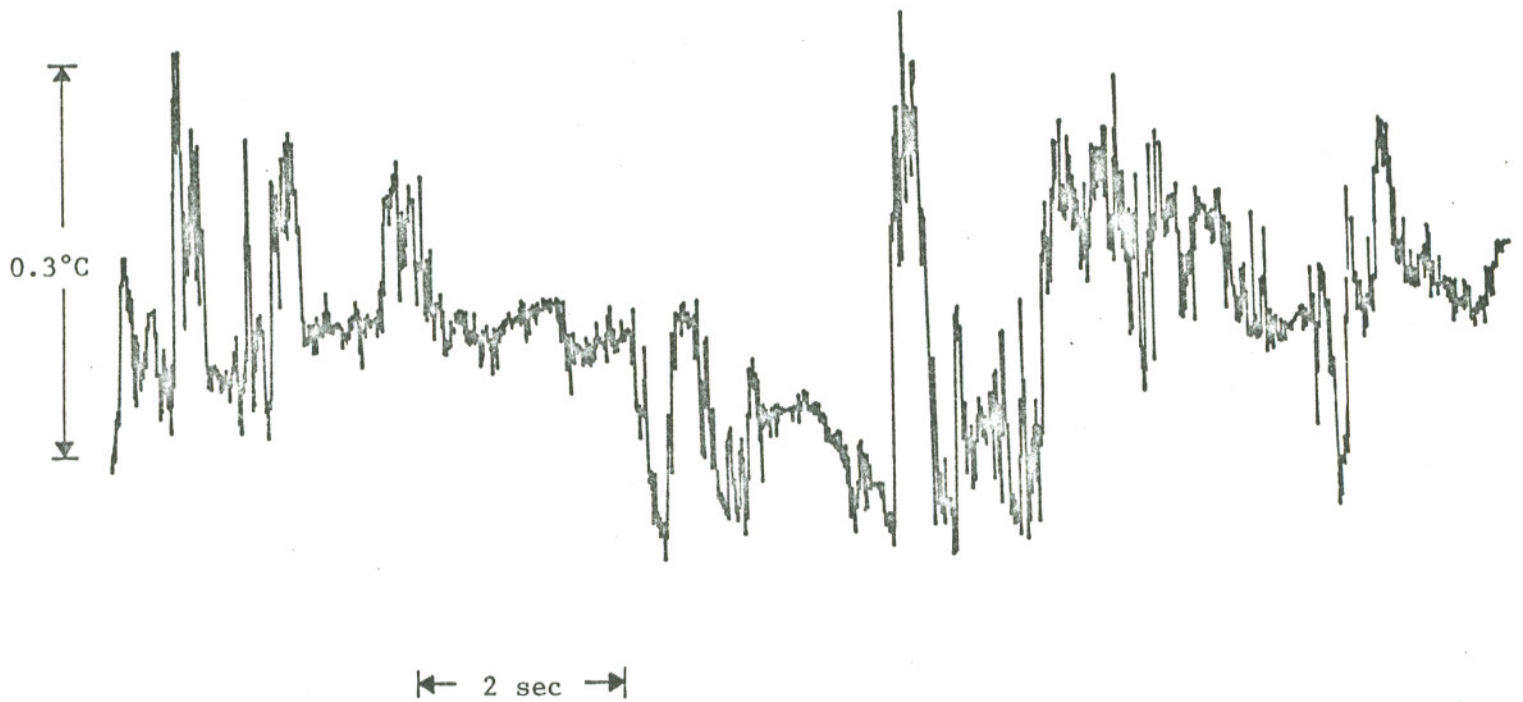

Figure II.2. Trace of temperature fluctuations at a single point in the atmosphere.

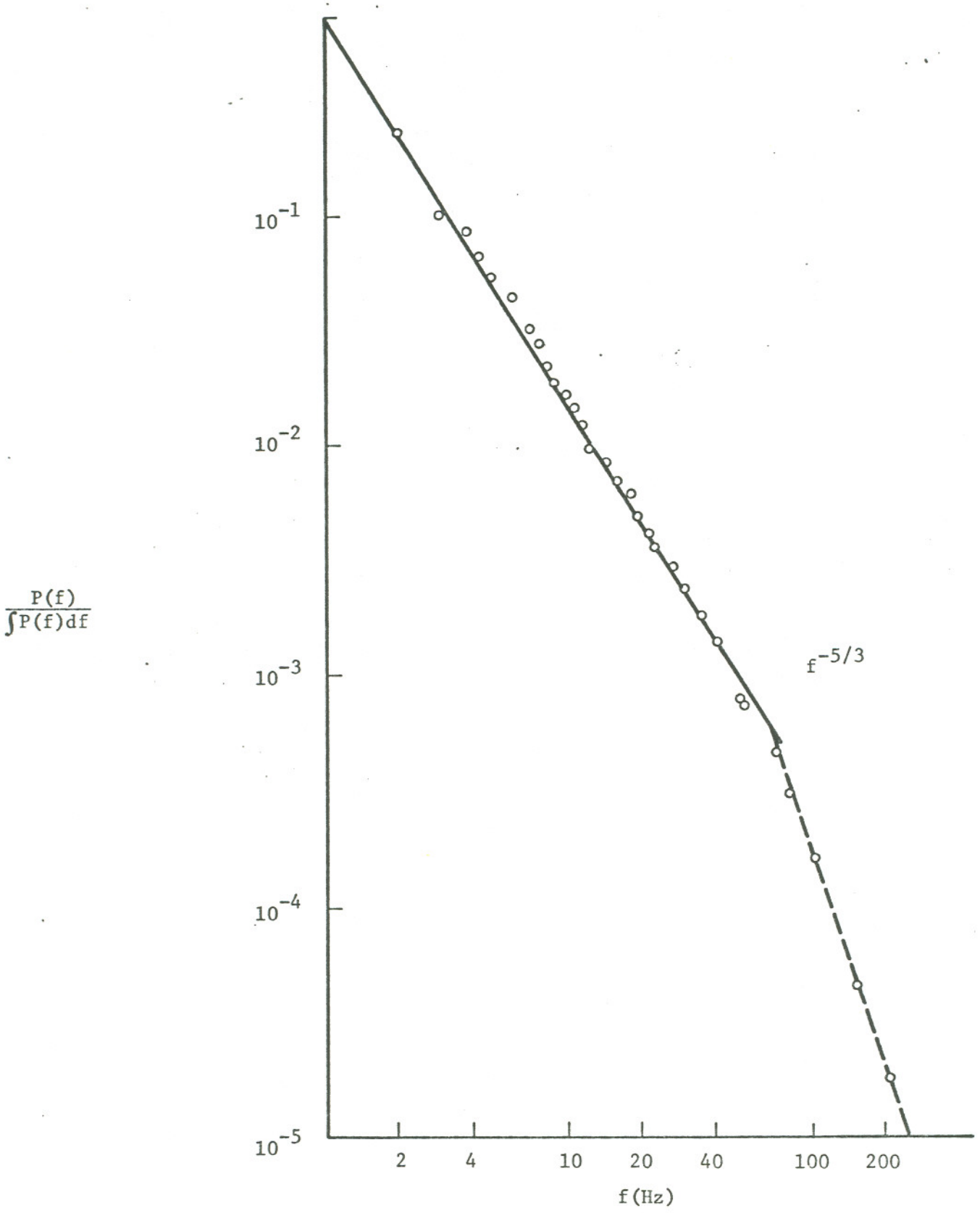

Figure II.3. Temporal Power Spectrum of single point temperature fluctuations. u = 1.5 m/sec.

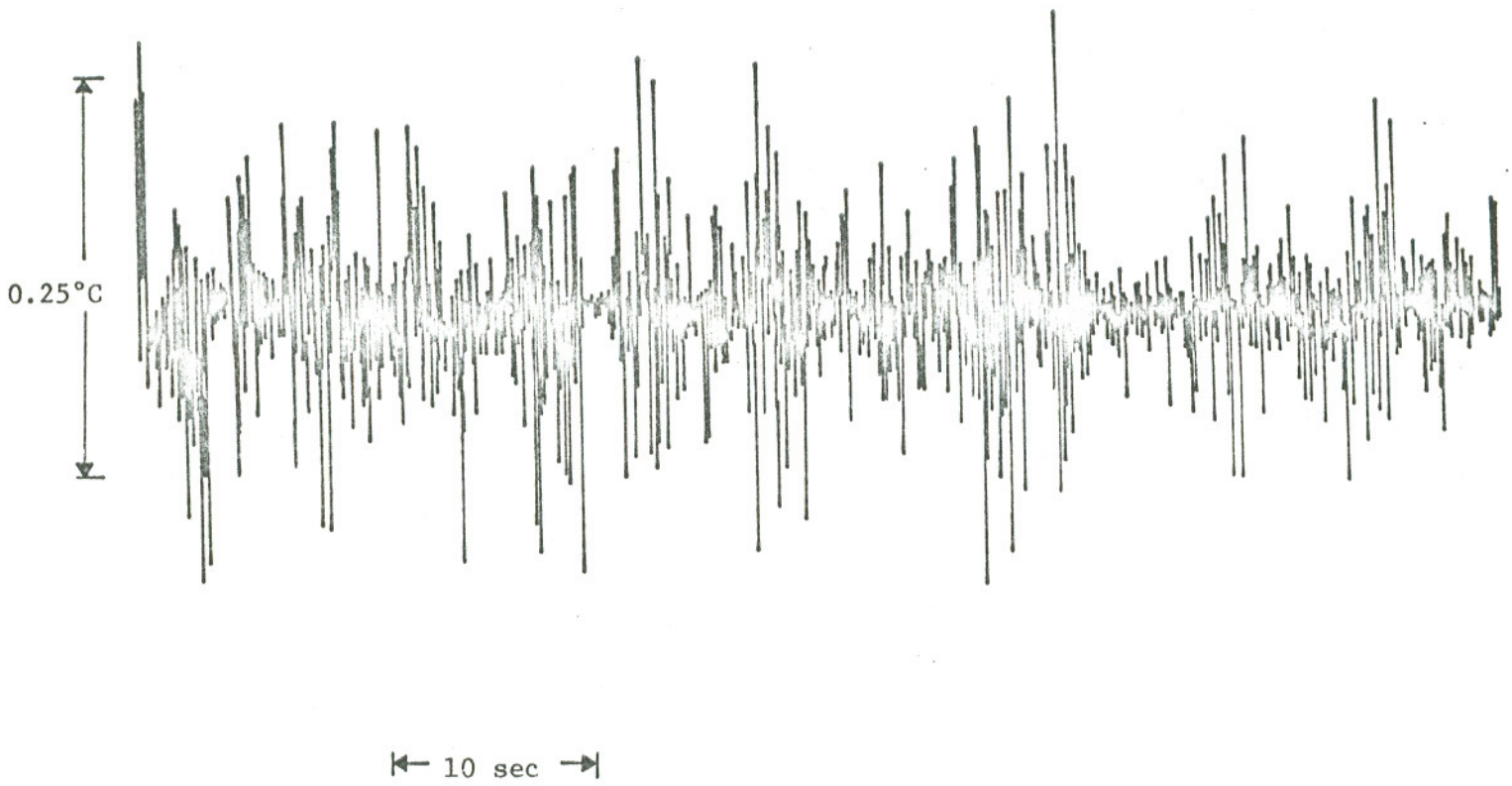

Figure II.4. Trace of fluctuations in temperature difference between two points in the atmosphere.

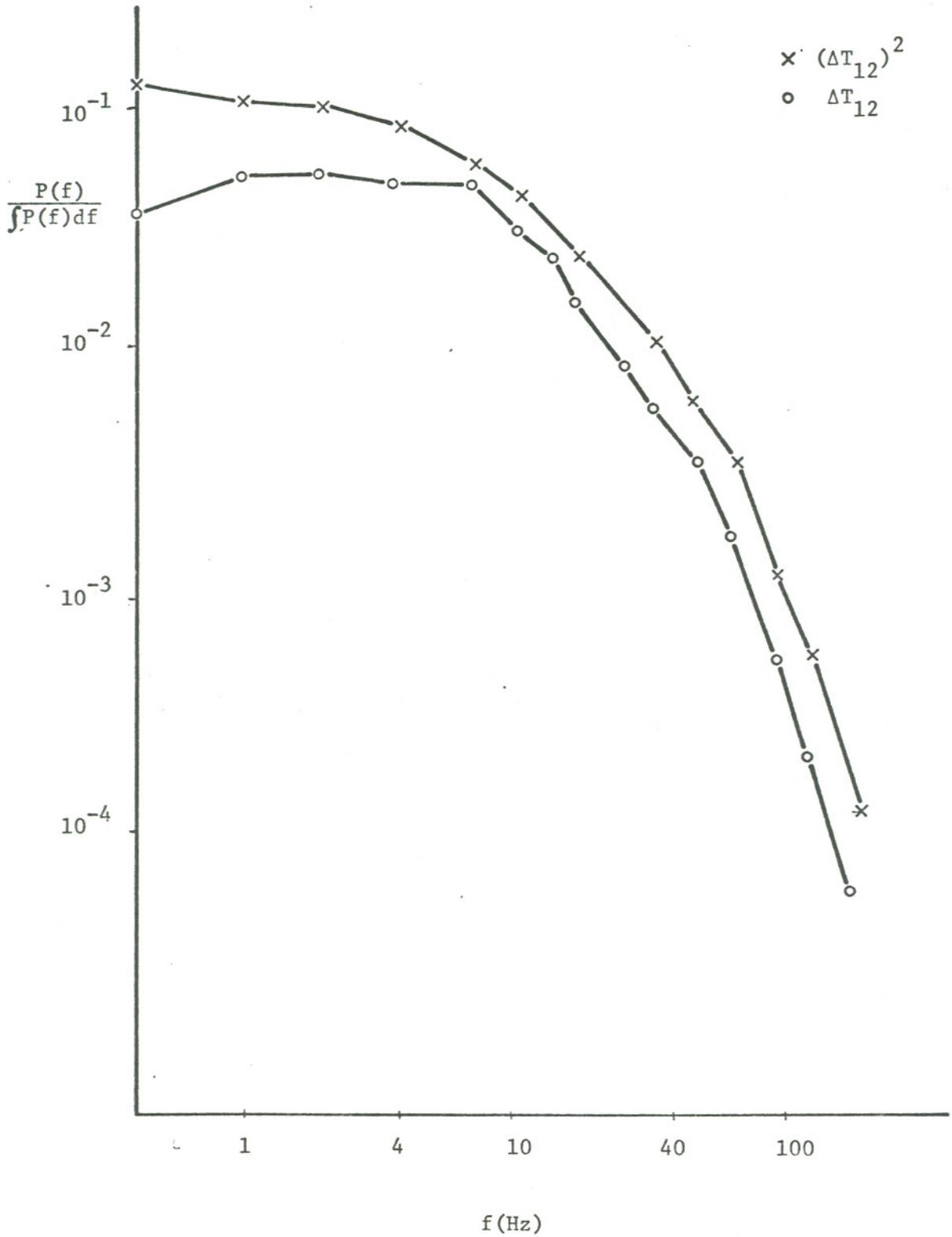

Figure II.5. Temporal power spectrum of two point differential temperature fluctuations ΔT_{12} and $(\Delta T_{12})^2$.

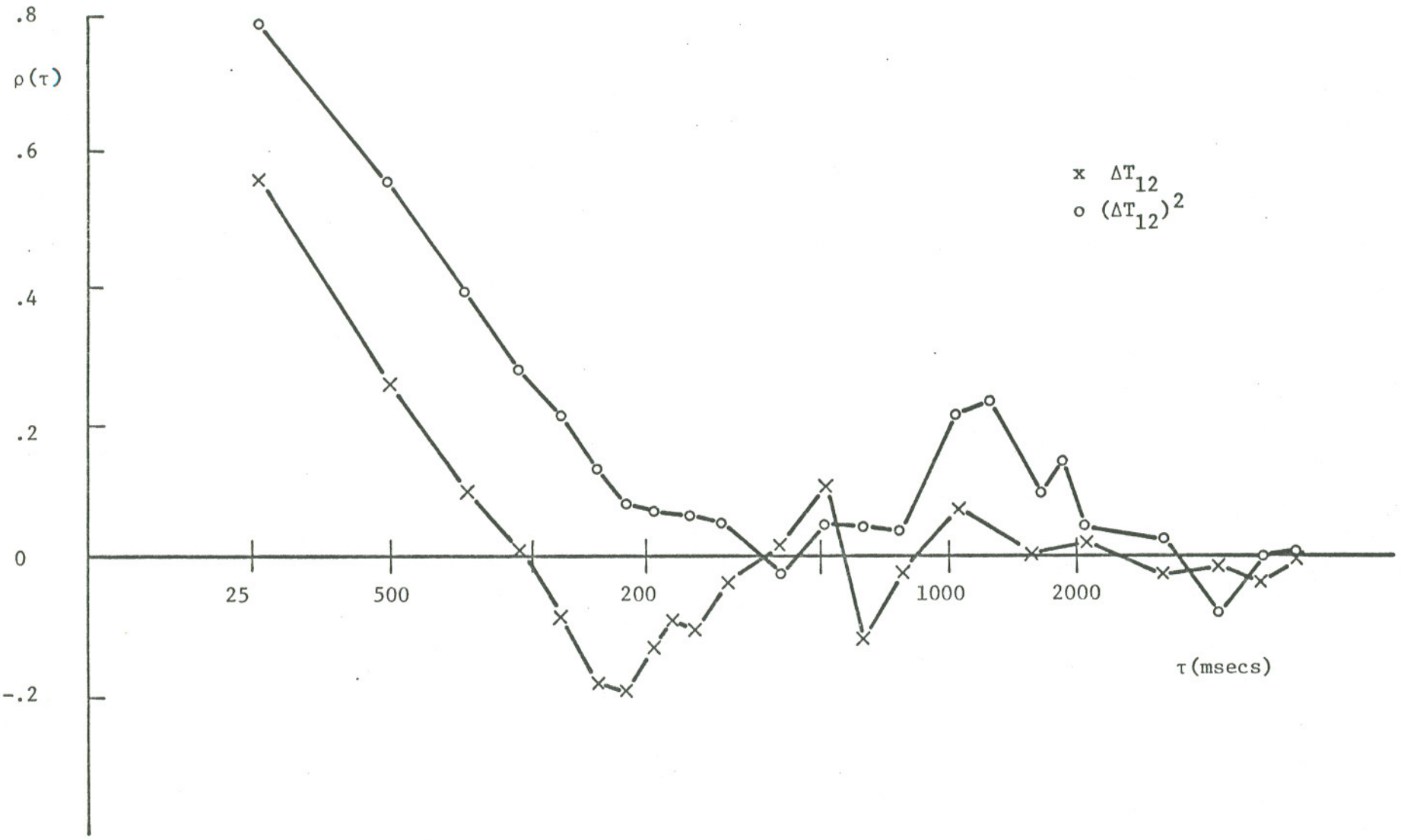

Figure II.6. Autocorrelation functions of ΔT_{12} and $(\Delta T_{12})^2$.

tistical properties of random processes) defined as

$$I = \int_0^\infty \rho(\tau)d\tau \qquad \text{(II.9)}$$

Since the correlation function $\rho(\tau)$ is the Fourier transform of the power spectrum $\phi(\omega)$, we know immediately that the integral of the correlation function, the integral scale, will be directly related to the value of the spectrum at zero frequency. The exact relationship will depend of course on the normalization used in defining the spectrum. From this relation it can be easily shown that the integral scale of the derivative of a process with finite integral scale, is zero. As the two probe differential temperature measurement is related to the average of the temperature derivative, its integral scale should also be zero. Figure II.6 shows the correlation function of ΔT_{12} fluctuating about zero at large τ allowing for the possibility of a zero integral scale. Actual calculation of the integral scales of these processes becomes difficult because the correlation function is significantly different from zero over such a wide range of τ. In the case of the $(\Delta T_{12})^2$ the autocorrelation function is nearly everywhere positive and thus the integral scale may be comparatively large.

Lumley (1970) discusses a theorem of Samarov (1958) relating to the above discussion of integral scales and correlation functions. Considering Gaussian processes, which in fact is not the case here as we shall see, Samarov proved that a process x(t) is better correlated than any function of it with the following exception: if the correlation function is anywhere negative, then the correlation function formed by taking the absolute value of the original correlation function is maximal. In terms of integral scales, the integral scale calculated from the absolute value of the original correlation function is greater than that of any function of the original process. This theorem could be very useful in making estimates of the integral scales of high order processes once the correlation function of the basic process is known.

II.4b. Probability Distribution Functions and Moments

The probability density function of the fluctuations ΔT at a single

point such as in Figure II.2 is asymmetric, amorphous and dependent on large scale, or low frequency fluctuations which are not of interest in this work. The PDF of the two probe differential temperature measurement however, is of particular interest in that it describes the distribution of the magnitude of index of refraction fluctuations in the size range of importance to the optical propagation problem. Figures II.8 and II.9 show cumulative probability distributions for the data shown in Figure II.7a and b respectively. On each graph a normal distribution of the same mean and variance is shown by the straight line for comparison. The PDF's of the temperature difference fluctuations are decidedly non-normal. There is a much larger probability in these distributions for very small values of ΔT_{12} and similarly for very large values of ΔT_{12} than in the corresponding normal distributions. This latter behavior, a large probability of extreme values, is of course the result of the small scale intermittent nature of the turbulence mentioned in regard to Figure II.4. These comments may be made more quantitative by investigating the central moments associated with the various distribution functions.

Also commonly used as descriptors of the probability distribution function are the 3rd and 4th central moments normalized by the variance, respectively the skewness S and the kurtosis K, defined as follows:

$$S = \frac{\langle \phi^3 \rangle}{\langle \phi^2 \rangle^{3/2}}$$

$$K = \frac{\langle \phi^4 \rangle}{\langle \phi^2 \rangle^2}$$

We note that for a normal distribution and in fact any symmetric distribution, S=0 and for a normal distribution, K=3. The calculated skewness and kurtosis of the distributions shown in Figures II.8 and II.9 are shown in the figures. We note that other turbulence parameters such as velocity and velocity derivatives have been observed with kurtoses as high as 40 (Gurvich 1967, Gibson, Stegen and Williams 1970, and Gibson and Masiello 1972).

Calculation of high order moments of distributions of atmospheric fluctuations are complicated by the necessity of long observation times for accurate estimates. Statistical errors in the calculation of the moments

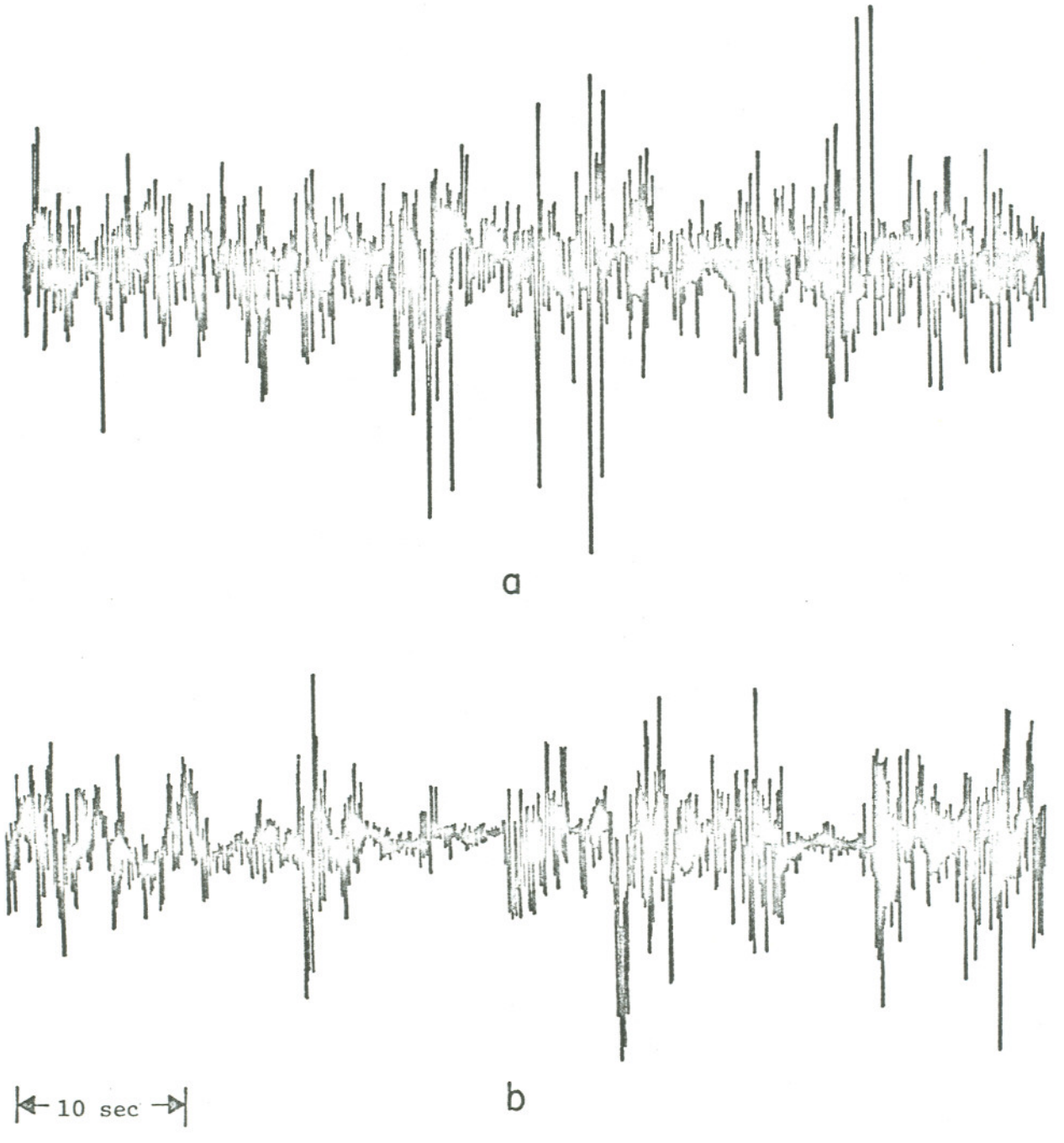

Figure II.7. Two probe differential temperature fluctuations

a, $\bar{u}$ = 4.5 meters/sec

b, $\bar{u}$ = 1.0 meters/sec

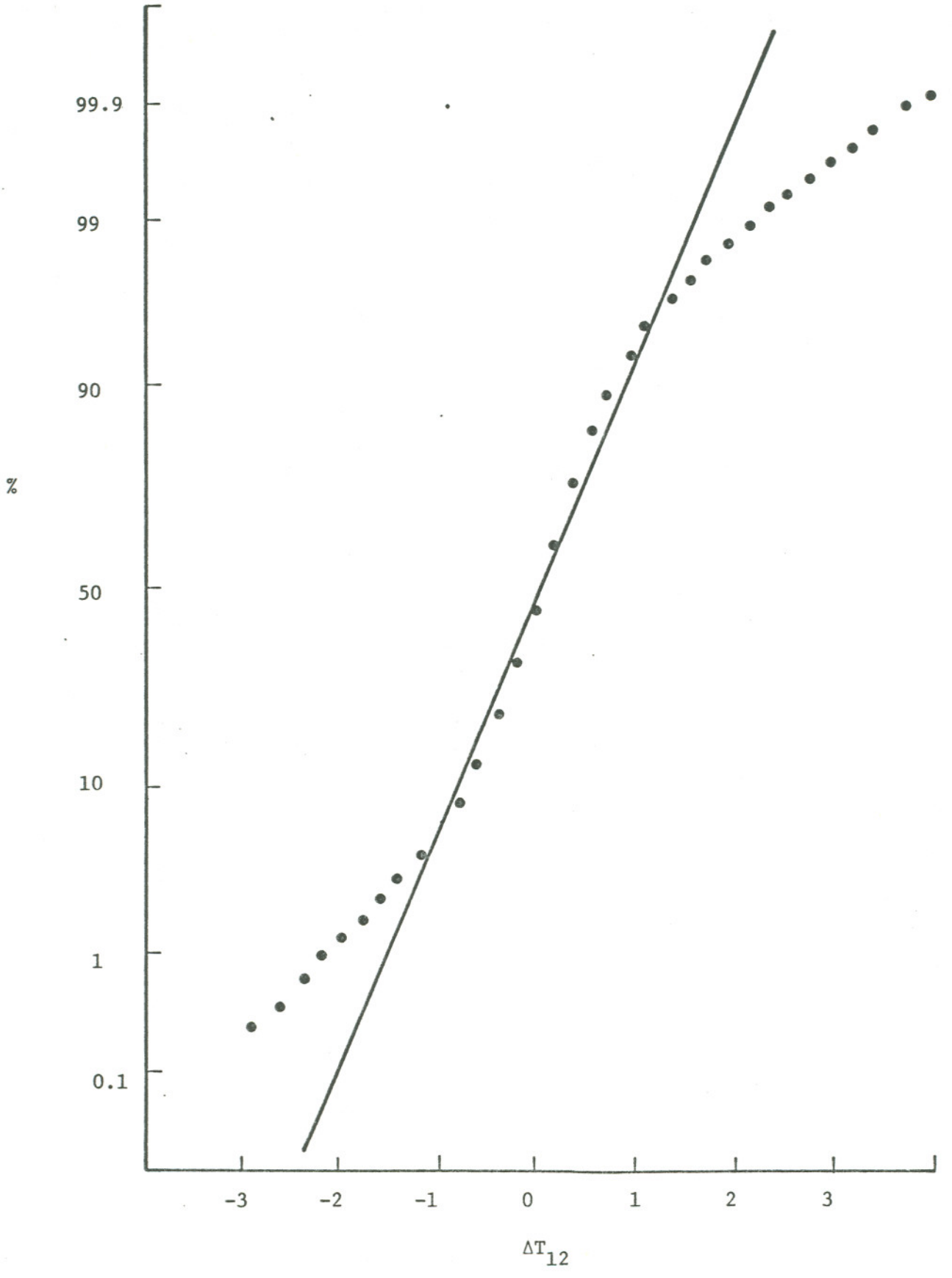

Figure II.8. Cumulative Probability Distribution (%) of ΔT_{12} associated with data of Figure II.7a. S = 0.06, K = 7.35

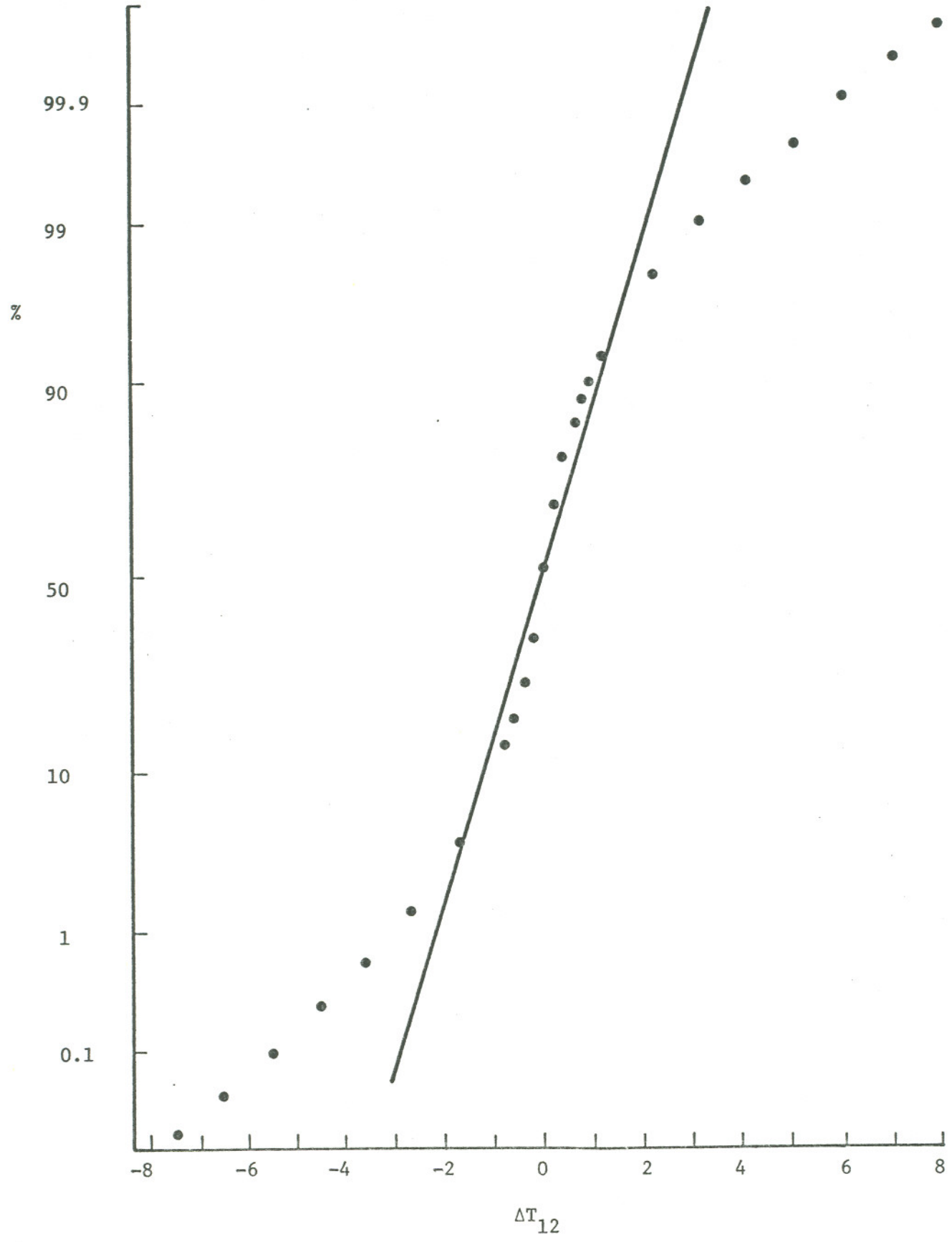

Figure II.9. Cumulative Probability Distribution (%) of ΔT_{12} associated with data of Figure II.7b. S = .02, K = 11.73

from a finite time sample of the data depend on two characteristics of the random process under investigation; the shape of the true distribution function and the temporal behavior of the random process described by the autocorrelation function. Tennekes and Wyngaard (1972) give formulae for the mean square error in the measurement of the variance (see also Ogura 1957 and Collins 1971) and fourth central moments averaged over a time τ as

$$\varepsilon^2(\sigma^2)_\tau = 2(K-1)\ T_2/\tau \tag{II.13}$$

$$\varepsilon^2(\mu^4)_\tau = 2(M_8/K^2-1)T_4/\tau \tag{II.14}$$

where T_n is the integral scale of the autocorrelation function of the n^{th} order process

$$T_n = \int_0^\infty \rho_n(\tau)d\tau$$

$$= \int_0^\infty \frac{<\chi^n(t)\chi^n(t+\tau)> - <\chi^n(t)^2>d\tau}{\mathrm{Var}[\chi^n(t)]} \tag{II.15}$$

and M_8 is the eighth central moment non-dimensionalized by the variance. These formulae are valid for $\tau >> T_n$. An obvious problem that develops in attempting to apply Eqs. (II.13) and (II.14) is that the error in the measurement of the second moment for example is dependent on (1) the integral scale of the squared process, itself an ensemble averaged quantity, and (2) the fourth moment of the process which will have a statistical error in its measurements given by Eq. (II.14).

Considering the discussion of the previous section indicating possible large values of T_2 and the large values of K seen here for turbulent temperature fluctuations, we might anticipate large errors in short time averages of the variance of ΔT_{12}. These short time effects will be discussed in Chapter IV.

The probability distribution of (ΔT_{12}^2) when averaged over some small volume or time period was predicted by Gurvich and Yaglom (1967) to

be lognormal (see section II.2 above). Figures II.10 and II.11 show distributions of $(\Delta T_{12}^2)_\tau$ for the data of Figure II.7 with a number of different averaging times. The solid lines indicate lognormal distributions with the same mean and variance as the experimentally determined distributions. The data of Figure II.11 was taken under very light wind conditions and we note a strong deviation from lognormality at both large and small values of (ΔT_{12}^2). In Figure II.10 we see similar deviations although to a much lesser degree. The deviations from lognormality at high and low values of (ΔT_{12}^2) and of the similarly distributed velocity derivative $\left(\frac{\partial u^2}{\partial t}\right)$ have been observed and reported numerous times in the literature (see Stewart, Wilson and Burling 1970, Gibson and Masiello 1972, and Chen 1971). Stewart et al suggest that the low probability density observed at large values of the fluctuations may arise from the cascade process, that is, the breakdown of large eddies into smaller eddies, consisting of too few steps because of low Reynolds number. Thus in the sum over ratios of the fluctuating parameter averaged over different volumes in Eq. (II.7), r is not large enough for the central limit theorem to apply and indicate a Gaussian distribution for log ϕ_r. They show that this assumption could account for the deviation of the distribution from lognormal at large values of the argument. We point out additionally there are inherent difficulties in attempts to experimentally verify that a process is lognormally distributed. These include the wide dynamic range over which the probability density is significantly different from zero necessitating extreme care in the design of experimental procedures (Tennekes and Wyngaard 1970), and the well known inability to strictly determine that a process is lognormal from the measurements of its moments (Orszag 1970). Whether or not the distribution of $(\Delta T_{12})_\tau^2$ is in fact exactly lognormal under any conditions cannot be answered. It is clear, however, that this distribution is highly asymmetric, has a large flatness factor, and is qualitatively similar to a lognormal. Again by the central limit theorem, we would expect that with long enough averaging times or distances, the distribution should approach a normal. It has been pointed out, however, that this approach may be exceedingly slow in the case of the fundamental distribution being lognormal, or excessively

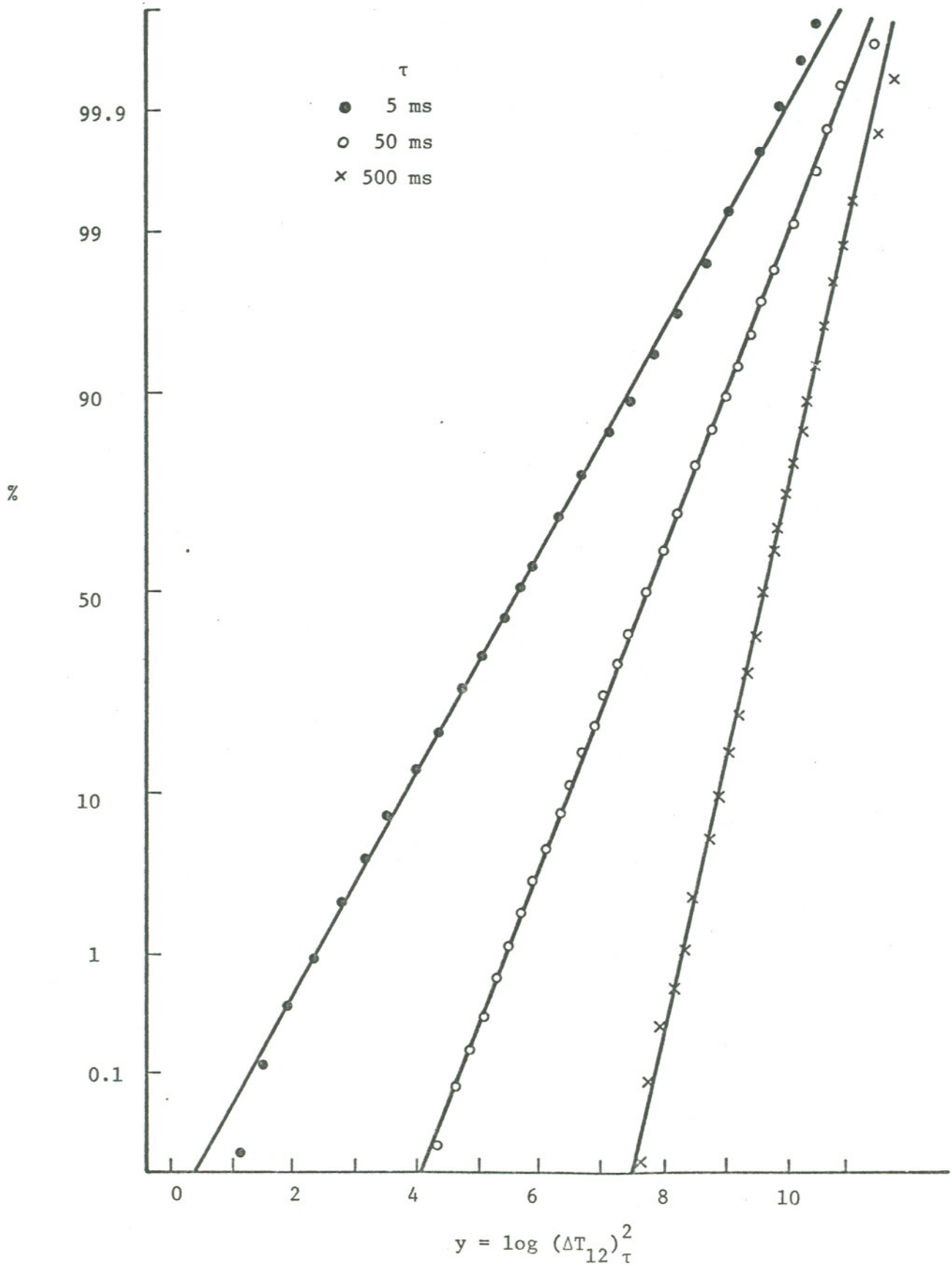

Figure II.10. Cumulative Probability Distribution (%) of $y = \log (\Delta T_{12}^2)$ associated with data of Figure II.7a.

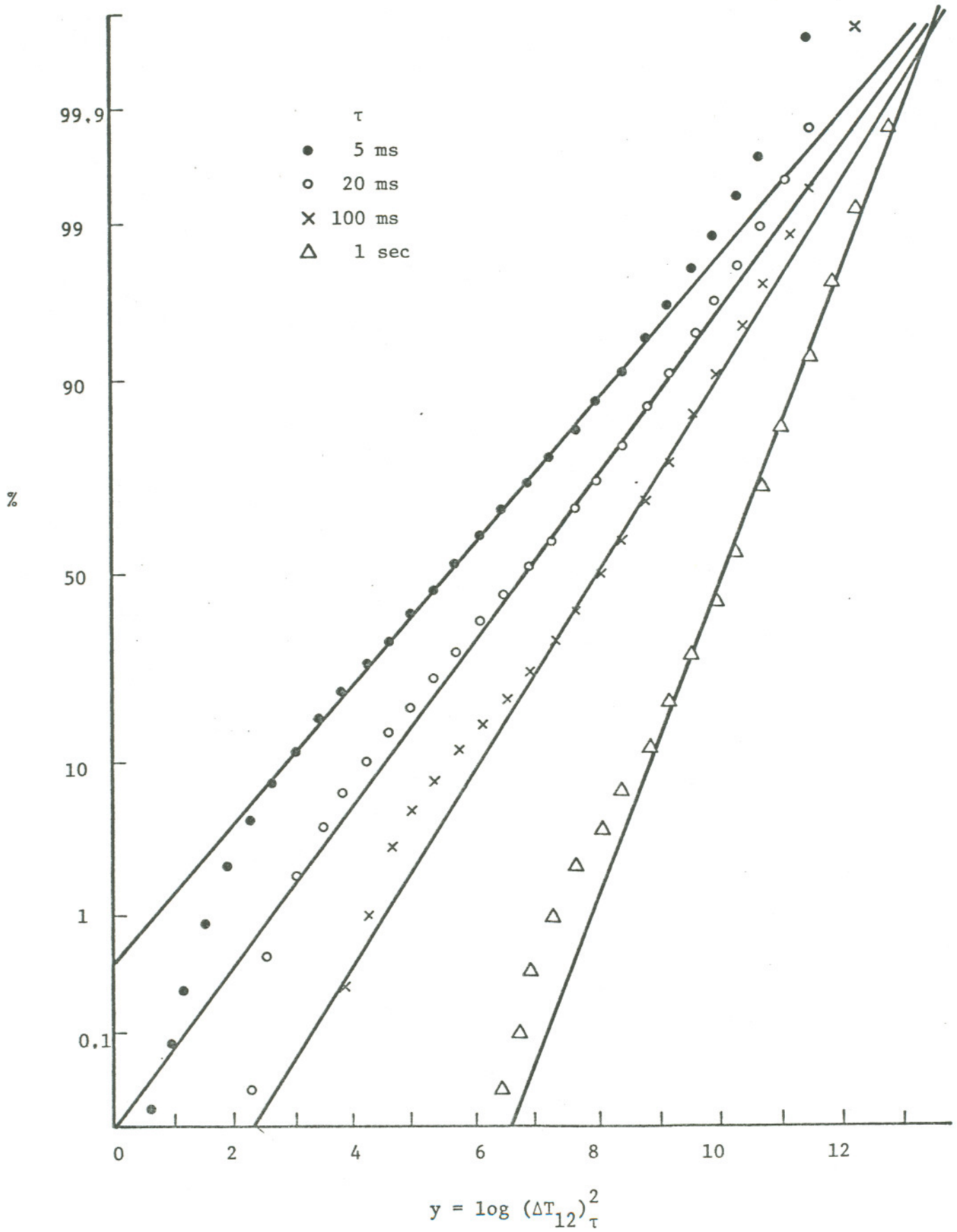

Figure II.11. Cumulative Probability Distribution (%) of $y = \log (\Delta T_{12}^2)$ associated with data of Figure II.7b.

skewed (Barakat and Blackman 1974, Mitchell 1968). We can illustrate the approach to a normal distribution by plotting the kurtosis K and the skewness S for a series of averaging times. Figure II.12 shows such a plot for distributions of $(\Delta T^2)_\tau$. We see that even for averaging times as long as 5 seconds, the distribution is extremely skewed and far from normal. The implications of the skewed distribution include the fact that the mode differs from the mean and thus a small number of short time measurements may yield an inadequate sample from which the true mean may not be derived with an acceptable accuracy.

II.5. Conclusion

The results presented above include the statistical properties of certain functions of the randomly fluctuating local temperature in the atmosphere which under certain conditions relate directly to those properties of the index of refraction. In general, atmospheric temperature fluctuations (two point differential measurements, ΔT_{12}) are characterized by non-gaussian probability distribution functions (flatness factors much greater than 3). Additionally, the autocorrelation functions show significant correlation at time lags (of the order of one second) large compared to the fundamental time scale of the fluctuations (of the order of milliseconds). The square of this process ΔT_{12}^2, whose mean is the variance of the temperature difference fluctuations, has a distribution which is highly skewed. When this process is time averaged over some short time, its probability distribution function appears nearly lognormal and very slowly approaches a normal distribution with increasing averaging time. The skewness and large flatness factors associated with the distribution of $\left(\Delta T_{12}^2\right)_\tau$ and the long time correlation (low frequency components in the power spectrum) combine to make short time averaged measurements of characteristics of this process subject to relatively large fluctuations. We will see further evidence of this in Chapter IV.

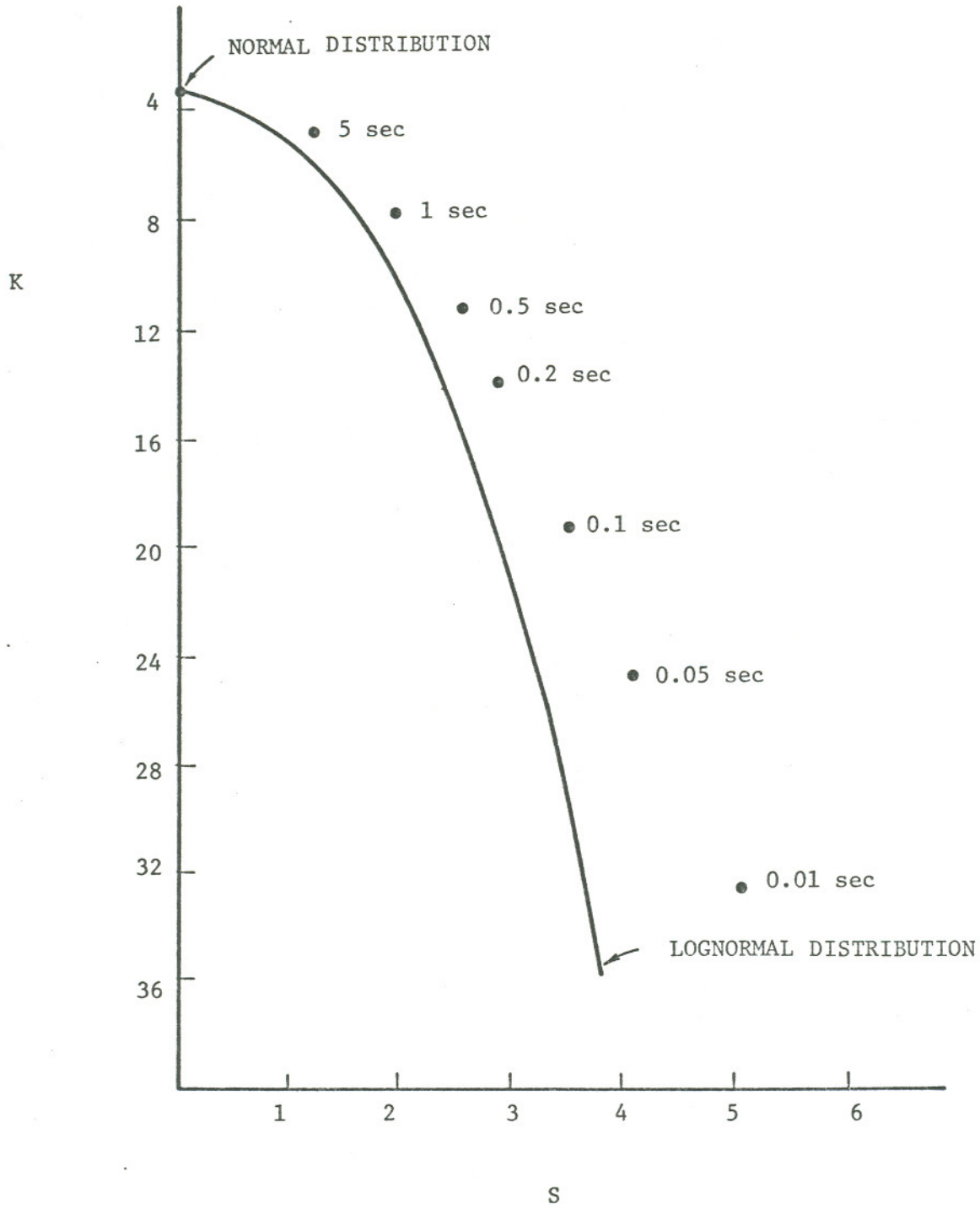

Figure II.12. Plot of kurtosis (K) versus skewness (S) for distributions $(\Delta T_{12})^2$ for averaging times between 0.01 and 5 seconds. The solid line is the locus of K, S values for the lognormal distribution.

CHAPTER III. Irradiance Fluctuations

III.1. Introduction

The fundamental statistical characteristics of amplitude fluctuations of an optical electromagnetic wave after propagation through the turbulent atmosphere are the subjects of this chapter. To begin, a brief review of the phenomenological models used to describe the measured statistical properties of amplitude scintillation are presented. This is followed by a description of the experimental propagation facility at which the measurements were made. We then present the results of observations and calculations of various statistical properties of the fluctuating optical amplitude. These include spectra and correlation functions, single point probability distribution function, and two point (in time) conditional probability distribution functions.

III.2. Background

The problem of amplitude scintillation, especially under low turbulence conditions has been reviewed extensively in the past (Lawrence and Strohbehn 1970, Tatarskii 1971, Kerr 1972). We mention here specifically a number of investigations relevant to the specific questions of interest. The problem of calculating the temporal frequency spectra of scintillation was described in detail by Tatarskii (1971) for the case of plane wave propagation. The basic assumption employed in the calculations was that the temporal variations in the optical field observed at a receiver are the result of a 'frozen in' turbulence field translated across the path with the mean wind velocity. Thus calculation of the power spectrum of these fluctuations basically involves calculation of the spatial covariance function of the irradiance at the receiver plane, transformation with Taylor's hypothesis to the temporal autocorrelation function and finally Fourier transforming to yield the power spectrum. Clifford (1971) extended the calculation to spherical wave propagation. The results of these calculations indicate a normalized spectrum dependent on a single parameter $\Omega = f/f_o$ where $f_o = \bar{u}_\perp/(2\pi\lambda L)^{1/2}$, where $\bar{u}_\perp$ is the wind speed transverse to the path.

The form of the probability distribution function of the fluctuating optical amplitude has been the subject of more intense study. Under very low turbulence conditions excellent agreement with the lognormal distribution has been observed (Kerr 1972 and Fried, Meyers and Kuster 1967). This distribution has also been predicted on the basis of a very simple physical argument (Strohbehn 1968). Recently however there has been increased study of the distribution function under high turbulence conditions. Prediction of a lognormal, Rayleigh and various modifications of these distributions have been made (deWolf 1973, Strohbehn, Wang and Speck 1975, Wang and Strohbehn 1974 a,b). In fact, Wang and Strohbehn (1974 a,b) have shown that over certain ranges of the 'turbulence level' the assumptions of Rayleigh or lognormal statistics of the amplitude fluctuations lead to unphysical results. Experimental investigations of these questions in the range of observable high turbulence conditions are currently in progress (Dunphy and Kerr, private communication).

III.3. Experimental

The optical experiments performed in this program were carried out at two wavelengths, 10.6 microns from a CO_2 laser (Sylvania Model No. 948) and 0.488 microns from an Ar ion laser (Coherent Radiation Model No. 52). The beams from the two lasers were formed into diverging beams such that at the receiver they appeared as effective point sources. The beams were also mechanically chopped at 9 kilohertz to avoid problems of the detection of DC light in the presence of ambient daytime light levels and to achieve better signal-to-noise characteristics in the receiver amplifiers. Following the chopping and the beam-forming optics, the two beams were combined spatially, such that all experiments were conducted with simultaneous, coaxial beams.

The atmospheric channel through which the beams travelled is 1.6 kilometers long and approximately 2 meters ($\pm$ 0.5 meters) above the ground. The terrain is extremely flat agricultural land with very few physical obstacles to the atmospheric flow within significant distance of the path, two exceptions being two small buildings at the ends of the

path, one housing the transmitter laser and optics and the other, the receiver and associated electronics. For point source (spherical wave) propagation the major contribution to the turbulence-induced amplitude fluctuations will arise from turbulence near the center of the path, with the contribution falling to zero near the ends of the path, so that the effects of the buildings are minimal.

The receivers for the two beams are effective point receivers,[+] under low turbulence conditions and are essentially coincident. The signals from the photodiodes are amplified and filtered to yield an information bandwidth of 1 kilohertz with a dynamic range of 80 db. The signal, representing the intensity of the optical field is passed through a log amplifier yielding a signal proportional to the normalized log intensity. This signal is then recorded on analog magnetic tape simultaneously with the atmospheric temperature fluctuations for later computer processing. Figure III.1 is a schematic block diagram of the propagation experiment.

III.4. Experimental Results

III.4a. Spectral Properties and Correlation Functions

Examples of the irradiance fluctuations observed over the 1.6 kilometer path are shown in the traces of Figure III.2. In the high turbulence case, $C_n^2 = 1.7 \times 10^{-13} m^{-2/3}$, the saturation of the intensity of the fluctuations of the 0.488 micron beam is indicated by the value of the log amplitude variance, 0.32, being substantially below the Rytov value predicted by Eq. I.5, $\sigma_\chi^2 = 3.15$. In the low turbulence case, neither beam exhibits saturation for this path length. Figure III.3 shows the normalized weighted power spectra for the low turbulence case. It is obvious from Figure III.2 that the 0.488 micron beam has higher frequency components than

---

[+] The covariance length, under low turbulence conditions, is approximately $\sqrt{\lambda L} >> d_r$ where d_r is the size of the receiver. At high turbulence, however, the covariance length decreases, and to avoid averaging over more than one covariance patch size, the detector size must decrease.

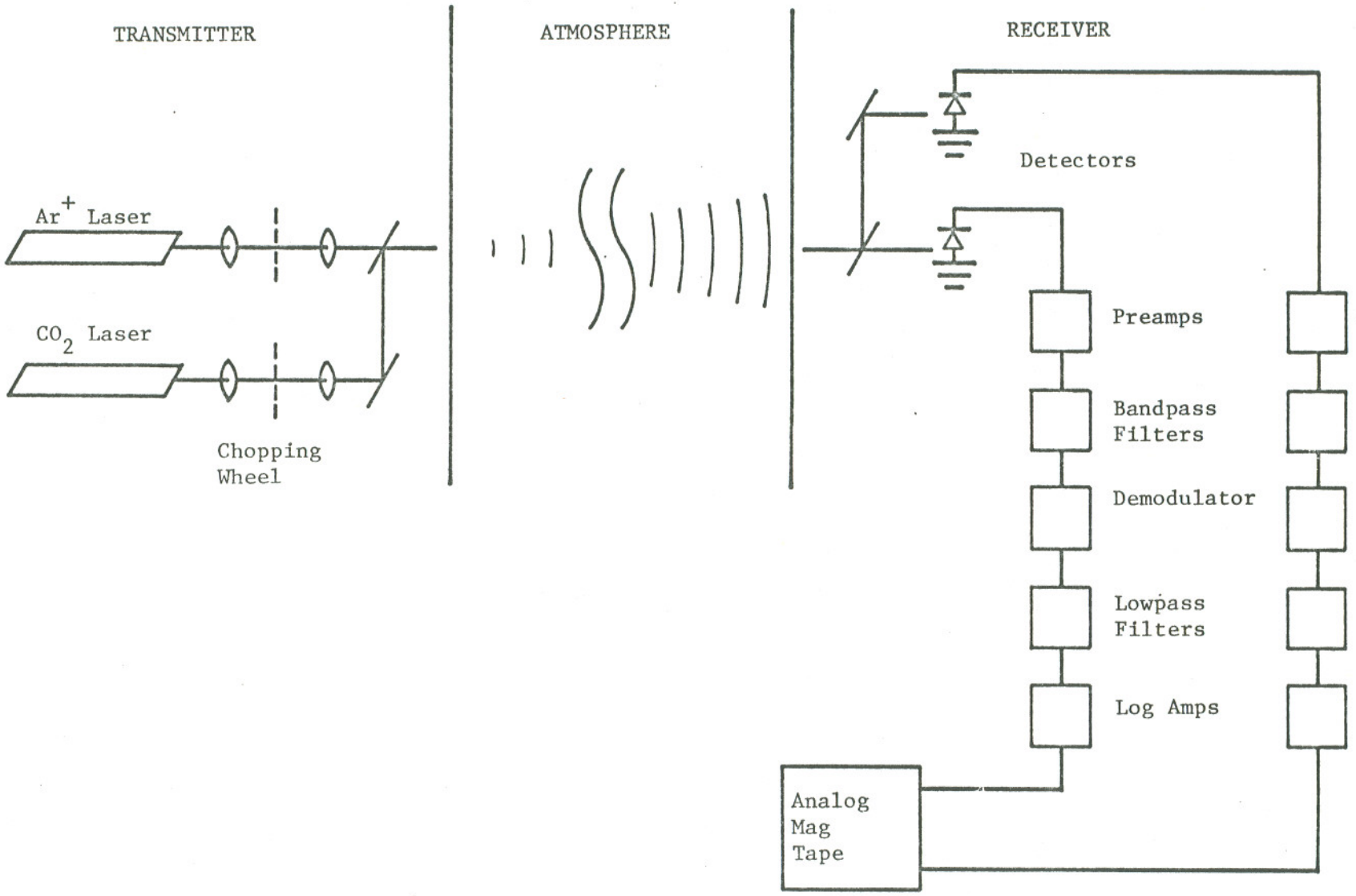

Figure III.1. Block diagram of propagation experiment.

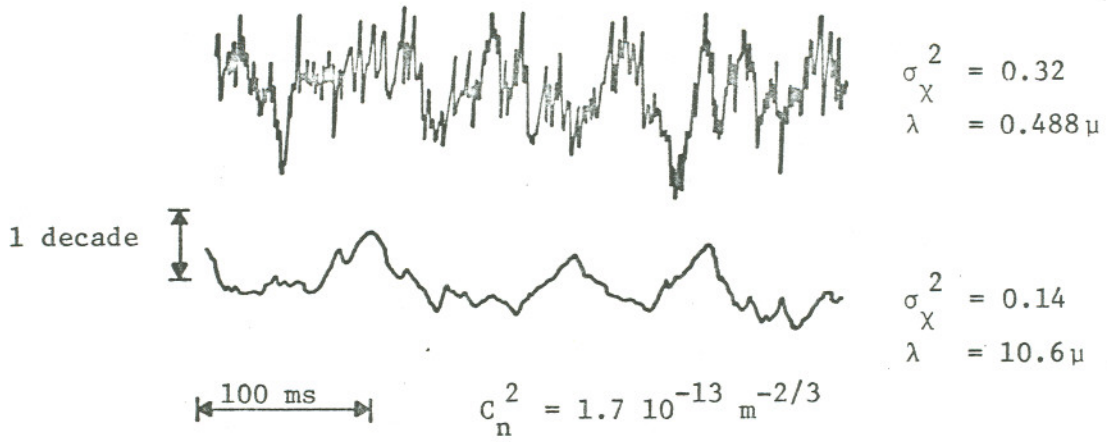

(a)

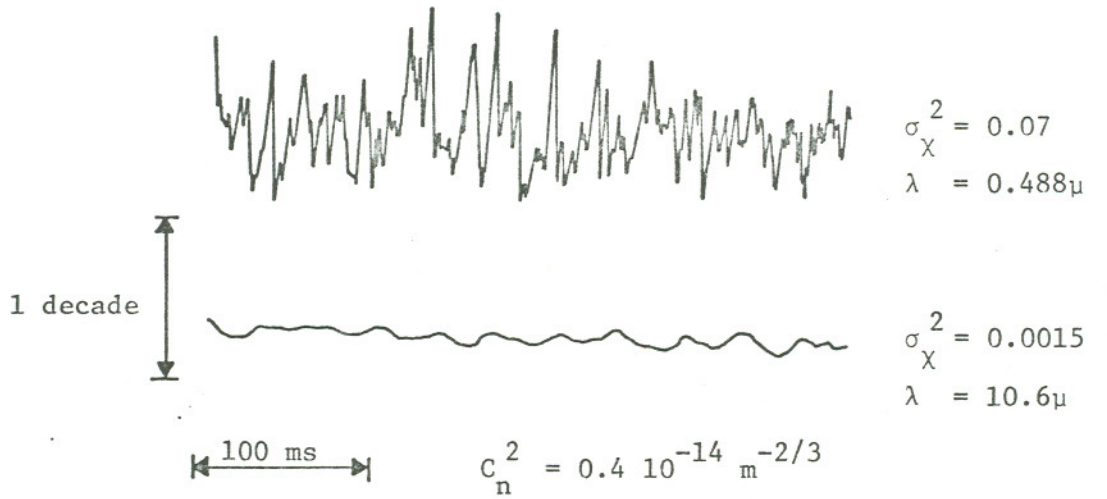

(b)

Figure III.2. Log amplitude fluctuations from 0.488μ and 10.6μ lasers under high (a) and low (b) turbulence conditions.

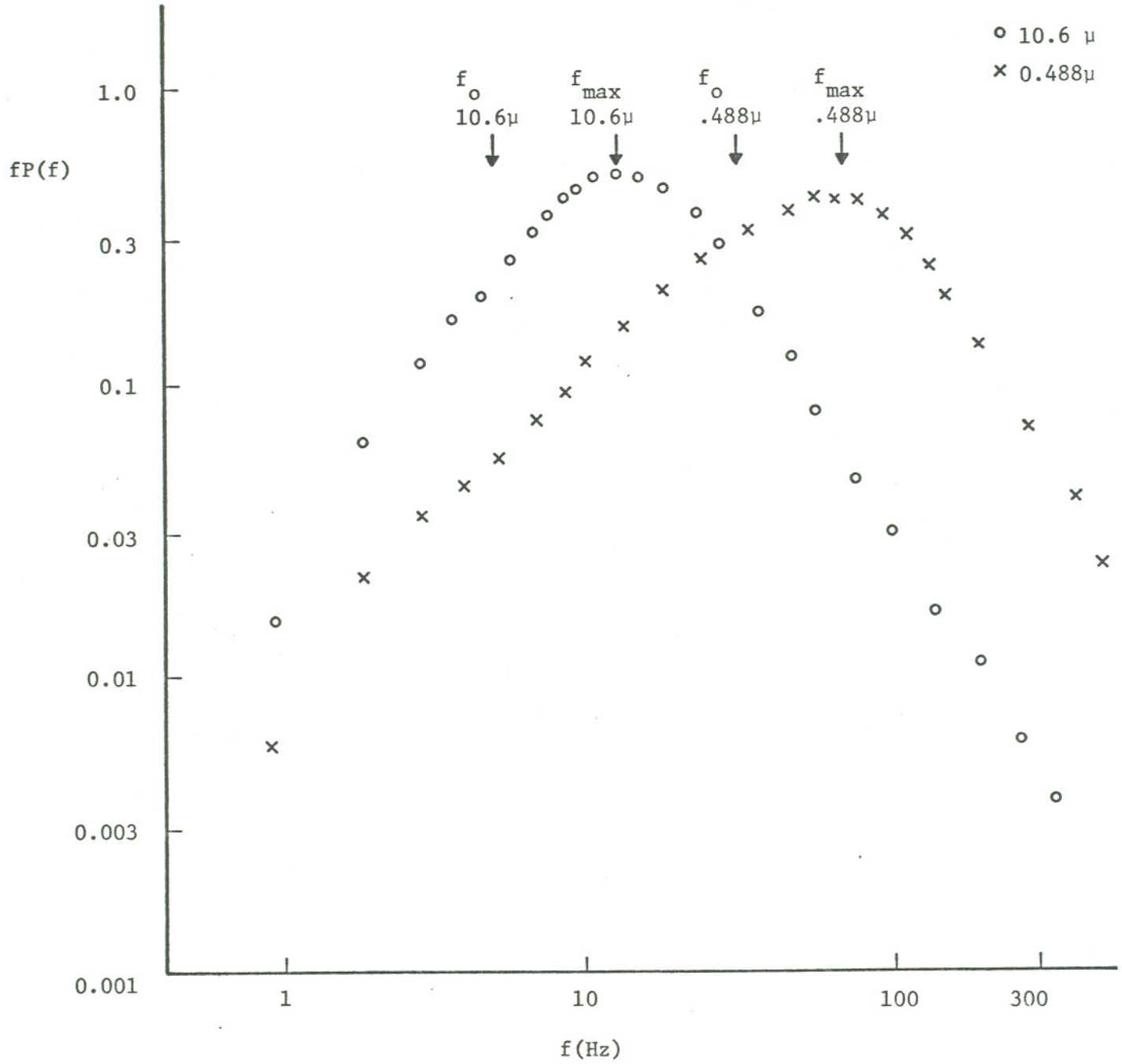

Figure III.3. Weighted power spectra of log irradiance fluctuations.

the 10.6 micron beam. This is clearly indicated by the locations of the peak positions of the two spectra in Figure III.3. The ratio of frequencies of the corresponding maxima is approximately 4.8 while the results of Clifford's analysis predict a ratio of $\sqrt{\frac{\lambda_1}{\lambda_2}} = \sqrt{\frac{10.6}{.488}} = 4.66$. Also shown in the figure are calculated values of f_o for the two wavelengths. These values are approximately one half the peak frequency also in agreement with Clifford's conclusions. From the calculated power spectra we can derive the autocorrelation function. For later reference we show three examples of the autocorrelation functions over a range of wind and turbulence conditions (Figure III.4).

III.4b. Probability Distribution Function and Moments

The expected probability distribution of the log amplitude and thus also the log irradiance fluctuations under low turbulence conditions is normal. Figures III.5 and III.6 show probability distributions of log I for the 10.6 micron beam under two turbulence conditions. Also indicated in the figure are the calculated log amplitude variance, skewness and kurtosis, the wind speed and a true normal distribution of the same mean and variance as the experimental distribution (solid line). Except for the slight skewness in the high turbulence example, the distributions and associated parameters indicate qualitative agreement with the lognormal hypothesis over a range of at least several standard deviations about the mean.

The distributions of the square of the log irradiance fluctuations averaged over various averaging times are related to the short time measurements in the log amplitude variance. As an example, Figure III.7 shows a series of such distributions for the high turbulence log irradiance fluctuations of Figure III.2a with averaging times ranging from one millisecond to one second. In this figure, a straight line would indicate a lognormal distribution. We point out that over the limited range shown

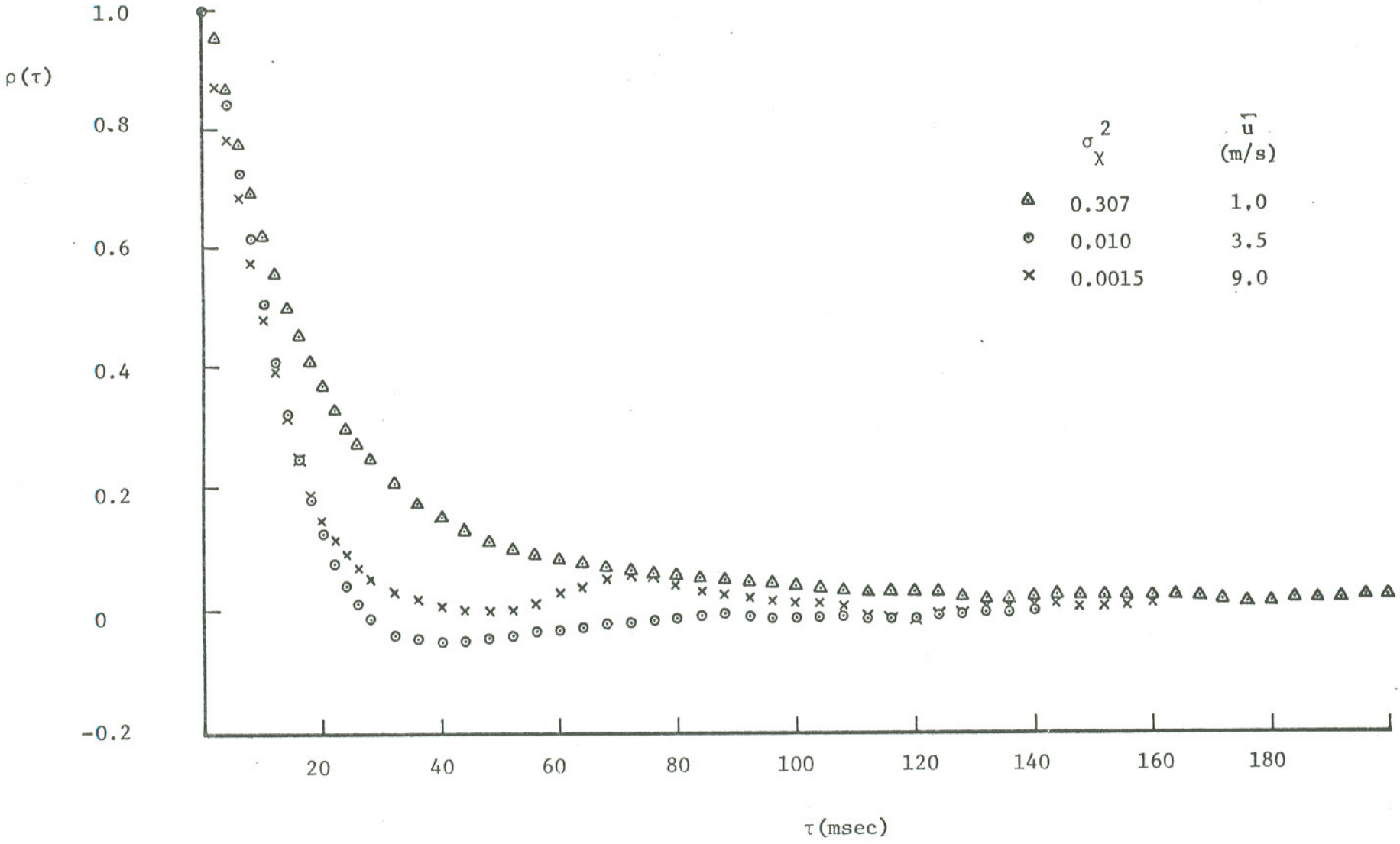

Figure III.4. Autocorrelation functions of log irradiance fluctuations. $\lambda = 10.6\mu$.

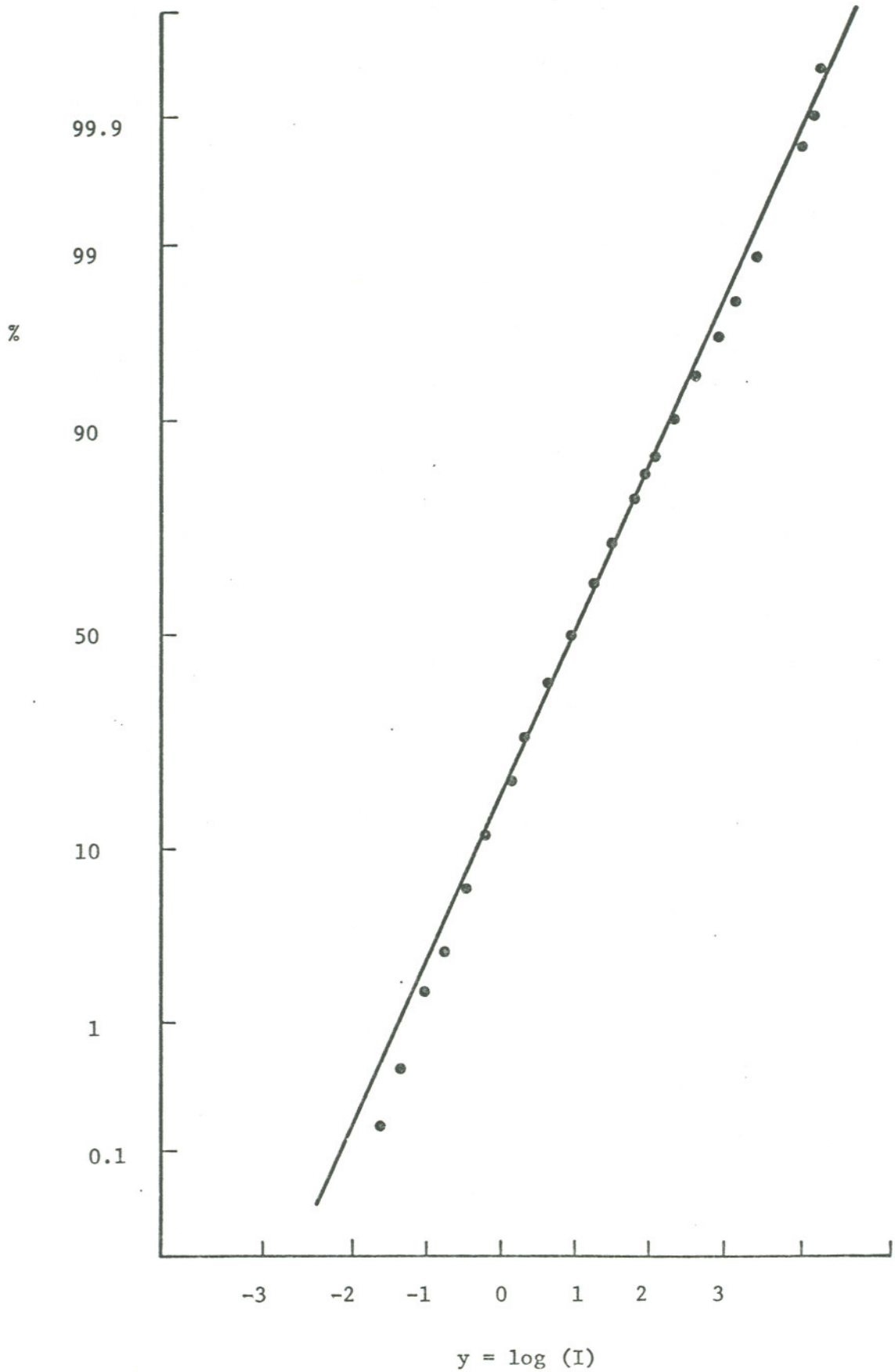

Figure III.5. Cumulative probability distribution (%) of log irradiance fluctuations under high turbulence conditions. S = .12, K K = 3.01, σ_{χ}^{2} = 0.14, u = 1.5 m/s.

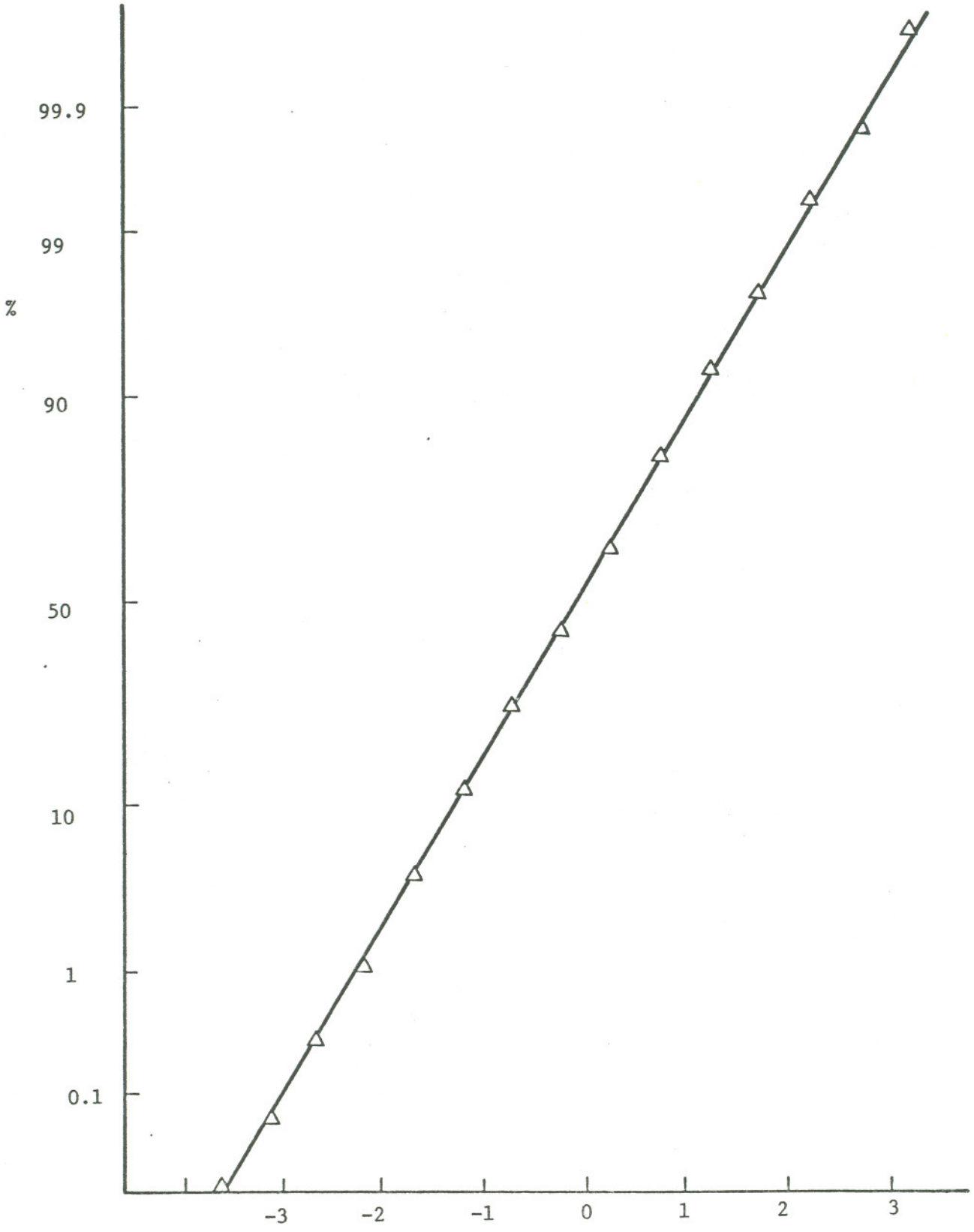

Figure III.6. Cumulative probability distribution (%) of log irradiance fluctuations under low turbulence conditions. S = 0.04, K = 3.06 σ_χ^2 = 0.0015, $\bar{u}$ = 9 m/sec.

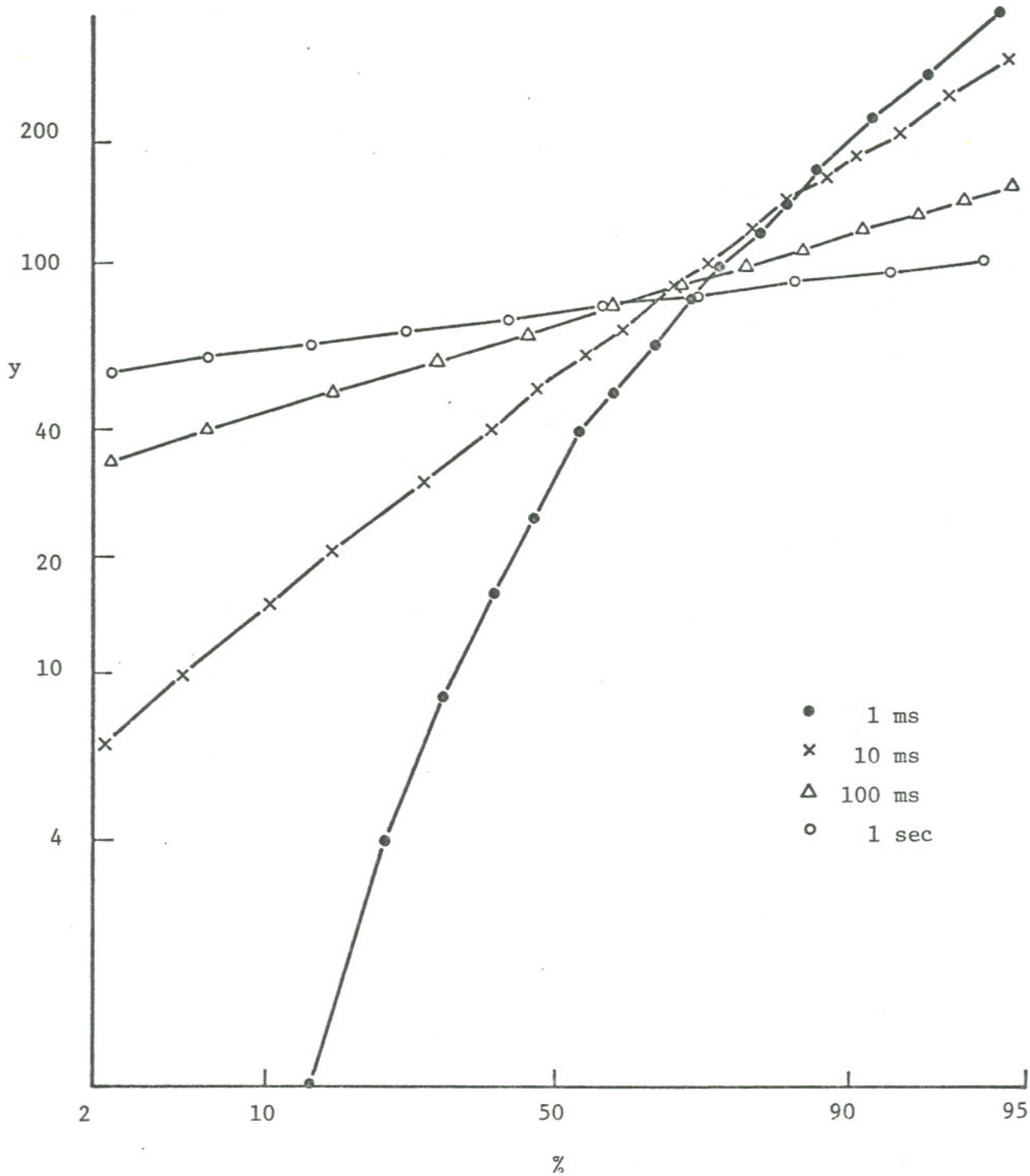

Figure III.7. Cumulative probability distribution functions of $(\text{Log } I)^2_\tau$ for data of Figure III.6.

there is little apparent difference between a lognormal distribution of very small variance, as in the case of the one second averaged square log irradiance fluctuations, and a normal distribution. Thus, in Figure III.8 showing the K-S diagram for these distributions, we see that for one second averaging, the parameters indicate agreement with those of a normal distribution. Note specifically the different scale for the kurtosis in this figure from the scale used in Figure II.12, for the squared temperature fluctuations. Here we see a much faster approach toward a normal distribution with increasing averaging time.

III.4c. Level Crossing and Conditional Probability

A further topic of interest regarding the statistical properties of the received optical signal is that of conditional statistics and level crossing. In terms of the irradiance fluctuations, we can state one practical problem as follows: given that the intensity of the received signal is equal to or greater than some given level Y_o at a time t_o, what is the probability distribution of the intensity at some time later, $t_o + \tau$. One particular application of the results of this problem might involve 'probing' the communication channel with an optical beam to determine when the channel is 'open', that is when the received signal is above some acceptable threshold level. In the 'open' condition, then, the channel is used to transmit a burst of information. Knowledge of the marginal probability density described above would allow prediction of the reliability versus use rate for such transmission.

The level crossing problem has been treated theoretically in detail (Rice 1954, and Blake and Lindsey 1973) specifically with regard to two general classes of random processes, Markov and Gaussian. (A Gaussian process is one for which for all n, the n-dimensional probability distribution function is an n-dimensional normal.) Doob (1953) defines, operationally, a Markov process as follows: a process χ_t is Markov in the wide sense if and only if the expectation value of $|\chi_t|^2$ is finite and the correlation function C satisfies the relation

$$C(r,t) = C(r,s)C(s,t) \quad r<s<t \qquad \text{(III.1)}$$

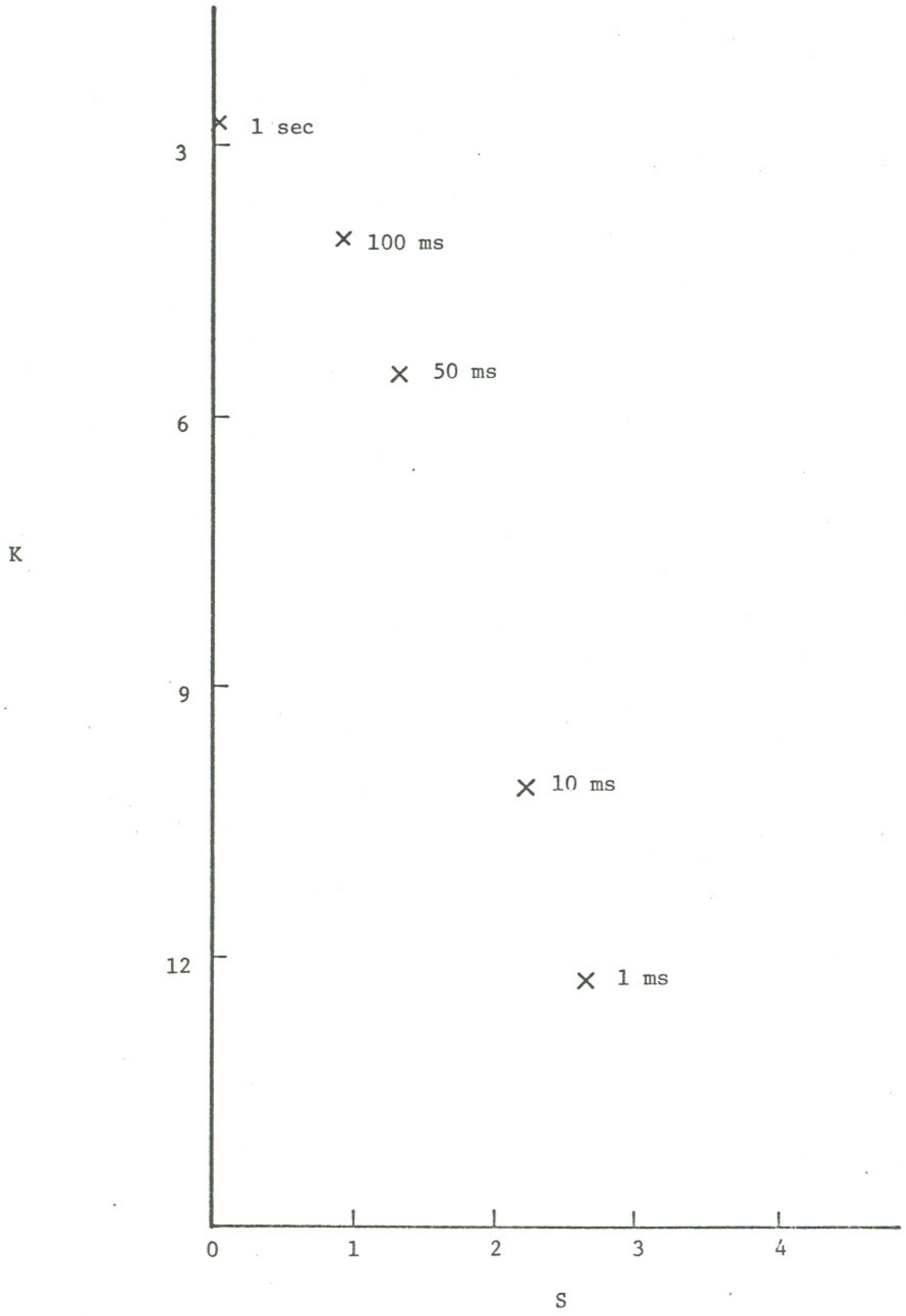

Figure III.8. Plot of S versus K for distributions of $(\ln(I))^2_\tau$ for τ between 1 ms and 1 sec.

If the process is real and stationary, this requires

$$C(t_o + t_1) = C(t_o)C(t_1). \tag{III.2}$$

Thus

$$C(\tau) = C(0) \exp(-c\tau). \tag{III.3}$$

The correlation functions of the log irradiance fluctuations are not of the exponential form, and thus we may conclude that these fluctuations are not Markoffian. We thus investigate the multidimensional probability distributions limiting our work here to the two point distributions which from a practical standpoint are most important. We have seen that under low turbulence conditions at least, the one point distributions of the log irradiance fluctuations are normal. Let us assume then that the two point or joint probability distribution is a bivariate normal. Thus

$$P(y(t),y(t+\tau)) = \frac{1}{2\pi\sigma_o (1-\rho(\tau)^2)^{1/2}} \exp\left\{-\frac{1}{2\pi\sigma_o^2 (1-\rho(\tau)^2)}\right.$$
$$\left.[y(t)^2-2\rho(\tau)y(t)y(t+\tau)+y(t+\tau)^2]\right\} \tag{III.4}$$

where $y(t)$ is the log irradiance fluctuation, a normally distributed random variable with zero mean, variance σ_o^2 and autocorrelation function

$$\rho(\tau) = \frac{\langle y(t)y(t+\tau)\rangle}{\sigma_o^2} \tag{III.5}$$

The conditional distribution of $y(t)$, the probability distribution of $y(t+\tau)$ given that $y(t) = Y_o$ is then

$$P(y(t+\tau)|y(t) = Y_o) = \frac{1}{2\pi\sigma_o(1-\rho^2)^{1/2}} \exp\left\{-\frac{1}{2\pi\sigma_o^2 (1-\rho^2)}\right.$$
$$\left.[y(t+\tau)-\rho(\tau)Y_o]^2\right\} \tag{III.6}$$

which is in fact a Gaussian distribution with a mean equal to $\rho(\tau)Y_o$ and a variance of $\sigma_o^2 (1-\rho(\tau)^2)$.

We have measured conditional distributions of the log irradiance fluctuations over a range of turbulence levels. For each experimental run, autocorrelation functions and conditional distributions for a number of different values of Y_o and τ were calculated. We point out that for each run, 400,000 data points sampled at one millisecond intervals were employed in the calculation. Table 1 indicates the turbulence conditions of the different experimental runs under consideration here. The correlation functions calculated for three of the runs analyzed here were shown in Figure III.4. Figure III.9 shows examples of the conditional distributions calculated for one of the low turbulence cases, in this case the log amplitude variance, $\sigma_\chi^2 = 0.0015$. Again the solid lines in the figure indicate normal distributions with the same means and variances as the experimental distributions. The values of the skewness and kurtosis for the conditional distributions of this low turbulence condition are given in Table 2. Here Y_o is the given threshold level (intensity) normalized by the standard deviation of the single point probability distribution. These values confirm the general qualitative agreement of the experimental distributions with Gaussian distributions seen in the figure. Finally we compare the observed mean and variance of the observed conditional distributions with those calculated from the assumption of the joint distribution being a bivariate Gaussian. Table 3 shows this comparison for the same low turbulence case. Again the values of Y_o and the calculated means and variances have been normalized by the standard deviation of the one dimensional distribution. Here we see excellent agreement between the observed and predicted values indicating that the assumption that the log irradiance fluctuations are 'Gaussian', may be valid. It should be emphasized that we cannot prove that the fluctuations are Gaussian to all orders, but merely that our observations are not inconsistent with this assumption.

We next investigate a higher turbulence case, $\sigma_\chi^2 = 0.14$. Again the distributions appear qualitatively Gaussian, and the skewness and kurtosis parameters of the conditional distributions seen in Table 4

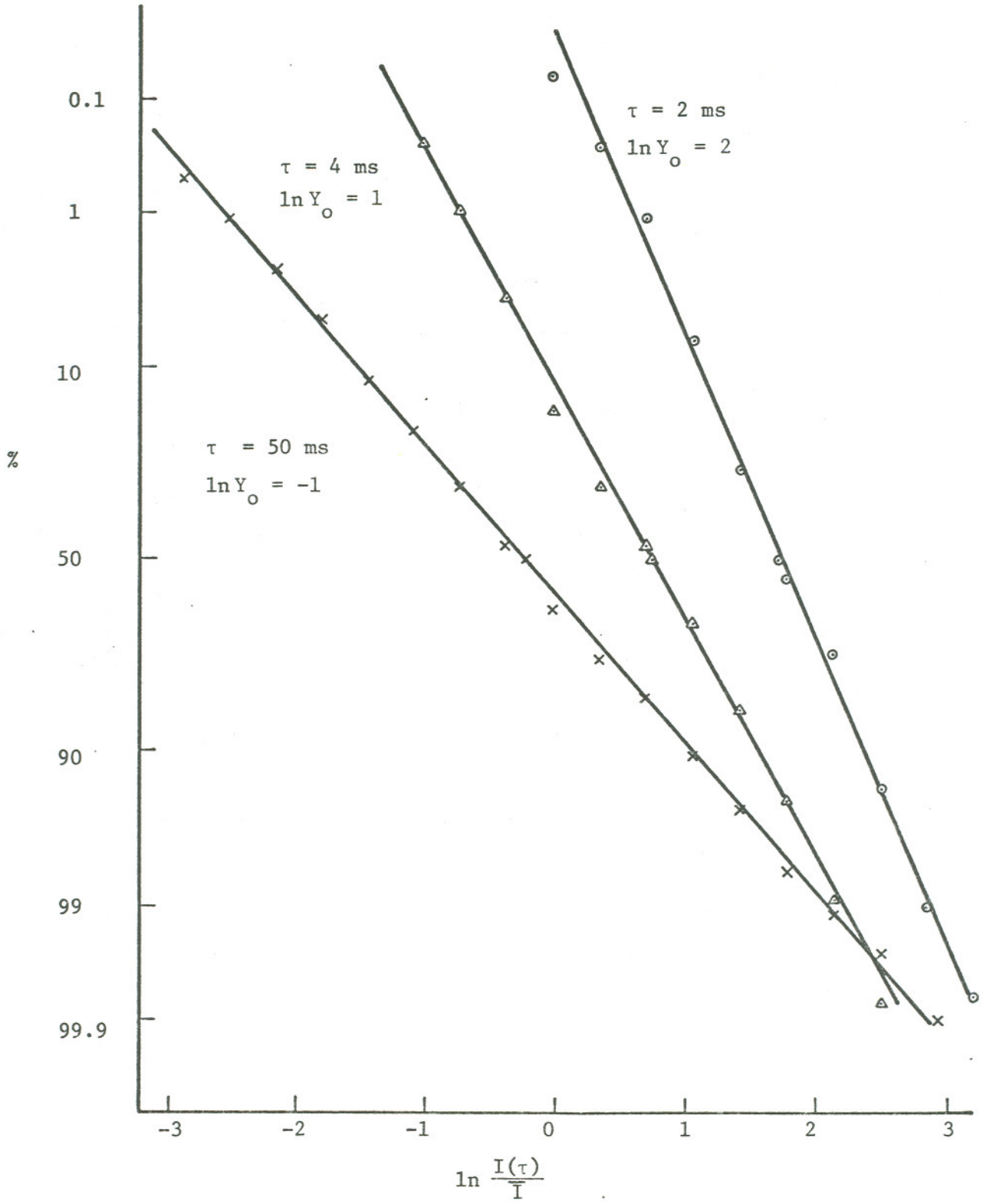

Figure III.9. Conditional probability distribution functions of normalized log irradiance fluctuations.

Table 1

Run	C_n^2 ($m^{-2/3}$)	Mean Wind Speed (meters/sec)	σ_χ^2	Optical Wavelength (Microns)
1	0.4×10^{-14}	9	0.0015	10.6
2	0.14×10^{-13}	3.5	0.010	10.6
3	0.4×10^{-14}	9	0.076	0.488
4	0.17×10^{-12}	1.5	0.14	10.6
5	0.59×10^{-12}	1	0.307	10.6

Table 2

Skewness (S) and Kurtosis (K) of $Pr(\chi(t+\tau)|\chi(t))$ for Run 3

S

$\frac{Y_o}{\sigma_o}$ \ τ(ms)	1	2	4	8	16
-1	.29	.13	.2	.022	.012
0	.03	.051	.056	.061	.068
1	-.12	-.017	.01	.13	-.055
2	-.0039	.047	.0080	-.0065	-.036

K

$\frac{Y_o}{\sigma_o}$ \ τ(ms)					
-1	4.2	3.59	3.83	3.29	3.18
0	3.20	3.16	3.089	3.05	3.04
1	3.27	3.21	2.69	2.77	3.17
2	2.83	2.84	2.95	2.98	3.08

Table 3

Comparison of Predicted and Observed $\frac{\text{Variance}}{\sigma_o^2}$ of Pr $\frac{\chi(t+\tau)}{\sigma} \quad \frac{\chi(t)}{\sigma_o} = Y_o$

For Run 3

$\frac{Y_o}{\sigma_o}$ \ τ(ms)		2	4	8	16
-1	Pred.	0.243	0.392	0.675	0.942
	Obs.	0.239	0.414	0.651	0.936
0	Pred.	0.243	0.392	0.675	0.942
	Obs.	0.236	0.406	0.686	0.961
1	Pred.	0.243	0.392	0.675	0.942
	Obs.	0.278	0.402	0.77	1.01
2	Pred.	0.243	0.392	0.675	0.942
	Obs.	0.254	0.439	0.765	0.99

Comparison of Predicted and Observed Mean of Pr $\frac{\chi(t+\tau)}{\sigma_o} \quad \frac{\chi(t)}{\sigma_o} = Y_o$

For Run 3

-1	Pred.	-0.87	-0.78	-0.57	-0.24
	Obs.	-0.89	-0.75	-0.60	-0.24
0	Pred.	0	0	0	0
	Obs.	-0.016	-0.016	-0.001	0.008
1	Pred.	0.87	0.78	0.57	0.24
	Obs.	0.85	0.72	0.50	0.21
2	Pred.	1.74	1.56	1.14	0.48
	Obs.	1.70	1.51	1.09	0.45

Table 4

Skewness

$\frac{Y_o}{\sigma_o}$ \ τ(ms)	2	4	8	16
-.92	9×10^{-4}	0.075	0.193	0.13
-.04	0.013	0.085	.055	0.107
1.07	0.048	0.074	0.048	0.06
2.03	-2.6×10^{-3}	-6.6×10^{-3}	-3.6×10^{-3}	0.013

Kurtosis

$\frac{Y_o}{\sigma_o}$ \ τ(ms)				
-.92	3.06	3.81	2.4	4.04
-.04	3.27	3.59	3.69	3.39
1.07	3.4	3.19	3.02	3.2
2.03	2.96	2.78	2.68	2.95

generally support this assertion. A comparison of observed and predicted variances of these distributions, Table 5, however shows large deviations of the measured variances from the variances expected assuming a 'Gaussian' process. In fact, the root mean square error between the observed and predicted variances in this case is 0.13, an average 13% error. Table 6 shows results of root mean square error calculations for the other experimental runs. The high turbulence cases ($\sigma_\chi^2 > 0.1$) for this sample show significantly higher deviations from the joint Gaussian behavior than the low turbulence cases.

More detailed error analysis appears to confirm the non-Gaussian behavior in the high turbulence cases. Eq. 18 describes the expected statistical error in a finite time measurement of the variance of a process. In this equation, $2T_2/\tau$, the integral scale divided by the observation time may be interpreted as the inverse of the number of uncorrelated samples in the data. In the above measurements we have in fact much fewer than the original 400,000 data points because of the conditional sampling. We might then modify Eq. (18) to account for the conditional sampling. This may be accomplished by changing τ, the total sampling time to reflect the number of samples actually used in the calculation. When this is done, the analysis in the low turbulence cases shows the observed variances to be within the probable statistical error of the variance predicted for a Gaussian process. In the high turbulence cases the results clearly indicate the deviations are, particularly for large values of Y_o, greater than the probable error. This would indicate non-Gaussian behavior of the unsaturated log intensity fluctuations under conditions of high turbulence.

III.5. Conclusion

In the previous sections we have presented the results of a basic statistical analysis of the observed fluctuations in the log irradiance of an optical wave which has propagated through the turbulent atmosphere. The qualitative picture that arises, at least from the low turbulence results, is that this random process is in a physical sense, a well behaved random process. It is for practical purposes normally distributed (a Gaussian process under very low turbulence conditions) with a correlation function which decays smoothly to zero in a time short compared to aver-

Table 5

Comparison of Predicted and Observed $\frac{\text{Mean}}{\sigma_o}$ of $P(x(t+\tau)|x(t) = Y_o)$

$\frac{Y_o}{\sigma_o}$ \ τ (ms)		2	4	8	16
-.92	Pred.	-.856	-.761	-.544	-.215
	Obs.	-.869	-.77	-.547	-.20
-.04	Pred.	.037	.033	.024	-.0094
	Obs.	4×10^{-3}	.033	.051	.01
1.07	Pred.	.995	.885	.632	.250
	Obs.	1.00	.896	.626	.248
2.03	Pred.	1.89	1.67	1.19	.475
	Obs.	1.87	1.54	.962	.314

Comparison of Predicted and Observed $\frac{\text{Variance}}{\sigma_o^2}$ of $P(x(t+\tau)|x(t) = Y_o)$

-.92	Pred.	.134	.32	.651	.945
	Obs.	.101	.314	.679	.94
-.04	Pred.	.034	.32	.651	.945
	Obs.	.088	.255	.615	.96
1.07	Pred.	.134	.32	.651	.945
	Obs.	.19	.47	.80	1.00
2.03	Pred.	.134	.32	.651	.945
	Obs.	.268	.603	.95	.99

Table 6

Run	σ_x^2	RMS Error
1	0.0015	0.04
2	0.010	0.037
3	0.070	0.027
4	0.14	0.13
5	0.307	0.11

aging times of practical interest. In the next chapter we specifically investigate the effects of short time averaging on a measure of this process, the variance, and the relationships between this variance and the atmospheric parameters.

CHAPTER IV.

IV.1. Introduction

In the previous two chapters, certain statistical characteristics of the random processes describing atmospheric temperature fluctuations and amplitude scintillation of an optical electromagnetic wave propagated through atmospheric turbulence have been presented. In this chapter we discuss with further experimental results, the relationship between these two random processes. We begin with the relationship between the measures of the intensity of these random processes, their variance, C_n^2 characterizing the atmospheric turbulence and σ_χ^2, the received optical field. Data spread in the short time averaged measurements of these characteristics is then presented and finally, the relationship between the observed data spreads in C_n^2 and σ_χ^2 is discussed.

IV.2. Experimental Observation of the Relationship Between σ_χ^2 and C_n^2

Equations (I.5) and (I.6) give the relationship, under conditions of low path integrated turbulence, of measurements of the log amplitude variance, σ_χ^2, and the index of refraction structure parameter C_n^2. These equations were derived with the assumption of ensemble or equivalently, long time averaging in the measurement of these variables. Figure IV.1 shows the results of relatively long time averaging, on the order of 10 minutes, on the measurements of σ_χ^2 and C_n^2. In this figure, σ_m^2 is the measured log amplitude variance (one quarter of the variance in the logarithm of the intensity of the optical signal) and σ_t^2 is the log amplitude variance predicted by Eq. (I.5) using the long time averaged value of C_n^2 measured at a point near the receiver. These experiments were performed on the 1.6 kilometer propagation facility described in Section III.3. In the figure, the open circles indicate data from the CO_2 laser with a wavelength of 10.6 microns and the solid circles are data from the Argon ion laser at 0.488 microns.

The straight line in the figure shows the expected linear relationship under low turbulence conditions between σ_χ^2 and C_n^2. Excellent agreement is observed between the measured and predicted variances in the low turbulence region below $\sigma_\chi^2 = 0.3$. We note the saturation effect of the log amplitude variance mentioned earlier for nearly all the data taken at the visible wavelength. It should be noted that the only requirement for

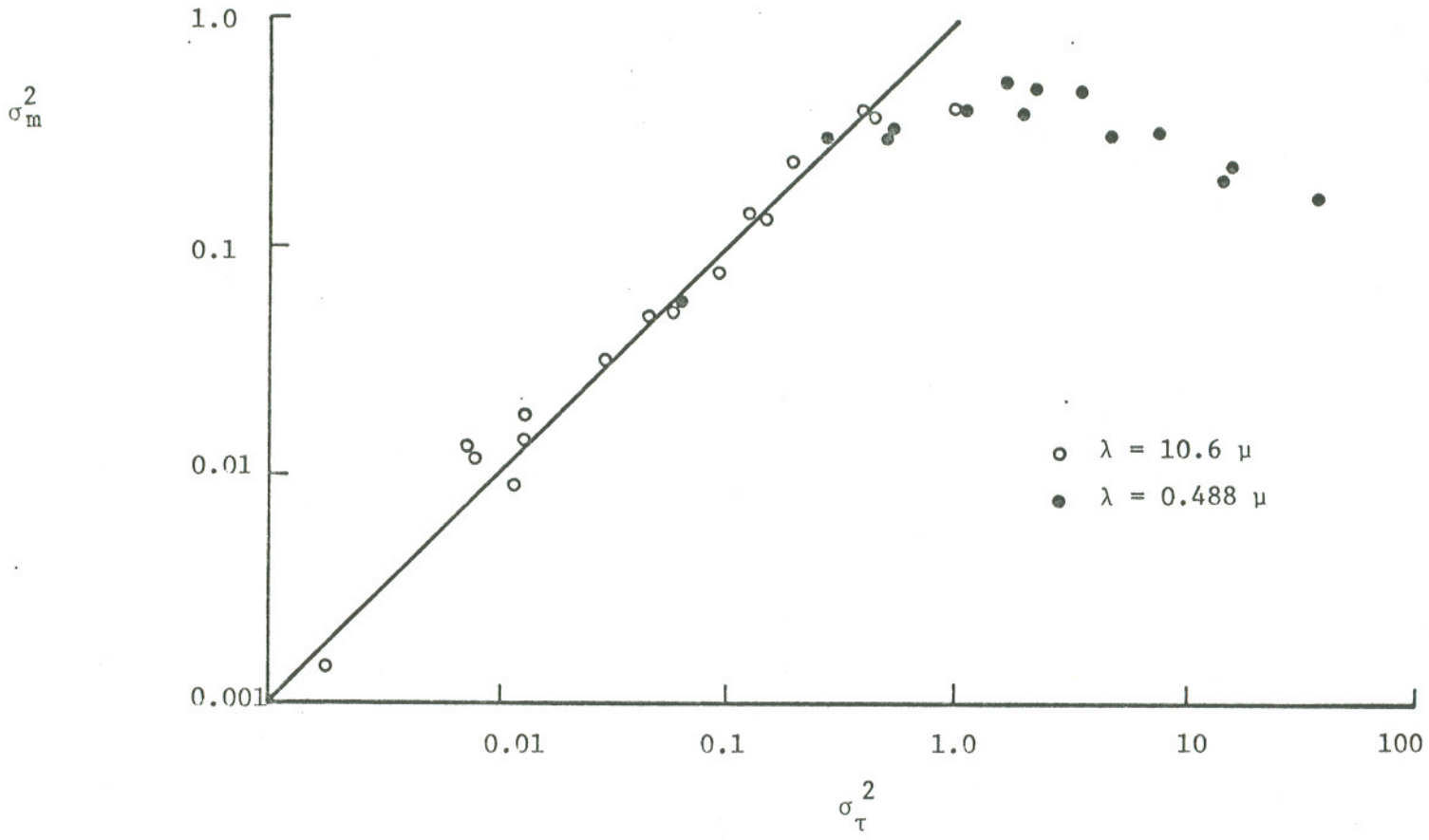

Figure IV.1. σ_m^2 versus σ_τ^2 for long averaging times.

selecting this data was that the sky cover was homogeneous during the experimental run, i.e., a clear sky or a uniform cloud cover in the absence of rain. Partially cloudy conditions generally produce data with very large fluctuations in the measured parameters dependent on such difficult-to-measure factors as the percentage of the sky covered by clouds and the motion of the clouds as they block the sun over the path. In these cases, extremely long averaging times would be necessary to yield data with the appearance of stationarity.

The results of Figure IV.1 are of interest primarily in that they show experimentally that with practical averaging times, the measurements agree quite well with the theoretical predictions. Of particular interest here however, are the effects on these same measurements of much shorter averaging times, of the order of seconds. Figure IV.2 shows the same data from the 10.6 micron laser as in Figure IV.1 for which the total observation time has been broken into successive short time averaging periods, in this case 10 second intervals, in each of which $(\sigma_m^2)_\tau$ and $(\sigma_t^2)_\tau$ were calculated. The mean and the standard deviation of the short time measurements were then calculated. The crossing point of the 'error bars' in the figure gives the mean value of the short time measurements, and the length of the bar on either side of the mean is equal to the standard deviation of the short time measurements. The means of the short time measurements are of course in exact agreement with the long time averages seen in Figure IV.1. The fluctuations in short time measurements of σ_t^2 are again due to fluctuations in short time averaged measurements of C_n^2. We indicate short time measurements of the variance from here on as $(\sigma_\chi^2)_\tau$ and $(C_n^2)_\tau$.

Figure IV.2 shows the possibilities of very large relative data spreads (standard deviation/mean $\equiv$ R) in the short time measurements, especially for $(C_n^2)_\tau$. In the past a number of authors have commented on the large data spreads observed in short time measurements of optical propagation variables. In particular, Kerr (1972) suggests that under poorly developed turbulence conditions (generally very low wind speed situations) deviations from the Kolmogorov spectrum of the turbulence may contribute to the data spreads observed in the optical measurements. Kleen and Ochs (1970) indicate that in well developed turbulence, for wind speeds greater than 2 meters per second, the effect of turbulence spectrum variations is minimal compared to the fluctuations in the turbulent inten-

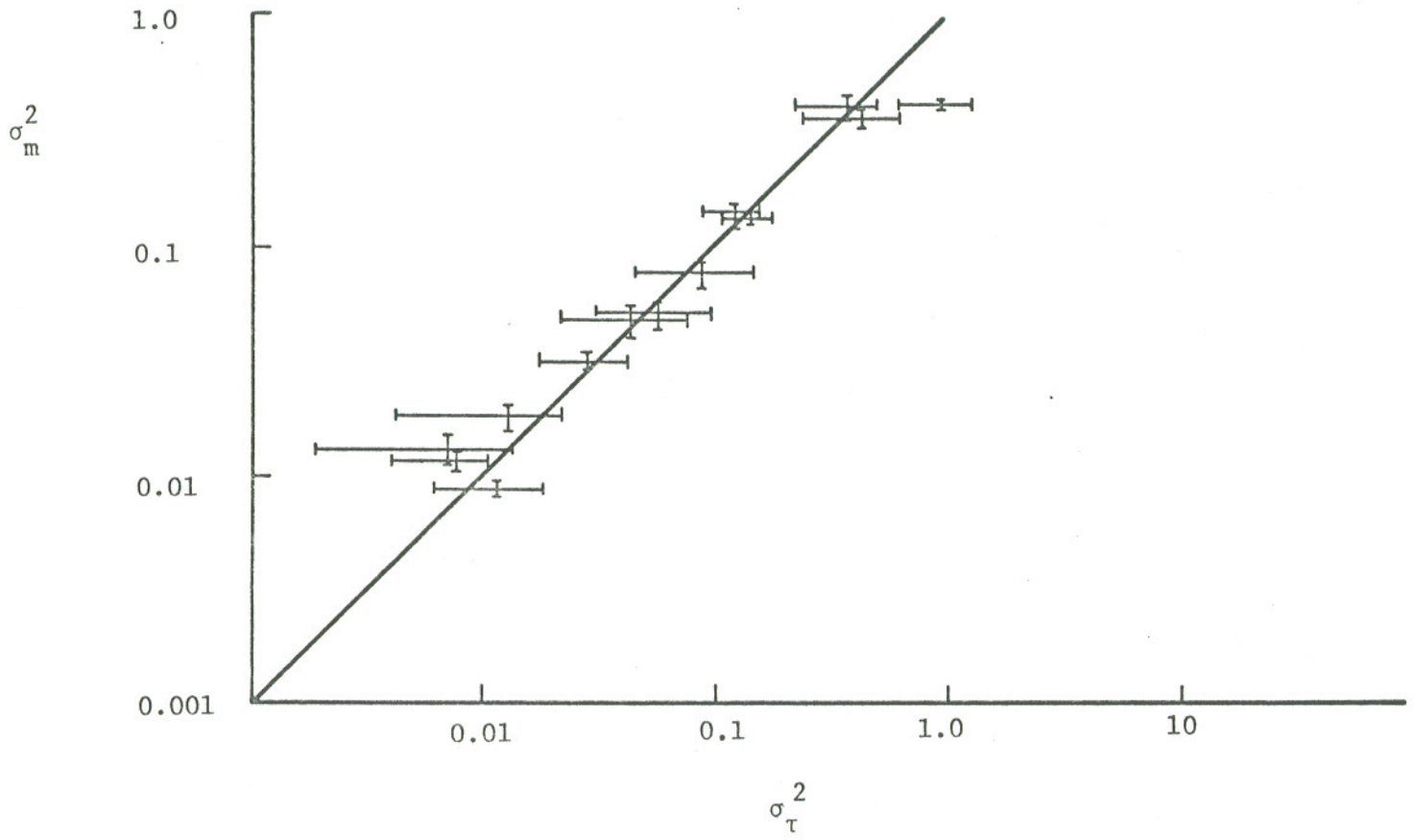

Figure IV.2. σ_m^2 versus σ_τ^2 for 10 second averaging time, including an indication of the data spread. λ = 10,6 microns.

sity, C_n^2, in contributing to the spread in the optical measurements.

IV.3. $(C_n^2)_\tau$

Before proceeding, we define specifically what is meant by short term averaging, particularly in regard to C_n^2. The definition of C_n^2 comes from the expression of either the structure function or the spatial spectrum of the index of refraction fluctuations, where C_n^2 is a coefficient of some power law dependence (see Eq. (II.5)). In practice we generally measure one point on the structure function of the temperature fluctuations with the spatial separation within the limits of the inner and outer scales of the turbulence. Thus

$$C_n^2 = D_n(r_o)/r_o^{2/3}$$

$$= \langle (T(r) - T(r+r_o))^2 \rangle / r_o^{2/3} \qquad \text{(IV.1)}$$

In order to write this expression or the equivalent spectral definition, it must be assumed that the measurement of the structure function is averaged over a scale size larger than the bounds of the inertial subrange. To be physically meaningful, the spatial averaging of C_n^2 must be over a scale greater than the outer scale, L_o, or equivalently, time averaging of a localized measurement must be greater than $\tau = (L_o/U)$ where U is the mean wind speed. For our experimental site, the outer scale should be of the order of one meter, and thus for wind speeds greater than one meter per second, time averaging of the microthermal measurements of the order of one second should yield physically meaningful values of short time averaged C_n^2.

IV.4. Characteristics of Data Spread

We now consider some of the properties of the spread observed in the short term C_n^2 measurements. Figure IV.3 is a plot of the normalized standard deviation of $(C_n^2)_\tau$ for τ = 10 seconds versus the mean value of C_n^2 obtained from long time average. We would expect that assuming no bias in the selection of the data, the data spread should be independent of the turbulence level. In fact, the data of Figure IV.3 visually confirms the independence of R and C_n^2, and a simple linear regression analysis of R on log (C_n^2) from this data yields the equation

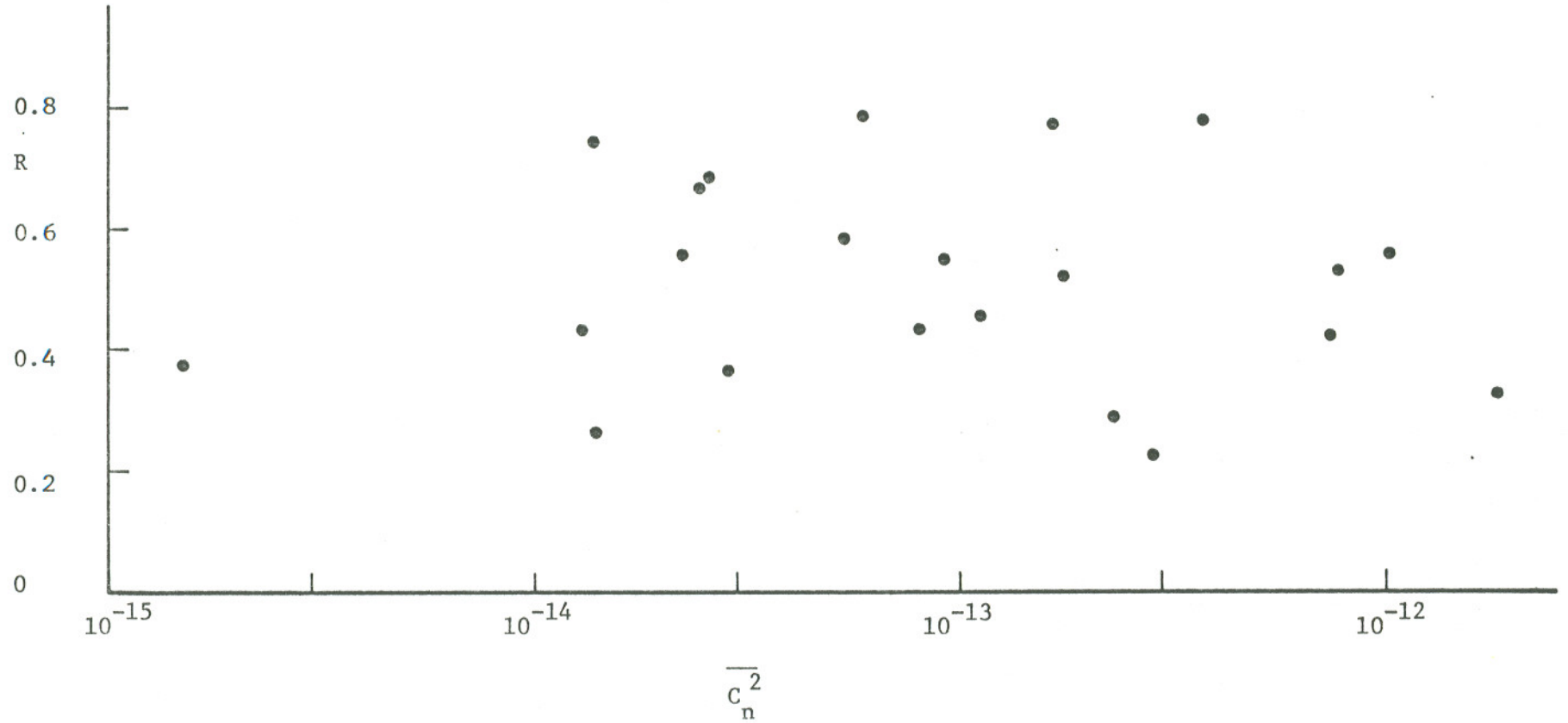

Figure IV.3. Normalized standard deviation of $(C_n^2)_{\tau=10\ sec}$ = R versus $\overline{C_n^2}$.

$$R = -0.013 \log C_n^2 + .50 \qquad \text{(IV.2)}$$

with a correlation coefficient of -0.06, giving a dependence of approximately 1% per decade change in C_n^2. This is within experimental error of a zero slope which would describe a uniform distribution of data spread with C_n^2.

Non trivial dependence of the spread in $(C_n^2)_\tau$ occurs in its relationships to the wind speed and the averaging time. Let us assume for the moment that the profile of $(C_n^2)_\tau$ over some area has some given 'frozen' spatial structure, that is we might assume that the Taylor frozen flow hypothesis be valid over distances much larger than the outer scale. A point measurement over some short averaging time will then 'see' some portion of the spatial profile of $(\Delta T_{12})^2$ blown by the sensor with the mean wind speed. As the wind speed increases, with a given structure of $(C_n^2)_\tau$, more of that structure will be seen by the sensor and consequently the deviations in short time measurements should decrease. Of course the Taylor hypothesis is not strictly valid over very large distances and the spatial structure is certainly dependent on wind speed; nonetheless, we expect a decrease in data spread with wind speed for a given averaging time. Figure IV.4 is a plot of the data spread in 10 second measurements of $(C_n^2)_\tau$ again indicated by the normalized standard deviation of the measurements versus the mean wind speed, U. While there is a great deal of scatter in the data, a linear regression analysis of $\log \left(\dfrac{\text{Var } C_{n_\tau}^2}{\overline{C_n^2}^2} \right)^{1/2}$ versus log (U) yields

$$\log\left(\frac{\text{Var}(C_n^2)_\tau}{\overline{C_n^2}^2}\right)^{1/2} = -1.01 \log \bar{U} + 0.053 \qquad \text{(IV.3)}$$

with a correlation coefficient of 0.59. Taking the antilog of Eq.(IV.3) gives

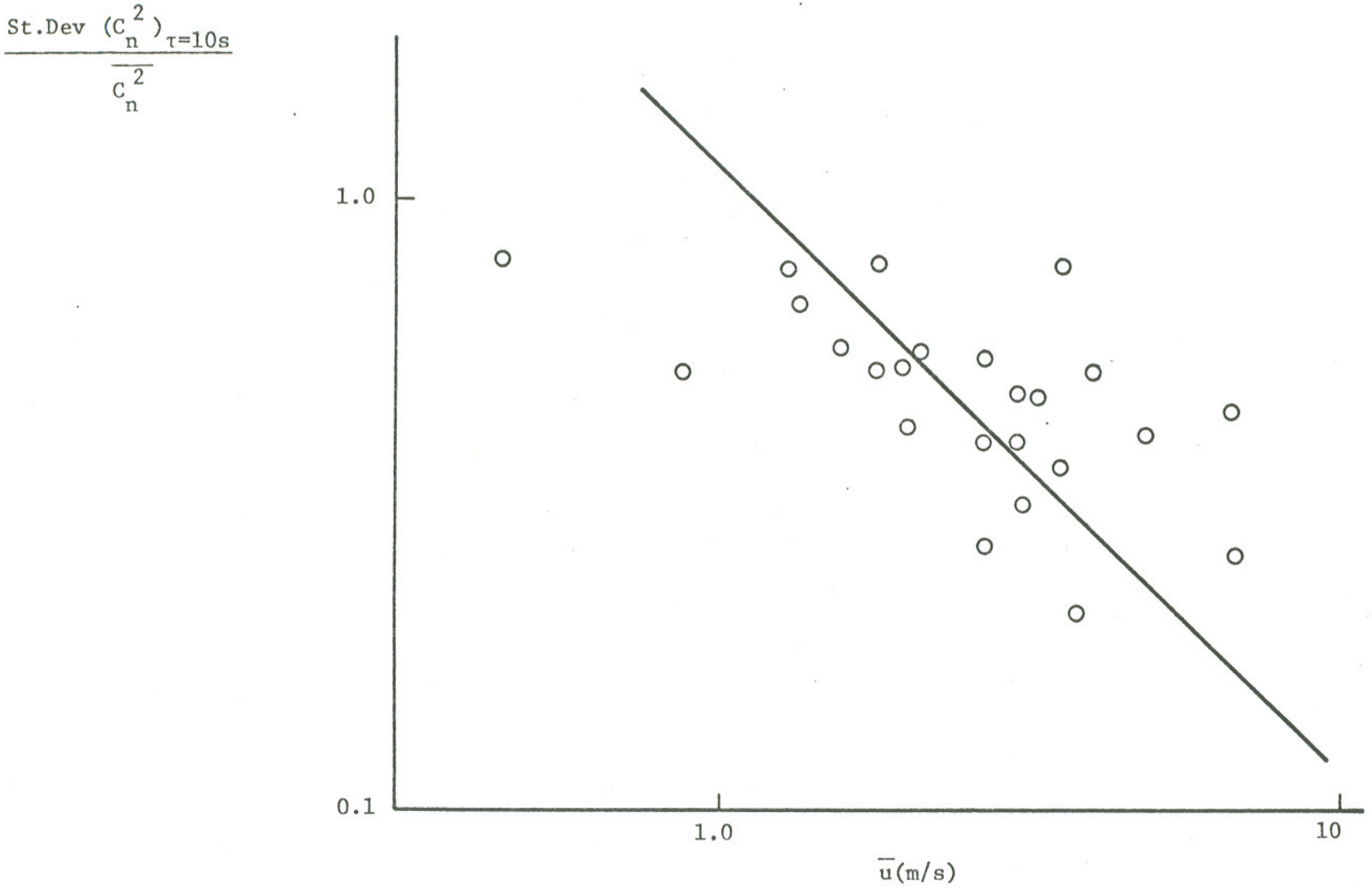

Figure IV.4. Normalized standard deviation of $(C_n^2)_{\tau = 10 \text{ sec}}$ versus mean wind speed $\overline{u}$. The straight line is a linear least square regression line to the data.

$$\left(\frac{\text{Var } (C_n^2)_\tau}{\overline{C_n^2}^2} \right)^{1/2} \approx \frac{1.13}{V} \qquad \text{(IV.4)}$$

As described in Section II.4b the averaging time dependence of the variance of a set of short time measurements of the second moment of a process y(t) for averaging times, τ, long compared to the integral scale T_2 of the square process $y^2(t)$ is given by

$$\frac{\text{Var } (y^2)_\tau}{\overline{y^2}^2} = \frac{2(K-1)T_2}{\tau} \qquad \text{(IV.5)}$$

where K is the kurtosis of y(t). Figures IV.5 and IV.6 show measurements of the data spread in $(C_n^2)_\tau$ and $(\sigma_\chi^2)_\tau$ respectively versus averaging time for a number of atmospheric conditions over a range of averaging times between 0.4 and 30 seconds. The wind conditions associated with each data run are listed in Table 7. In both figures, the slopes of the curves of log (normalized variance) versus the log (τ) range from near zero to a value of -1 for long averaging times in agreement with Eq. (IV.5). This range of behavior will be further discussed below.

IV.5. Analytical Relationship Between Data Spreads in $(\sigma_\chi^2)_\tau$ and $(C_n^2)_\tau$

In this section we describe the relationship between the observed data spreads measured in short term averaged $(C_n^2)_\tau$ and $(\sigma_\chi^2)_\tau$ described above and seen in Figure IV.b. We begin by rewriting Eq. (I.6) relating ensemble values of the indicated variances as

$$\langle \sigma_\chi^2 \rangle = \int_0^L d\eta \, f(\eta) \langle C_n^2(\eta) \rangle \qquad \text{(IV.6)}$$

where $f(\eta)$ is a general path weighting function dependent on the propagating beam geometry, given specifically for point source propagation in Eq.

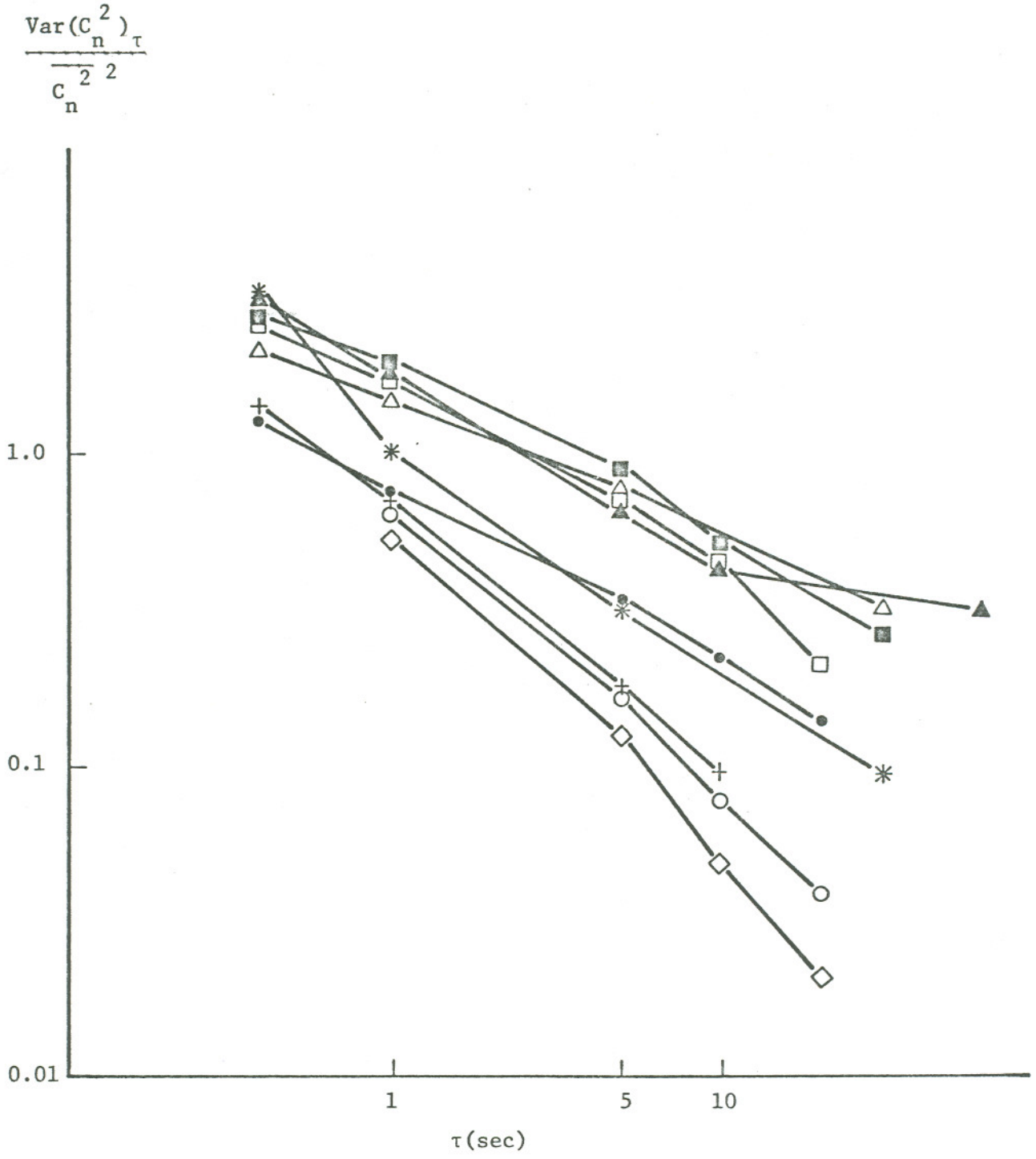

Figure IV.5. Normalized variance of $(C_n^2)_\tau$ versus τ.

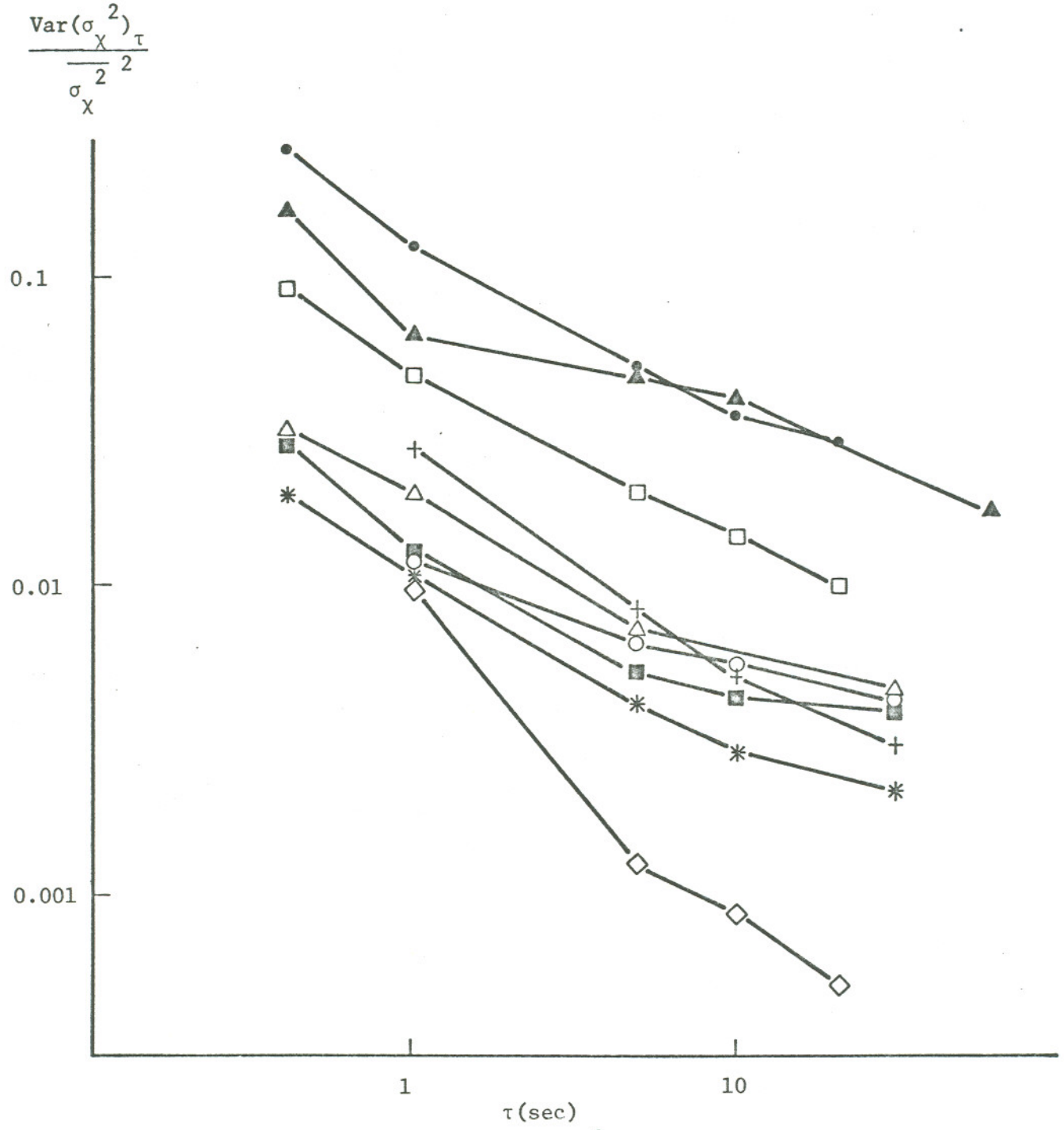

Figure IV.6. Normalized variance of $(\sigma_\chi^2)_\tau$ versus τ.

Table 7

Data Run	Symbol	$\overline{V}$ (m/sec)	Wind Direction Relative to N-S Optical Path	$\overline{C_n^2}$ ($m^{-2/3}$)
A	O	3.5	0°-S	1.89×10^{-12}
B	□	<1	0°-S	0.59×10^{-12}
C	◇	3	0°-S	2.9×10^{-13}
D	△	3.5	0°-N	1.5×10^{-14}
E	+	9	∿15°-S-SE	4.0×10^{-13}
F	*	3.5	∿15°-N-NE	1.37×10^{-14}
G	●	4	∿45° SE	2.1×10^{-13}
H	▲	0.5-2	90° W	3.2×10^{-13}
I	■	1.5	90° W	1.7×10^{-13}

(I.6). This equation is rewritten again where it is now assumed that the relationship holds for short time averaged measurements of $(C_n^2)_\tau$ and $(\sigma_\chi^2)_\tau$ described above. Thus

$$(\sigma_\chi^2)_\tau = \int_0^L d\eta\, f(\eta)(C_n^2(\eta))_\tau \qquad \text{(IV.7)}$$

The viewpoint adopted here is that the path is considered to be a homogeneous field with regard to $\langle C_n^2 \rangle$, but that $(C_n^2)_\tau$ is dependent on η the position along the path due to the averaging time used in the measurement of the structure parameter being smaller than some time scale of significant fluctuations of C_n^2.

One now considers that a large number of measurements of $(\sigma_\chi^2)_\tau$ and $(C_n^2)_\tau$ at some point along the path are made. The average of these individual measurements, being in a sense an ensemble average, will yield results described by Eq. (IV.6), as evidenced by Figure IV.2. The spread in the data will be described by the normalized variance or standard deviation of the short time measurements. Starting with Eq. (IV.7) one calculates the variance of $(\sigma_\chi^2)_\tau$

$$\mathrm{Var}(\sigma_\chi^2)_\tau = \langle(\sigma_\chi^2)_\tau^2\rangle - \langle(\sigma_\chi^2)_\tau\rangle^2$$

$$\mathrm{Var}\,(\sigma_\chi^2)_\tau = \int_0^L\int_0^L d\eta_1 d\eta_2\, f(\eta_1)f(\eta_2)\left\{\langle(C_n^2(\eta_1))_\tau(C_n^2(\eta_2))_\tau\rangle\right.$$

$$\left. -\langle C_n^2(\eta_1)\rangle\langle C_n^2(\eta_2)\rangle\right\} \qquad \text{(IV.8)}$$

With the assumption of long term homogeneity, and defining a normalized spatial correlation function of short time averaged $(C_n^2)_\tau$ as

$$C_{C_n^2}(\eta_1-\eta_2) = \frac{\langle(C_n^2(\eta_1))_\tau(C_n^2(\eta_2))\rangle - \langle C_n^2\rangle^2}{\mathrm{Var}\,(C_n^2)_\tau} \qquad \text{(IV.9)}$$

one finds that the normalized variance in measurements of the log amplitude variance is given by

$$\frac{\mathrm{Var}\,(\sigma_\chi^2)_\tau}{\langle\sigma_\chi^2\rangle^2} = \frac{\mathrm{Var}\,(C_n^2)_\tau}{\langle C_n^2\rangle^2} \frac{\int_0^L\int_0^L d\eta_1 d\eta_2\, f(\eta_1) f(\eta_2) \mathbf{C}_{C_n^2}(\eta_1-\eta_2)}{\left[\int_0^L d\eta f(\eta)\right]^2} \qquad \text{(IV.10)}$$

Thus the observed data spread in the optical measurements (normalized variance of $(\sigma_\chi^2)_\tau$) should be directly related to the observed spread in the measurements of $(C_n^2)_\tau$ (normalized variance of $(C_n^2)_\tau$) times a factor related to the spatial correlation of $(C_n^2)_\tau$ along the propagation path and the specific beam geometry. Before presenting measurements of the spatial correlation function and application of Eq. (IV.10), a simplified, but useful approximation to this equation is described.

IV.6. Discrete Model of Path-Data Spread

Let the propagation path be broken into a number of discrete slabs of turbulent activity. Within each slab $(C_n^2)_\tau$ has a constant value over the slab, and the correlation between $(C_n^2)_\tau$ measured in any two different slabs is assumed to be zero. Thus in equation (IV.10) the integrals over the path are replaced by summations over N discrete slabs along the path and the correlation function $\mathbf{C}_{C_n^2}(\eta_1-\eta_2)$ is replaced by a Kronecker delta yielding

$$\frac{\mathrm{Var}\,(\sigma_\chi^2)_\tau}{\langle\sigma_\chi^2\rangle^2} = \frac{\mathrm{Var}\,(C_n^2)_\tau}{\langle C_n^2\rangle^2} \frac{\sum_{i=1}^{N}\sum_{j=1}^{N} f_i f_j \delta_{ij}}{\left(\sum_{i=1}^{N} f_i\right)^2} \qquad \text{(IV.11)}$$

$$= \frac{\mathrm{Var}\,(C_n^2)_\tau}{\langle C_n^2\rangle^2} \frac{\sum_{i=1}^{N} f_i^2}{\left(\sum_{i=1}^{N} f_i\right)^2} \qquad \text{(IV.12)}$$

Here f_i is the discretized version of the path weighting function. If we

consider the case of a uniform path weighting function (f_i = constant), the ratio of sums in Eq. (IV.12) is 1/N, and one has the simple, physically intuitive result that the normalized variance of $(\sigma_\chi^2)_\tau$ is equal to the normalized variance of $(C_n^2)_\tau$ reduced by the number of independent slabs of turbulence along the path. For any given physically realizable path weighting function, one has

$$\sum_{i=1}^{N} f_i^2 \Big/ \left(\sum_{i=1}^{N} f_i\right)^2 = 1/N' \qquad \text{(IV.13)}$$

where N' will be less than N, the total number of slabs along the path and thus

$$\frac{\text{Var}\,(\sigma_\chi^2)_\tau}{\langle\sigma_\chi^2\rangle^2} = \frac{\text{Var}\,(C_n^2)_\tau}{\langle C_n^2\rangle^2} \cdot \frac{1}{N'} \cdot \qquad \text{(IV.14)}$$

N' is then the effective number of turbulent slabs along the path which contribute to the decrease in the optical data spread.

This simple physical picture can now be compared with the experimental results. N, the total number of uncorrelated slabs along the path, is equal to L, the path length, divided by twice the correlation length of $(C_n^2)_\tau$ along the path. The correlation length, ℓ_z, will be given by the mean wind speed along the path times the correlation time T_2 of $(C_n^2)_\tau$. For τ, the averaging time long compared to the integral scale of the unaveraged fluctuations of $(C_n^2)_\tau$, Appendix II yields

$$T_2 = \tau/2 \qquad \text{(IV.15)}$$

Thus

$$N = L/(U_z \tau) \qquad \text{(IV.16)}$$

Table 8 gives representative results of the determination of N from Eq. (IV.16) and of N' from measurements of $\dfrac{\text{Var}\,(C_n^2)_\tau}{\langle C_n^2\rangle^2} \Big/ \dfrac{\text{Var}\,(\sigma_\chi^2)_\tau}{\langle\sigma_\chi^2\rangle^2}$ for 10 second averaging time used in the short time variance measurements.

Table 8

Run No.	C_n^2	U_z m/sec	N	N'	N'/N
1	1.3×10^{-14}	5.4	29.6	40	1.38
2	1.8×10^{-13}	0.8	20	29.6	1.4
3	8.3×10^{-14}	2.2	71.4	22.8	.32
4	8.0×10^{-13}	1.8	88.9	61.5	.69
5	1.0×10^{-13}	7.8	20.5	24.2	1.18
6	2.9×10^{-13}	5.0	32.0	12.1	.38
7	1.9×10^{-12}	3.2	50.0	33.0	.66
8	3.9×10^{-13}	1.8	88.9	80	.9
9	1.5×10^{-14}	5.4	29.6	19.0	.64

There is qualitative agreement with the above picture in that N' is of the same order of N, although there is much scatter in the ratio N'/N and in a number of cases, the measured N' exceeds the value of N estimated from Eq. (IV.16), an unphysical result indicating a breakdown in this discrete description, or errors in the measurements, for example, of the mean wind speed along the path.

Onecan also compare the averaging time dependence of N' predicted under the above simple picture with observed results. One must first distinguish two cases depending on the relationship of the wind direction to the path. In the first case, with the mean wind along the path direciton, one expectsthe 'z' or path direction correlation of $(C_n^2)_\tau$ to increase with increasing averaging time. Thus $N = \frac{L}{U\tau}$ as in Eq. (IV.16). N' from Eq. (IV.13) will then decrease essentially as $1/\tau$. Figure IV.7 is a plot of $1/N'$ calculated from Eq. (IV.13) versus the averaging time for data taken with the wind along the path. Again the symbols refer to the conditions listed in Table IV.1. In all cases but one as the averaging time increases beyond 5 seconds there is an increase of $1/N'$ with increasing averaging time, in qualitative agreement with the above discrete model.

In the second case the wind is transverse to the path. Under this condition one wouldnot expect the 'z' (path) correlation length of $(C_n^2)_\tau$ to be dependent on τ, for τ much greater than L_o/U. This is because the effective spatial averaging will be along the same direction as the wind, in this case, transverse to the direction along which the spatial correlation is measured. Thus the z correlation length and N should be relatively independent of τ. From Eq. (IV.13) then, N' will be independent of τ. Figure IV.8 shows calculations of $1/N'$ versus τ for the wind transverse to the path. Again the expected behavior is qualitatively observed for large τ. Note that Run H showing $1/N'$ decreasing with τ was observed under particularly low and variable wind conditions which may have contributed to the observed anomalous behavior.

Returning to the averaging time dependence of the spread in $(\sigma_\chi^2)_\tau$, one cannow employ the above discussion on the τ dependence of N' and Eq. (IV.14) to complete the discussion of Section IV.4. Eq. (II.12) again

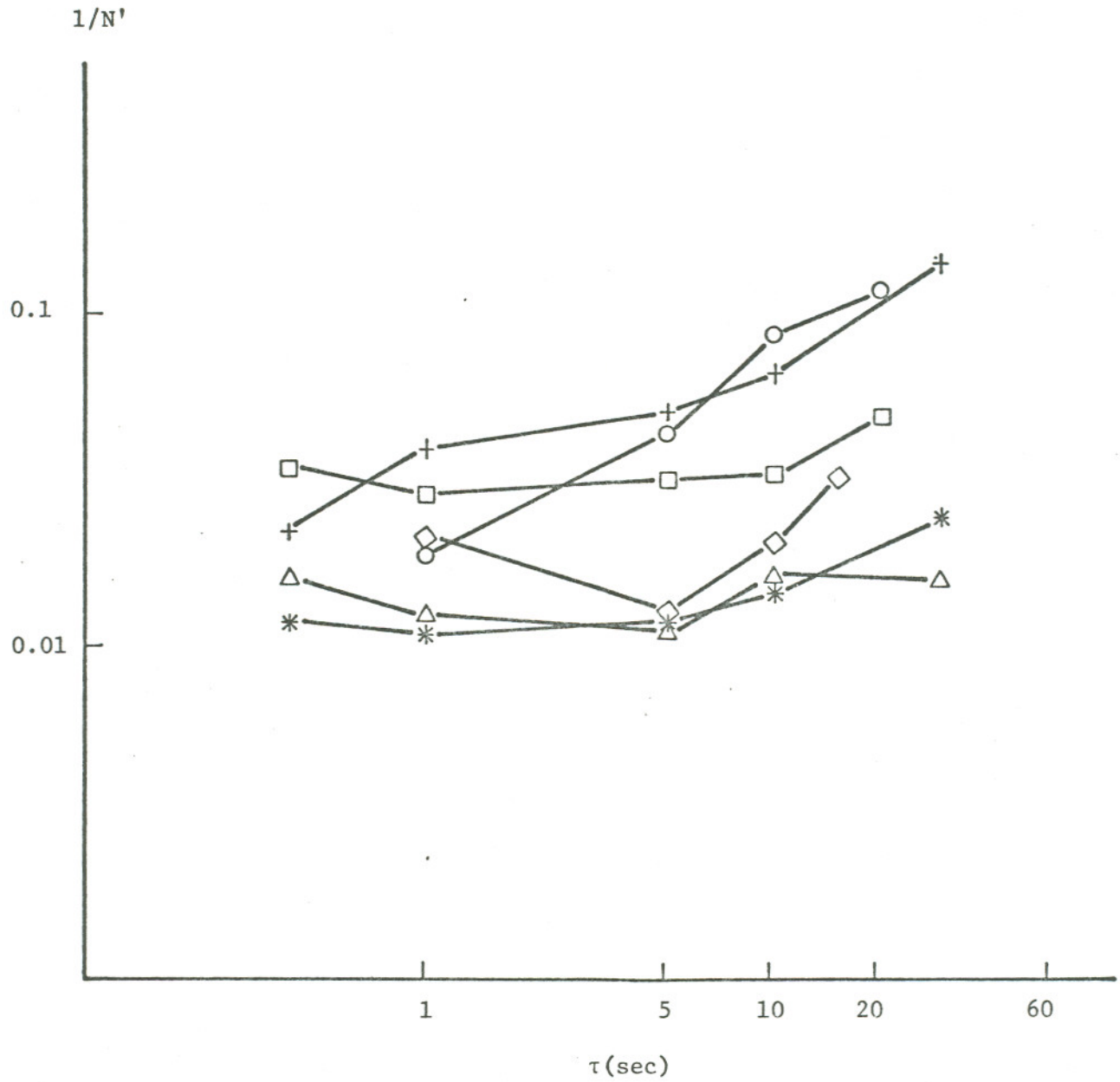

Figure IV.7. 1/N' versus τ, $\bar{u}$ parallel to the propagation direction.

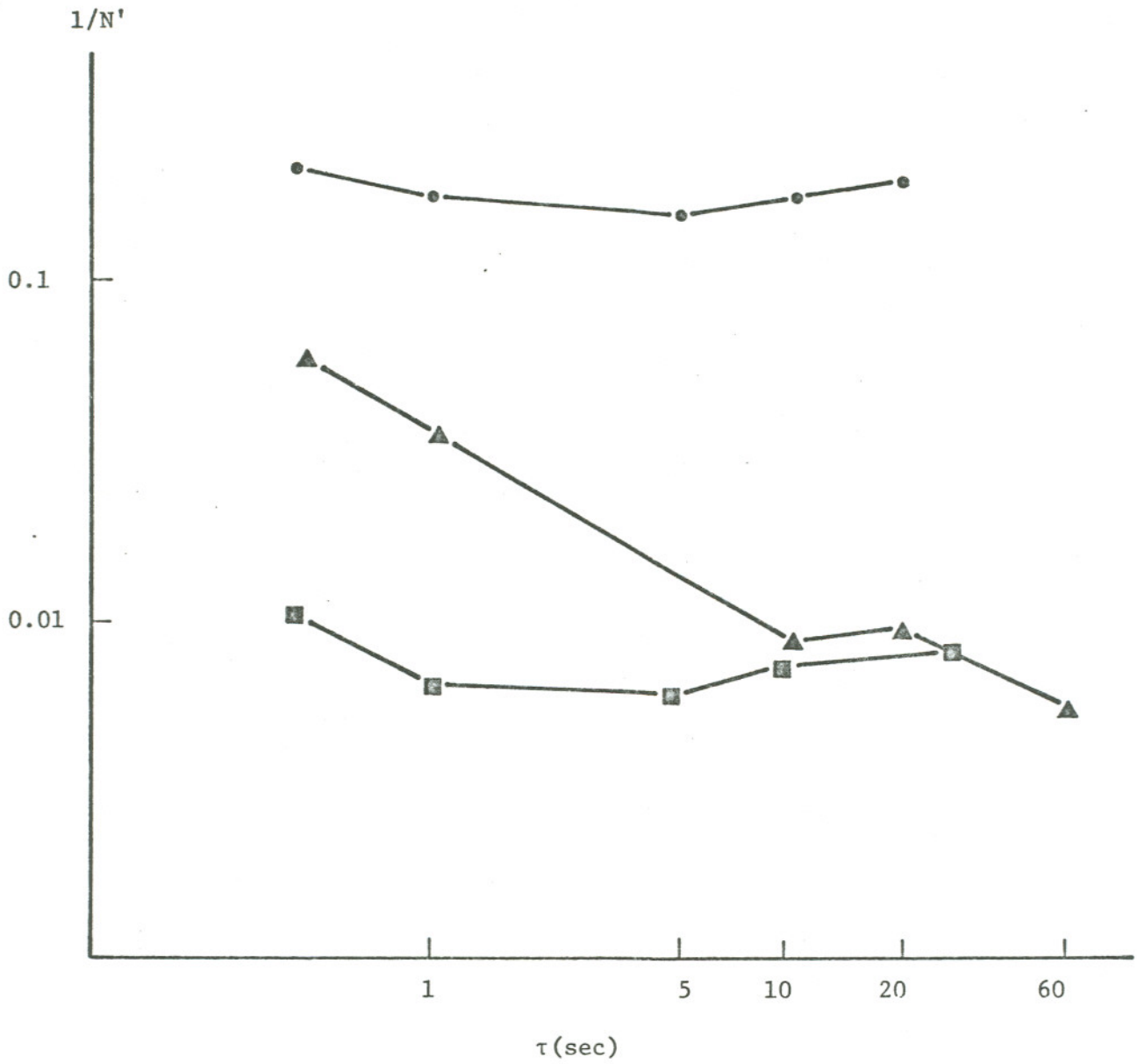

Figure IV.8. 1/N' versus τ, $\bar{u}$ normal to the propagation direction.

gives the τ dependence of variance of $(C_n^2)_\tau$ as $1/\tau$ for long averaging times and in the two wind direction conditions discussed above, N' varies as $1/\tau$ for the wind along the path and is independent of τ for the wind transverse to the path. Thus Eq. (IV.14) implies that in this simple model, the variance of $(\sigma_\chi^2)_\tau$ should vary as $1/\tau$ for the wind transverse to the path and be independent of τ for the wind along the path. The results of Fig. IV.6 however are not in agreement with this conclusion. A number of factors may account for the discrepancy. Probably the most important factors are that the above discrete model assumed a constant wind field and a frozen flow field of the turbulence strength. The actual wind velocity is a locally fluctuating quantity as is the local temperature. Even over the large scales of interest, there will be significant fluctuations in wind velocity. (A number of possibilities for causes of such large scale fluctuations arise from such known atmospheric turbulence structures as convective plumes, dust devils and vortex rolls). Similarly, the turbulence field is constantly undergoing decay and production processes and the frozen flow model is unrealistic over distances many times the outer scale. This randomness of the wind velocity and the turbulent field will cause a tendency for the basic statistical relationship described by Eq. (IV.5) to dominate and the slopes of all the curves in Figure IV.6 will tend toward minus one. There is also the question of the magnitude of the integral scale of these processes defining $(C_n^2)_\tau$. The dependence indicated in Eq. IV.5 is of course only valid for τ much greater than the integral scale of the second order process, which under conditions of large scale correlations in $(C_n^2)_\tau$ could become invalid for τ on the order of several seconds. By returning to Eq. (IV.10) and measuring the actual spatial correlation function of short time averaged $(C_n^2)_\tau$ along the path, one should be able to relate the measured spreads in the optical and turbulent parameters without the necessity of assumptions such as a frozen flow and constant wind velocity.

IV.7. Measurement of Spatial Structure of $(C_n^2)_\tau$

Measurement of the spatial correlation function of $(C_n^2)_\tau$, $C_{C_n^2}(\eta_1-\eta_2)$ (assuming long time homogeneity of the turbulent structure along the path) requires the use of a number of thermal sensors and the ability to

process simultaneous signals from the different sensors. For this work, five units equivalent to the one described in section II.3 for measuring C_n^2 were available. Short time averaged signals proportional to $(C_n^2)_\tau$ from each unit along with calibration signals and a signal proportional to the averaged wind speed were multiplexed onto a single channel of the FM magnetic tape recorder and later demultiplexed and processed by the PDP-11 computer.

The processing of interest here involves calculation of the auto-correlation functions of the individual $(\Delta T^2)_\tau$ signals, and cross-correla-functions among the different signals from the spatially separated thermal sensors. From the correlation coefficient or zero lag value of the cross-correlation function of different pairs of sensors and the spatial separation of the pair, the actual spatial correlation function can be generated. Additionally, the effect of increased time averaging on the various correlation functions can be observed by digital filtering of the 'signals' stored in the computer.

Typical configurations of the thermal sensors for these measurements are indicated in Figure IV.9. In case a, the temperature probes are oriented into the wind and the sensor units are stationed nearly along the wind. In fact an angle of 15°-30° was allowed between the line along the sensors and the observed wind direction to attempt to minimize the effects of the turbulent wakes produced by the upwind sensors. In this configuration, one measures the spatial structure along the wind and the motion of the structure with the wind. In case b the sensors lie along a line perpendicular to the wind and the spatial structure of the turbulence transverse to the mean motion is observed,

Figure IV.10 shows a portion of the demultiplexed signals from four sensor units with 0.4 second averaging time. These sensors were configured as in Figure IV.9a along the optical path, with spatial separations as indicated in the caption to the figure. The mean wind speed was 3.5 meters per second. Figures IV.11 and IV.12 show the calculated cross-correlation functions for the signals from the different pairs of sensors separated by the indicated distances. The general characteristics of each of the cross-correlation functions is similar. Each peaks at some nonzero time lag, with the position of the peak moving toward longer time lags as

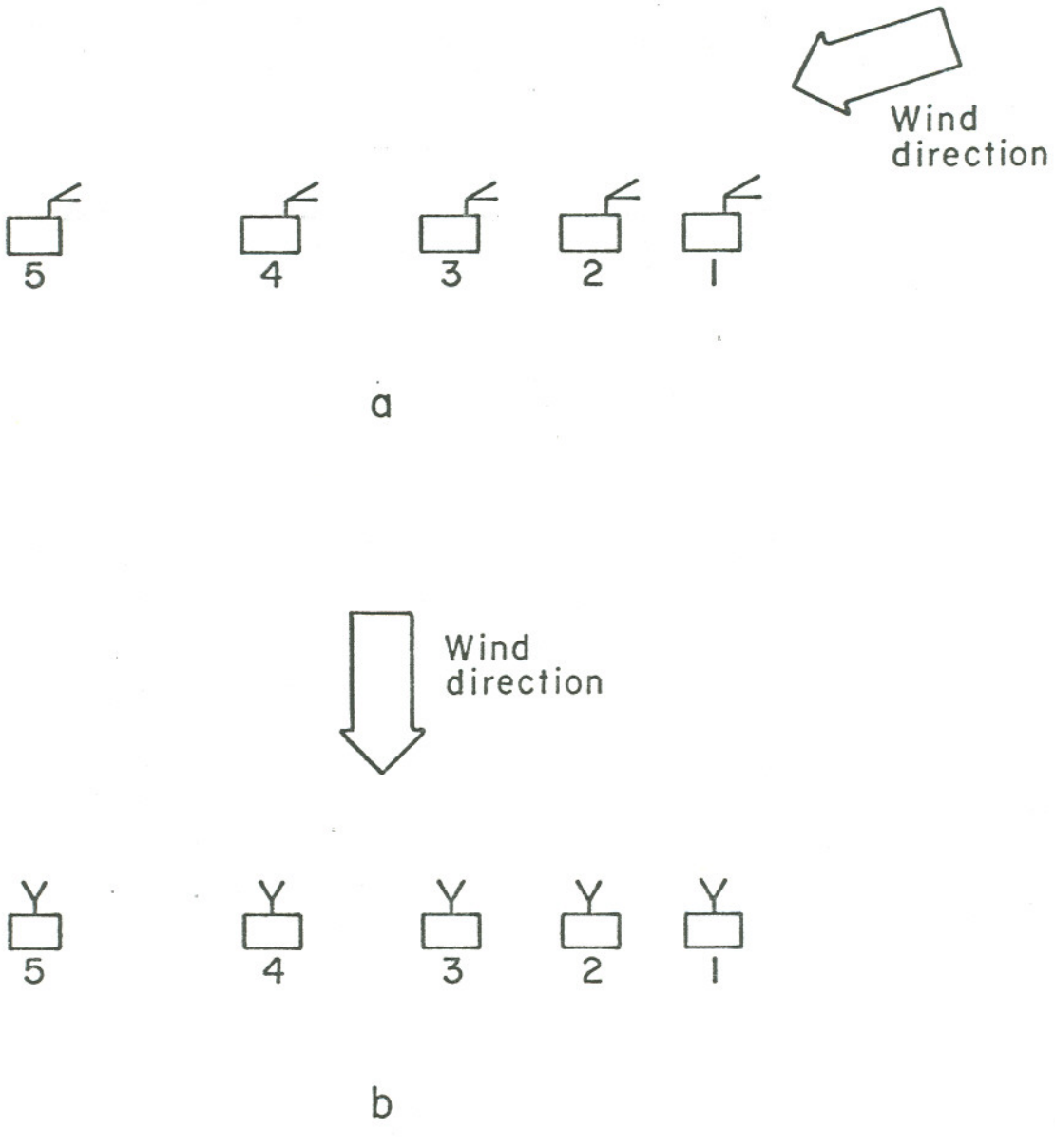

Figure IV.9. Typical configurations of turbulence sensors for measurement of spatial correlation function of $(C_n^2)_\tau$.

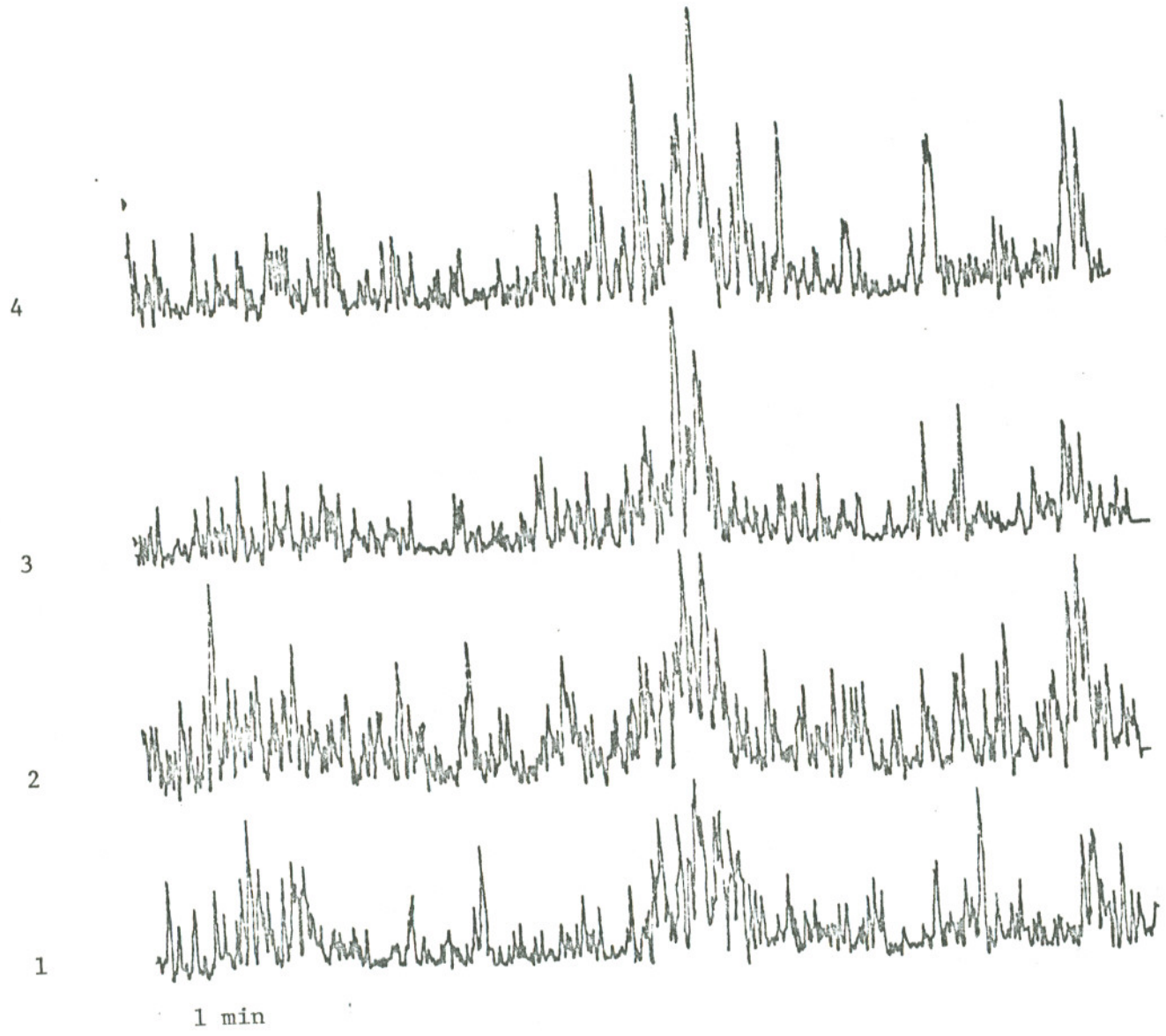

Figure IV.10. Traces of $(C_n^2)_{\tau = -/4 \text{ sec}}$ versus time from 4 sensors situated as in Figure IV.9a. Spatial separation: 1-2 = 2.5 m: 2-3 = 4 m: 3-4 - 6 m.

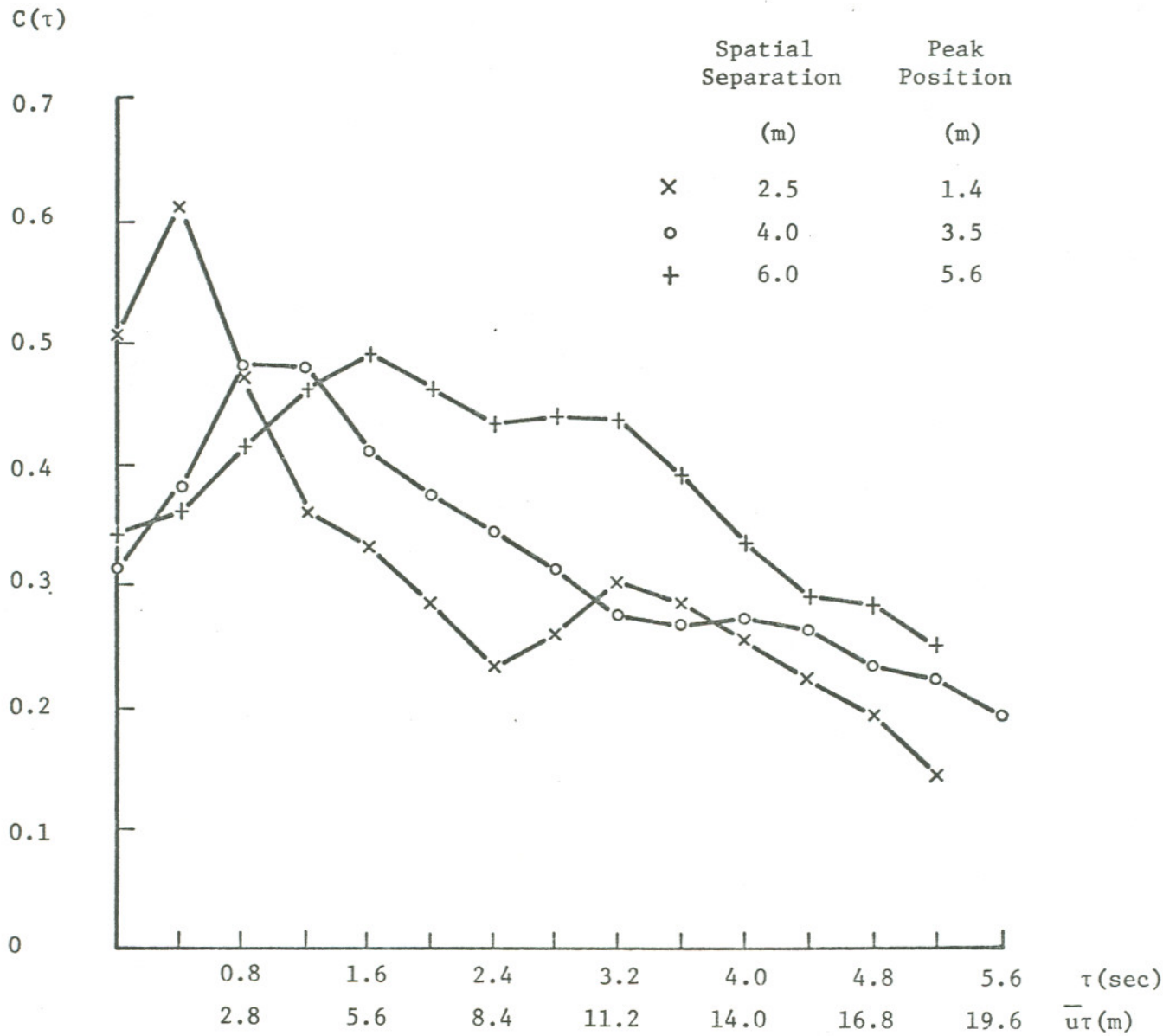

Figure IV.11. Cross correlation function of $(C_n^2)_\tau$ for data of Figure IV.10.

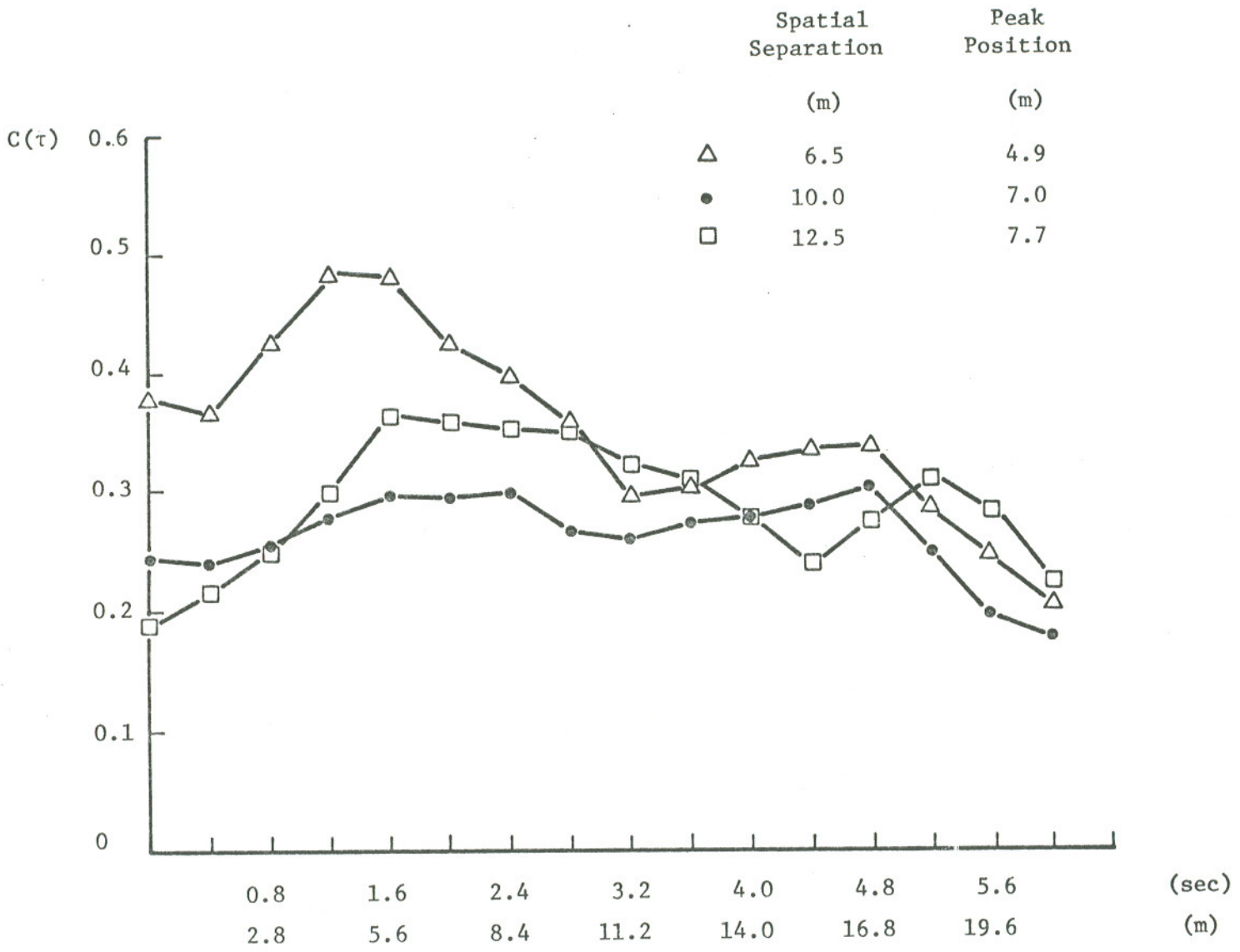

Figure IV.12. Cross correlation function of $(C_n^2)_\tau$ for data of Figure IV.10.

the spatial separation of the sensors increases. Thus the 'turbulence' which appears at one sensor at time t appears at another sensor downwind at a time $t + \tau$. Of course the turbulent structure is continually evolving as it moves with the wind. Were the turbulence field a 'frozen in' structure, each cross-correlation function would peak to a value of unity. The decrease in the peak heights from unity indicates the average decay or evolution of the turbulent structure with distance. The spatial correlation function constructed from the zero lag values as described above, for these data is shown in Figure IV.13. Also shown in this figure is the temporal autocorrelation function calculated from the individual $(C_n^2)_\tau$ signals. The time lag axis has been transformed to a spatial lag by multiplication by the mean wind speed. The separation of the two correlation functions at about 8 meters indicates absolutely the breakdown of the frozen flow hypothesis.

Using the calculated spatial correlation function one can return to Eq. (IV.10) to compare the predicted and observed data spread in the variance of the log amplitude of the optical fluctuations. The path weighting function f, for a spherical wave propagation is defined in Equation (I.6). The integrations of Eq. (IV.10) were performed numerically with a grid spacing along the path of 2 meters and an averaging time for the variance calculation of 0.4 seconds. The following indicates the numerical results of those calculations for this particular example:

$$\frac{\text{Var } (\sigma_\chi^2)_\tau / \langle\sigma^2\rangle^2}{\text{Var } (C_n^2)_\tau / \langle C_n^2\rangle^2} = 0.015$$

$$\frac{\int_0^L \int_0^L d\eta_1 d\eta_2 \; f(\eta_1) f(\eta_2) \; C_{C_n}{}^2 (\eta_1 - \eta_2)}{\left\{ \int_0^L d\eta f(\eta) \right\}^2} = 0.0115$$

While this example shows good agreement between the experimental measurements of data spread in short time averages of $(\sigma_\chi^2)_\tau$ and $(C_n^2)_\tau$, the spatial structure of $(C_n^2)_\tau$, and the derived relationship between these quantities, further attempts at such measurements yielded significantly higher deviations between observed and predicted data spread in $(\sigma_\chi^2)_\tau$. Under con-

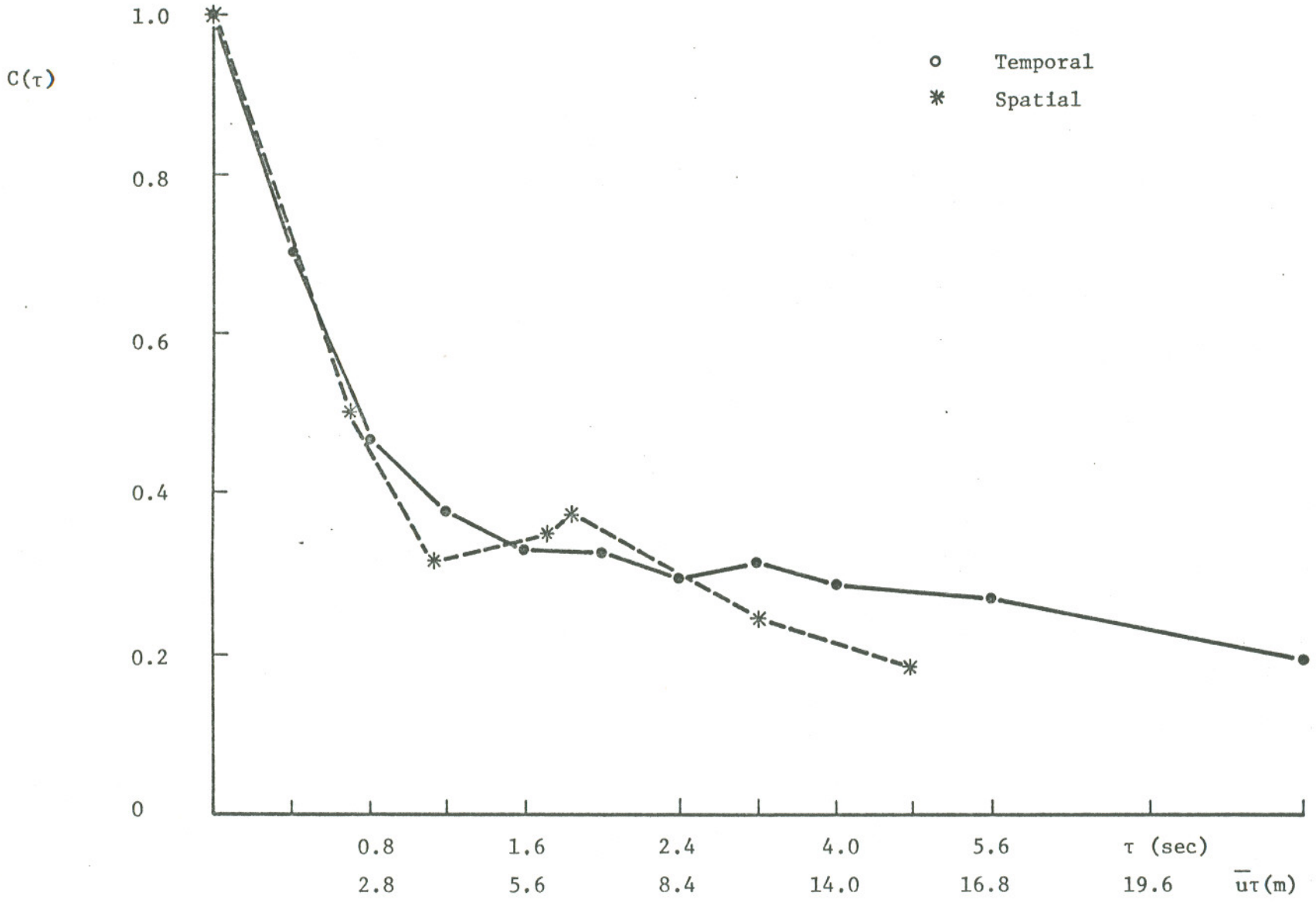

Figure IV.13. Spatial and Temporal correlation functions of data of Figure IV.10.

ditions of low wind speed, the agreement was particularly poor due possibly to inhomogeneity of the spatial profile of $(C_n^2)_\tau$ along the path.

Finally a number of examples of spatial correlation functions observed under the two configurations illustrated in Figure IV.9 are displayed. Figures IV.14 and IV.15 show spatial correlation functions under two different wind speeds with the wind along the sensors. In addition each figure includes results with three different averaging times. As the averaging time increases, the values of the correlation function increase, and thus the integral scale increases as shown in Appendix II. In the case of correlations measured transverse to the mean wind direction, one expectsminimal increase in the correlation function with averaging time as discussed above. Figure IV.16 shows such transverse correlations with a wind speed of 1.5 meters per second and one notes that at large separations there is little increase in the correlation with averaging time. Figure IV.17 also shows transverse correlations. In this case, however, there is significant correlation at large separations and a tendency to increase with averaging time.

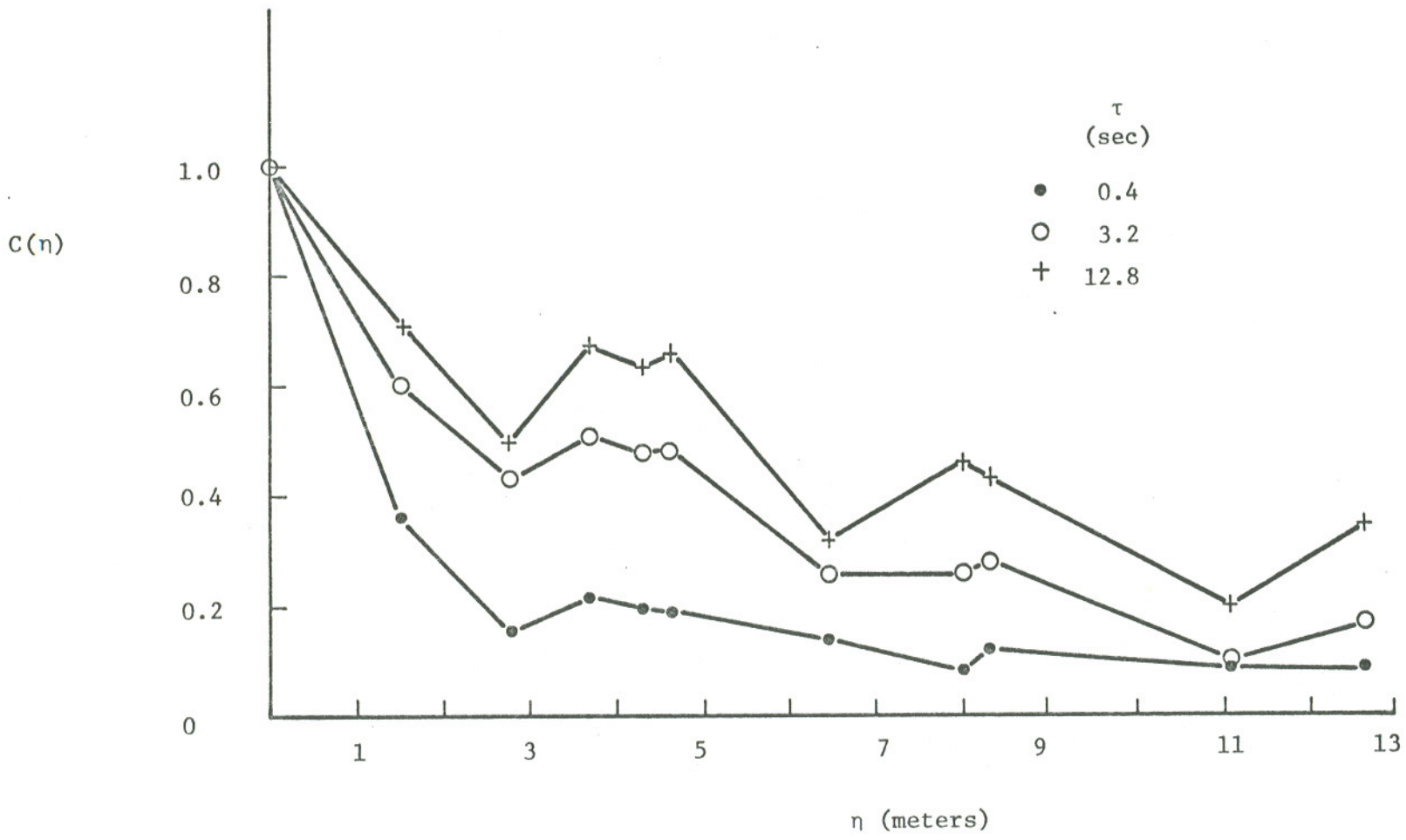

Figure IV.14. Spatial correlation function of $(C_n^2)_\tau$ parallel to the mean wind direction. $\bar{u}$ = 1.5 m/sec.

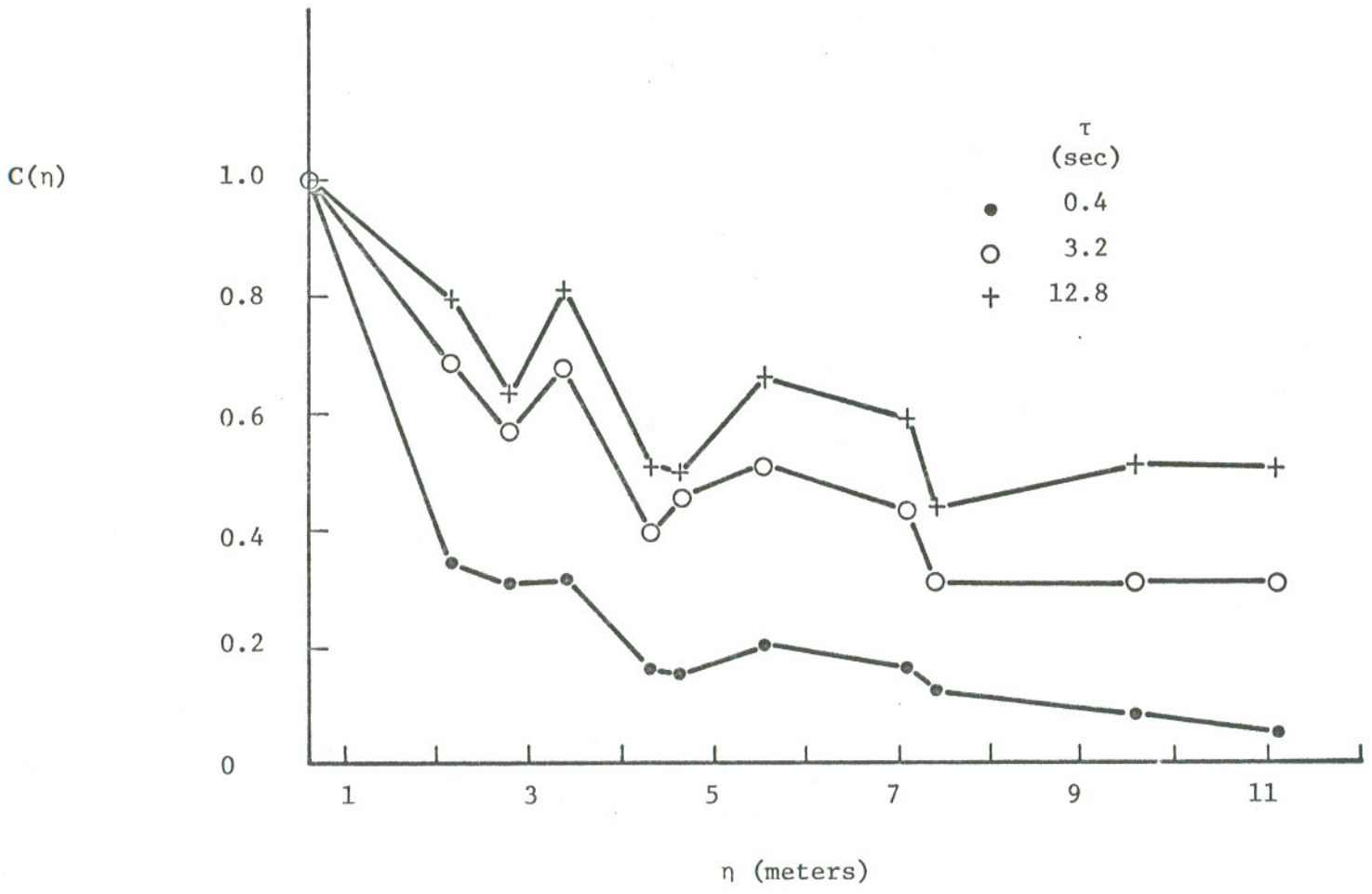

Figure IV.15. Spatial correlation function of $(C_n^2)_\tau$ parallel to the mean wind direction. $\bar{u}$ = 4.6 m/sec.

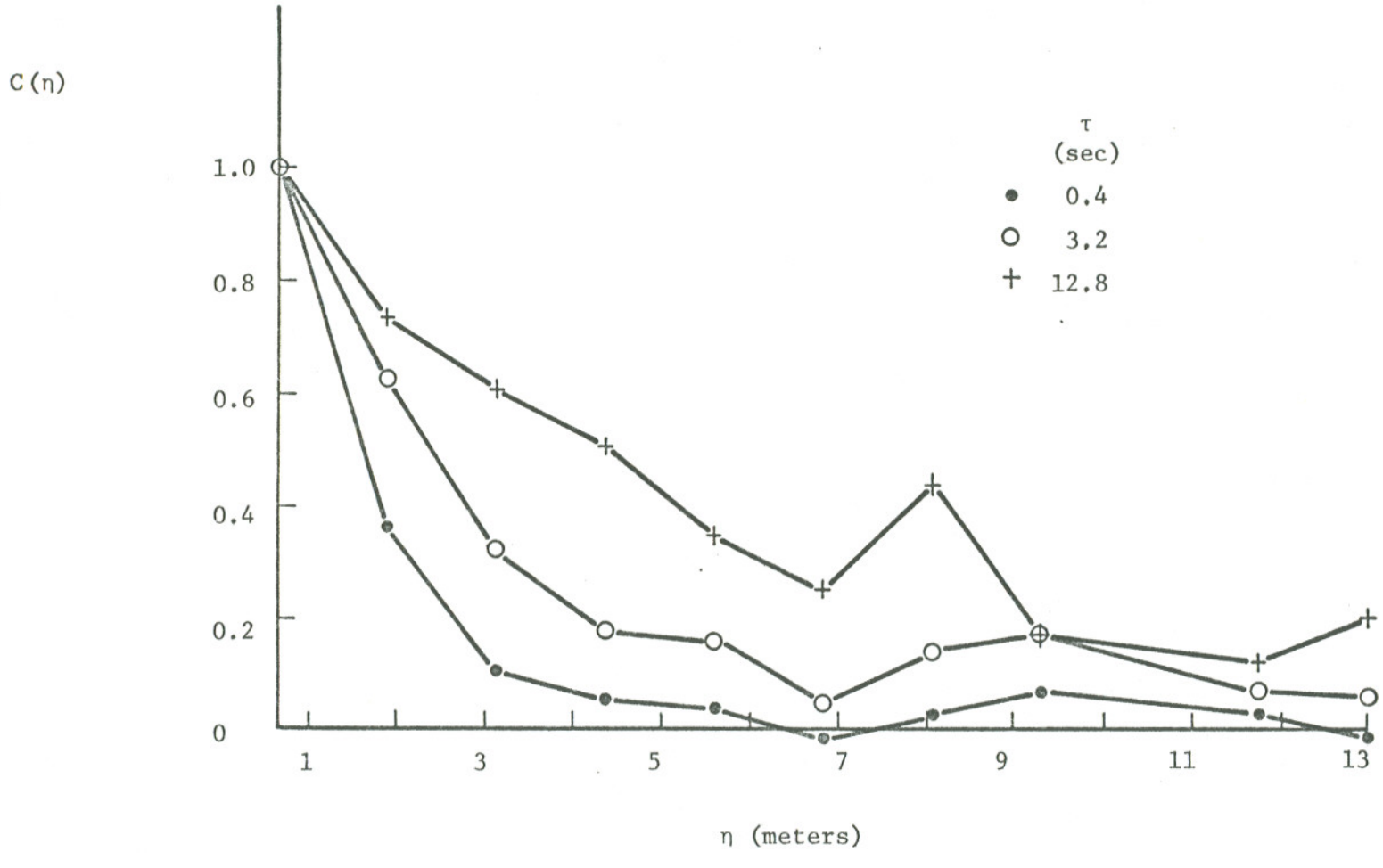

Figure IV.16. Spatial correlation function of $(C_n^2)_\tau$ normal to the mean wind direction. $\bar{u}$ = 1.5 m/sec.

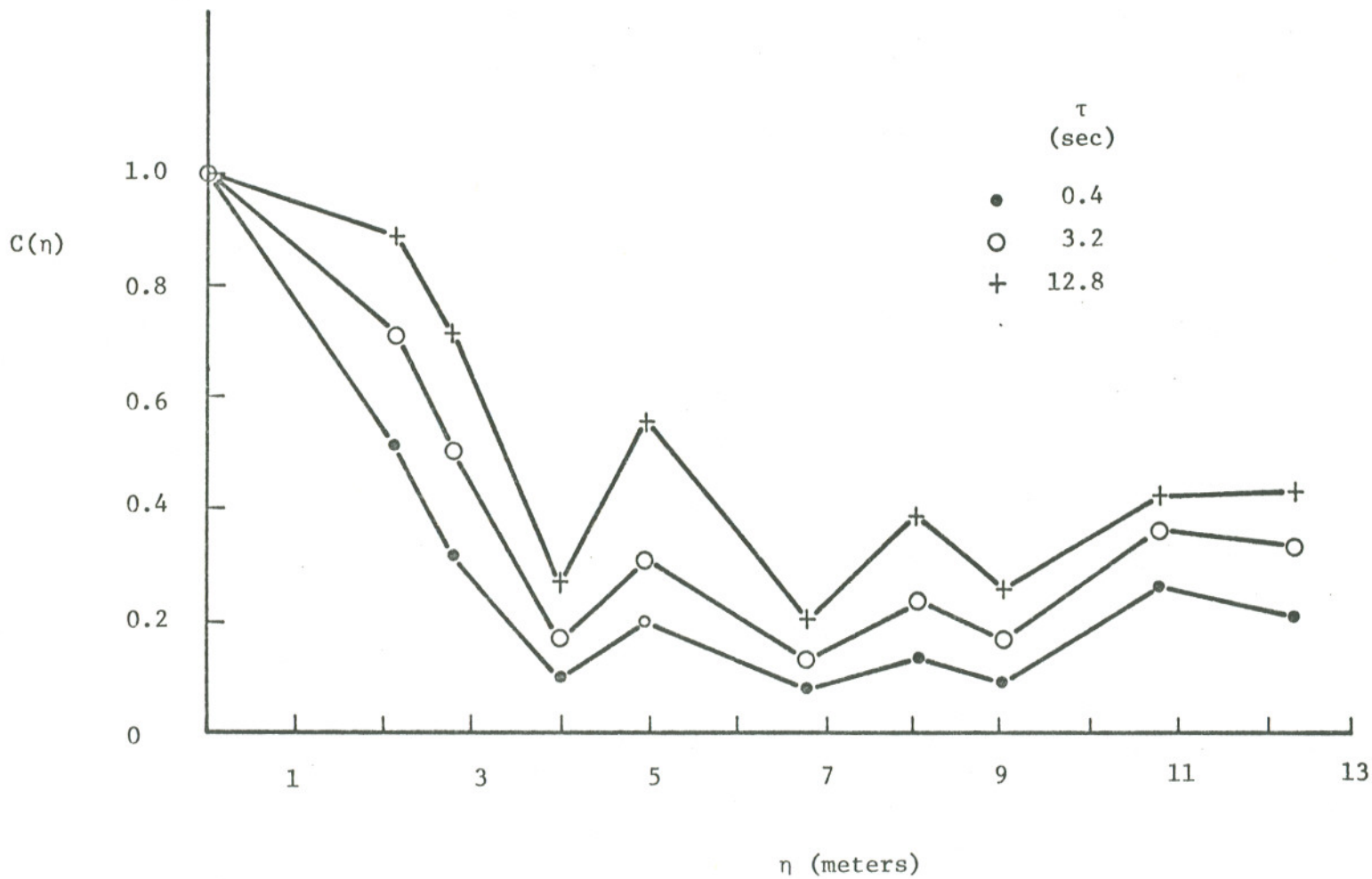

Figure IV.17. Spatial correlation function of $(C_n^2)_\tau$ normal to the mean wind direction. $\bar{u}$ = 0.9 m/sec.

CHAPTER V. Atmospheric Intermittency

V.1. Introduction

In this chapter one observed property of atmospheric turbulence mentioned in previous chapters, namely its large scale intermittent nature is discussed. This property is best described pictorially as in Figure V.1 showing traces of two probe differential temperature fluctuations and their absolute magnitude. An important difference is noted between Figure V.1 and, for example, Figure II.4, depicting temperature difference fluctuations under different atmospheric conditions. In Figure V.1 the fluctuations appear to occur in 'bursts' between one and five seconds in length followed by relatively quiet periods of similar duration. This sporadic character in the temperature fluctuations on such a time scale is denoted as large scale intermittency. This is in fact a pragmatic viewpoint. An intermittent process defined here is one in which the 'envelope' of the process, or its average intensity varies slowly compared to the fundamental fluctuating process, but which varies significantly over observation times of interest. Thus in Figure V.1, measurements of the variance of the temperature fluctuations over five second intervals for example, would yield very different results as the observation intervals were moved along the trace. Questions of stationarity of the process are not of practical concern here because the interest is primarily in short time averages.

V.2. Background

The first report of intermittency in turbulent flows appears to be that of Batchelor and Townsend (1947) in their observation of small scale turbulent velocity fluctuations. Since then the problem of spatial intermittency of turbulent variables has been described repeatedly from different viewpoints. The work of Kolmogorov (1962), Oboukhov (1962) and finally Gurvich and Yaglom (1967) described in Chapter II arose from the problem of small scale intermittency of velocity fluctuations and the resultant dissipation rates of the turbulence. Kuo and Corrsin (1971) experimentally investigated small scale intermittency of velocity fluctuations including measurements of the intermittency factor, γ, the fraction of space or time occupied by the fine structure turbulence. Their work

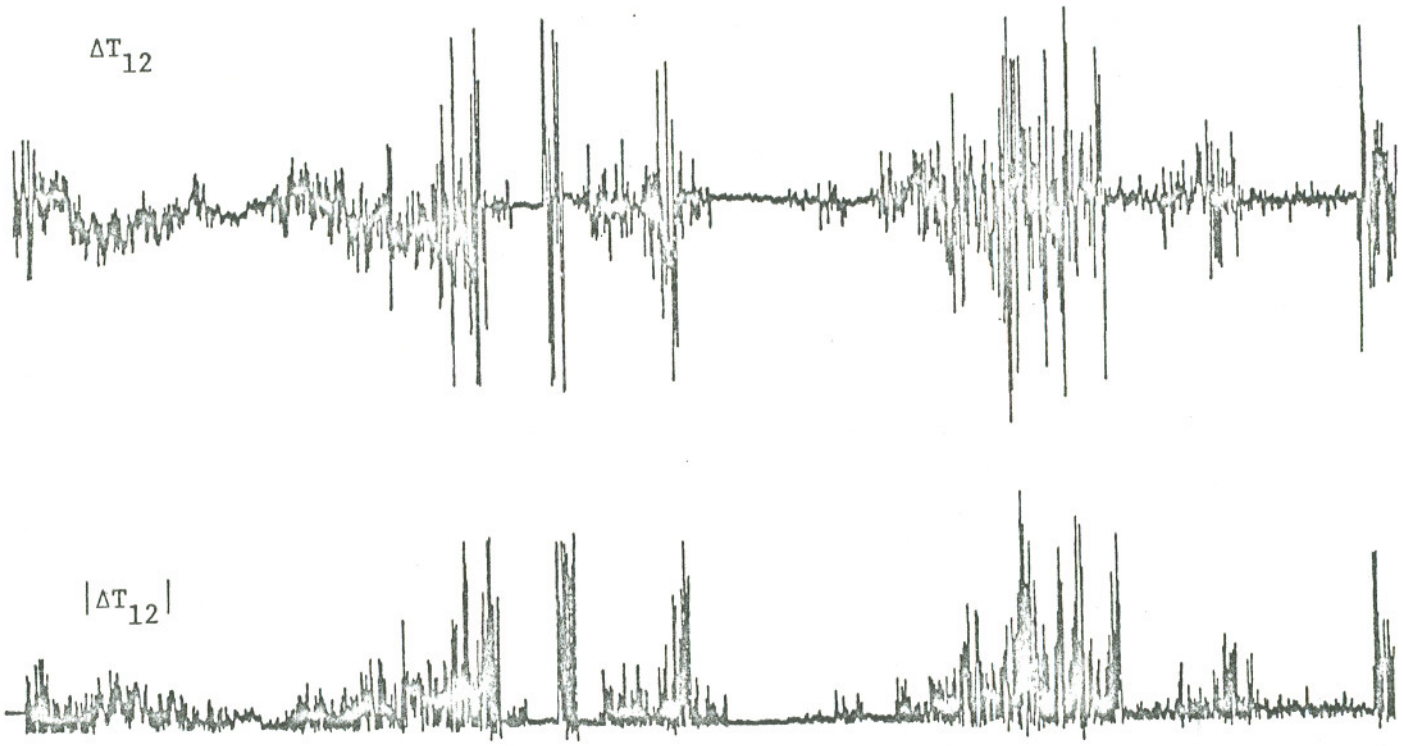

Figure V.1. Intermittent temperature fluctuations ΔT_{12} and $|\Delta T_{12}|$.

was at relatively low Reynolds numbers compared to the atmospheric flows of interest here. Of particular interest though, is their discussion of the lognormal distribution (as the distribution of the average dissipation rate of the turbulence, ε) and intermittency. Their concluding remark, that for a lognormal distribution, as the variance increases, "the probability density at very large and very small values of ε will increase and that at intermediate values of ε will decrease" depicts precisely one of the characteristics of observed intermittency. Thus a lognormally distributed variable with a large variance may in itself tend to appear intermittent. More recently work has progressed on describing the origins of intermittency. Mollo-Christensen (1973) reviewed this aspect of the problem indicating that the observed intermittency is caused by 'bursts' in the generation of turbulence rather than continuous production of turbulence followed by aggregation of regions of high turbulent activity. The bursting generation of the turbulence is the result of a coupling of instabilities of the flow of a number of different scale sizes. Experimental measurements concerning bursting phenomena of turbulence and coupling of different size instabilities have been made under laboratory controlled conditions (Lu and Willmarth 1973, Lauffer and Narayanan 1971).

Discussions of larger scale intermittency with which we are principally concerned are more limited in the literature. Lawrence, Ochs and Clifford (1970) noted intermittent turbulence as seen in Figure V.1 and modeled the observed fluctuations as the product of two random processes, one a Gaussian process with zero mean describing the rapid small scale fluctuations and the other, a slow two level process acting as a modulation function. They noted some qualitative agreement with a predicted probability distribution function under this model and their measured distribution of the temperature difference fluctuations. Kerr (1973) discussed some implications of modeling the intermittent turbulent process as the product of two processes with widely disparate time scales, noting particularly problems associated with short time averaged measurements. Further comments on large scale intermittency and data spread were made by deWolf (1973 b). He derives an expression for the data spread in optical propagation parameters similar to (Eq. IV.10) above in terms of the spectrum of the large scale or intermittent fluctuations in C_n^2.

He concludes that it is "unclear whether intermittent phenomena can be distinguished from random sampling of a statistical process with a known probability distribution", especially because the large scale phenomena are not universal but rather dependent on terrain and atmospheric conditions. This is essentially true; however in this case, of intermittent thermal fluctuations, one has phenomena occurring qualitatively over widely separated frequency regions and one may expect to gain some understanding of the consequences of strong intermittency by modelling it as a process separate from the 'fundamental temperature fluctuations'. The descriptions of a two level multiplicative process of Lawrence, Ochs and Clifford (1970) and Kerr (1973) provide such a model.

V.3. Plumes

A possible physical mechanism for the simple model of intermittent temperature fluctuations described above may be found in the phenomena of convective plumes. These structures of the lower boundary layer of the earth's atmosphere are near vertical parcels of air with well defined boundaries, within which both the air temperature and the intensity of the thermal turbulence are significantly greater than that in the surrounding air. Boston (1971) described the appearance of 'ramp-like' structures in traces of temperature fluctuations at a single point in the atmosphere, and attributed these to the passage of convective plumes by the sensor. Kaimal (1974) and Kaimal and Businger (1970) present details of their observations of plumes including characteristics of their shape and motion. These plumes are columns of rising warm air, slightly tipped in the downwind direction and are easily recognized by the sharp drop in the temperature at the upwind edge. This of course contributes to the appearance of ramp-like structures in the temperature traces. Following the drop in the temperature, thus after the plume passes the sensor, and until the appearance of the next plume, the turbulence level may appear to be extremely low. This description of the temperature fluctuations at a single point, when translated into that expected from the two probe differential measurements corresponds well with the fluctuations observed under intermittent conditions (Figure V.1).

Several examples are shown of observations of single point thermal fluctuations indicating the presence of convective plumes. In these examples four independent probes were operated simultaneously at a height of two meters, situated as shown in Figure V.2.

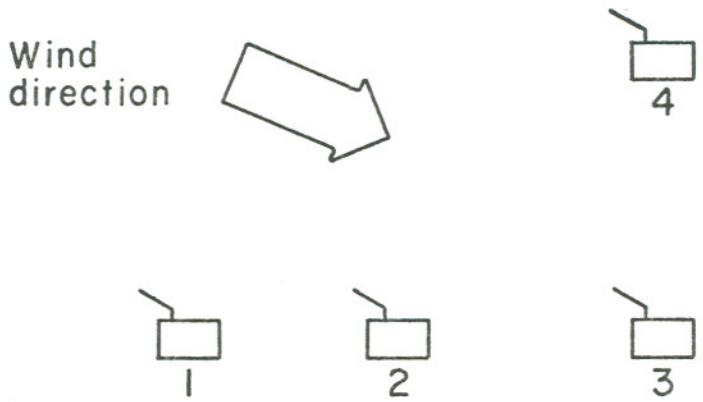

Figure V.2

During the observation period, the wind speed varied between three and five meters per second. Figures V.3 and V.4 show the results of two separate observations of the temperature fluctuations at the four sensors. The arrows indicate the times of the probable passage of the upwind edge of plumes sequentially by the three sensors. The fourth sensor is separated from the others in a direction transverse to the wind direction and the temperature trace from this sensor does not appear correlated with the other traces. From the known spatial separation of the sensors, and the measured time delay between the appearance of the plume at each sensor, the translation speed of the plume can be calculated. Table 9 shows the results of such calculations for the two examples of plumes indicated in the figures. The observed translation speeds are approximately 3.5 and 5 meters per second, consistent with the independent measure of the wind speed. Kaimal (1974) observed plume passage at two heights (4 m and 16 m) and found the translation speed of the plume to be essentially independent of height unlike the mean wind velocity which increases with height. Only at the lower boundary of the plume does its translation speed equal the mean wind speed.

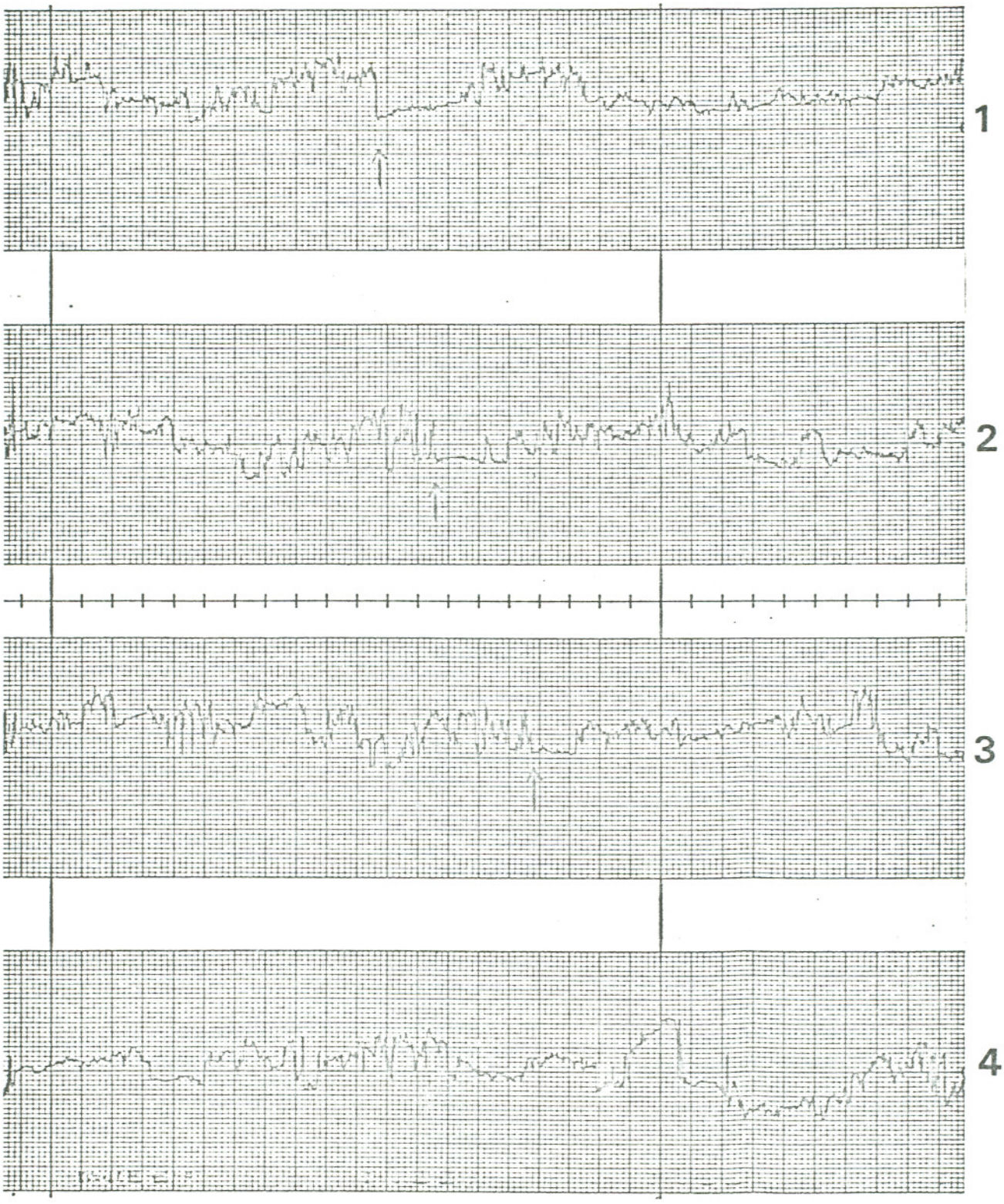

Figure V.3, Traces of single point temperature fluctuations. Plume No. 1.

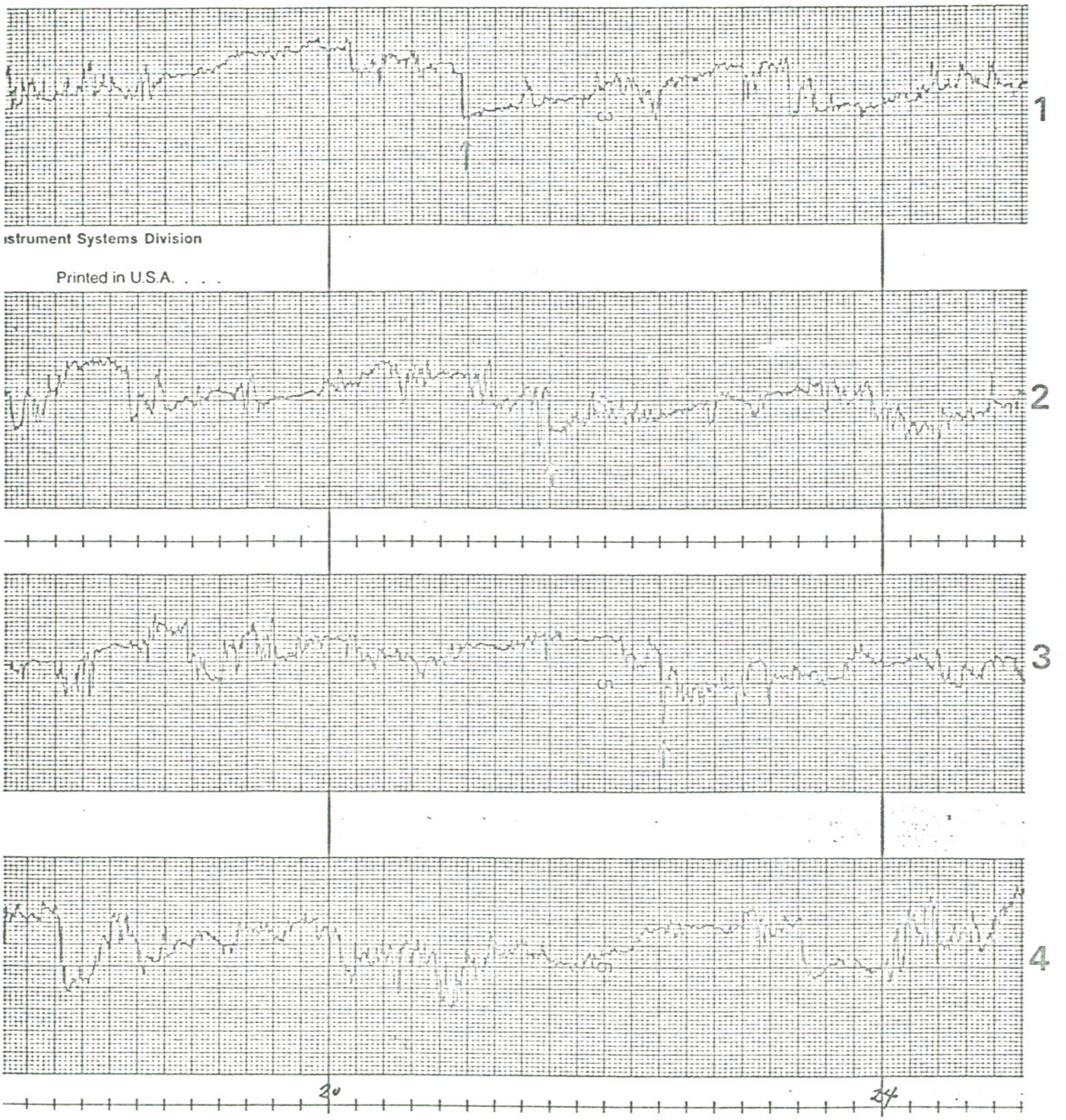

Figure V.4. Traces of single point temperature fluctuations, Plume No. 2.

Table 9

Plume 1

Sensor pair	Sensor Separation (m)	Observed time lag (sec)	Velocity of Plume (m/sec)
1-2	2	0.4	5
2-3	2.9	0.6	4.83
1-3	4.9	1.0	4.9

Plume 2

1-2	2	0.64	3.1
2-3	2.9	0.8	3.6
1-3	4.9	1.44	3.4

V.4. Effects of Intermittency on Turbulence Spectra and Probability Distribution Functions

Despite the fact that the two level plume model of Lawrence, Ochs and Clifford and Kerr is an oversimplification of the physical situation, it does provide a framework within which one can investigate the effects of strong intermittency on various finite time statistical measures of turbulence described in the previous chapters. One denotes the observed intermittent temperature fluctuations as $z(t)$ and assume $z(t) = x(t) \cdot y(t)$, where $x(t)$ is a zero mean random process describing the non-intermittent rapid temperature fluctuations and $y(t)$ is a non-negative essentially two level process describing the on-off character of the intermittency.

These processes are schematically illustrated in Figure V.5. Also shown in Figure V.5 is $z^2(t)$ which translated into the temperature fluctuation domain corresponds to the intensity of the fluctuations, and whose average over some short time is related to $(C_n^2)_\tau$. Figure V.5 additionally indicates the power spectral representations of each of these processes. $x(t)$ is essentially a bandpass limited function whose cutoff points are determined by the high frequency cutoff of the thermal sensing equipment or the temperature fluctuations themselves and the low frequency cutoff characteristic of the differential measurement technique. $y(t)$ should contain only very low frequency components indicative of the intermittency time scale in the range one to ten seconds.

The power spectrum of $z(t)$ will be related to the convolution of the power spectra of $x(t)$ and $y(t)$. The effect of the modulation of $x(t)$ by $y(t)$ is simply to 'broaden' the spectrum of $z(t)$ over that of $x(t)$ (introduction of narrow sidebands around a carrier frequency by amplitude modulation). Essentially no significant amount of energy is introduced into the low frequency region of the spectrum of $z(t)$ by the slow modulation of the intermittency. This is important in that the correlation function of $z(t)$, at long time lags which is sensitive to the low frequency portions of the spectrum, will not be significantly affected by the intermittency. In particular, the integral scale of the intermittent process will not differ from that of the non-intermittent process. In the case of $z^2(t)$ however, there is energy in the low frequency region of the spectrum and the added intermittency increases the energy density and thus consequently increases the integral scale of the process.

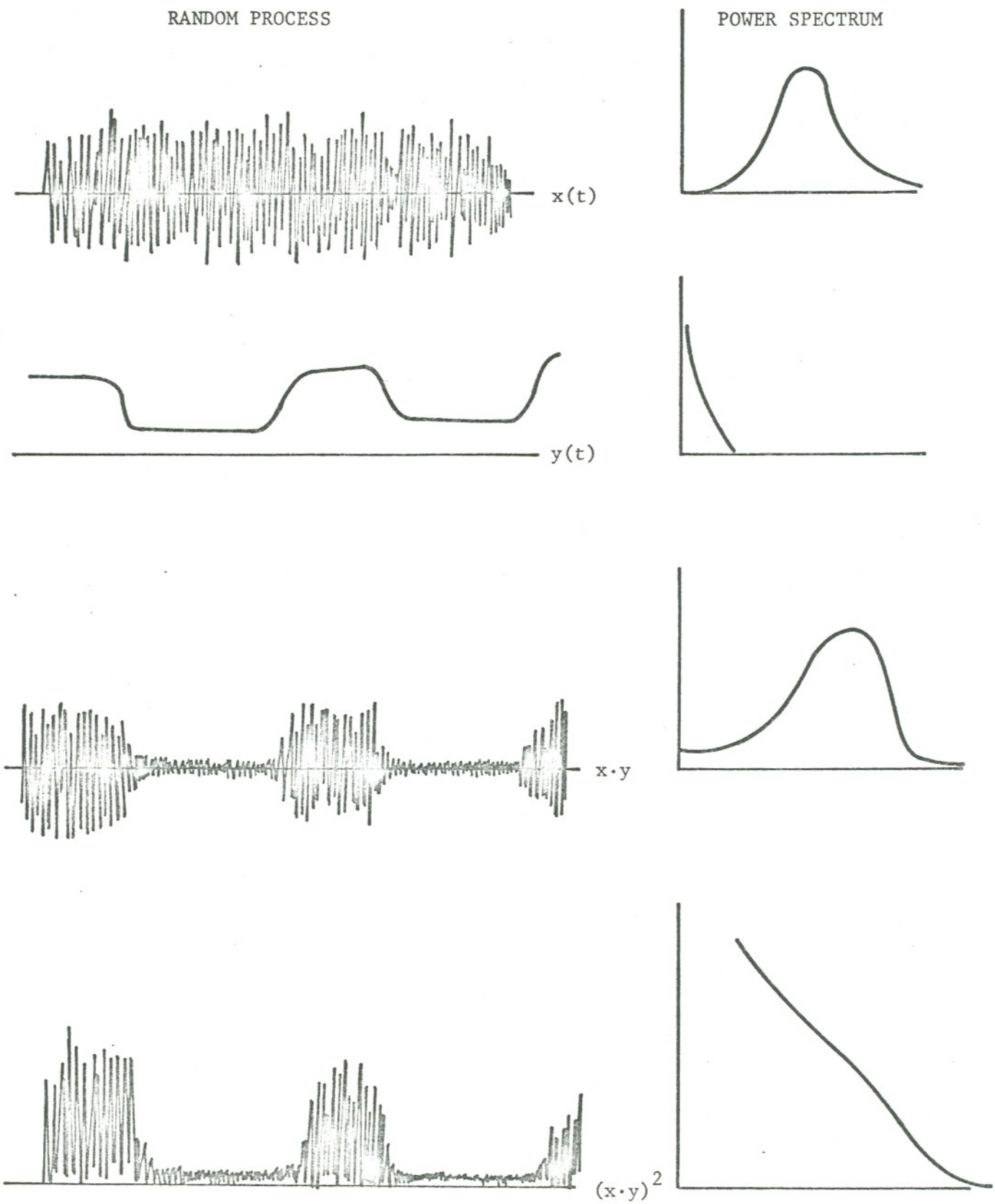

Figure V.5. Pictorial description of intermittent random process.

The effects of intermittency on the probability distribution function can be similarly described. The probability distribution function of $x(t)$, $p_x(x)$, is symmetric about zero, and qualitatively bell shaped. Thus the skewness is zero and the flatness factor will be greater than or equal to three (the deviation from three is one possible measure of the deviation of the distribution from gaussian). The distribution function of $y(t)$, $P_y(y)$, depends on the description of the modulating function. If the intermittency is described by a two level process, then $p_y(y)$ would equal the sum of two delta functions, their relative weights depending on the relative probabilities of the two levels. The distribution function of $z=x\cdot y$, $P_z(z)$, is then given by

$$P_z(z) = \int_0^\infty P_x(z/y)\ P_y(y) 1/y\ dy$$

The distribution of z will qualitatively be described by zero skewness, and generally a higher flatness factor than the distribution of x due to the increased probability density at small absolute values of z which gives the distribution function a relatively wider extent.

The distribution function of the squared non-intermittent process, $x^2, P_x{}^2(x^2)$, will have the same characteristics as the distribution of the absolute magnitude of x, with a change in scale. As the distribution of x is symmetric about zero, the distribution of $|x|$ will be proportional to the distribution function of x for x greater than zero and equal to zero for x less than zero. This of course yields a highly asymmetric distribution function with a very large flatness factor for $P_x{}^2(x^2)$. In the intermittent case, the same holds true, and the distribution of z^2, $P_{z^2}(z^2)$, will be related to the distribution $P_z(z)$, with an appropriate scale change, for z greater than zero and equal to zero for z less than zero. Again this yields a highly asymmetric distribution function with a very large flatness factor, and non-zero probability density at z equal to zero.

The effect of time averaging of x^2 or z^2 leads to a narrowing of the distribution function and specifically to a decrease in the probability

density at x^2 or z^2 equal to zero. Section II.2 included a discussion of the probability distribution function of $(\Delta T_{12})^2$ including the prediction of lognormality for a certain range of averaging times τ. The probability density must go to zero at x^2 or z^2 equal to zero for the distribution to be lognormal. Referring to examples in Chapter II, Figure II.7a is an example of relatively non-intermittent fluctuations, while those in Figure II.7b are intermittent. The distribution function of ΔT_{12}^2 for the non-intermittent case, which appears in Figure II.10 shows good agreement with lognormality. With the added slow modulation of intermittency, figure II.7b, the equivalent distribution in Figure II.11 is decidedly not lognormal.

Another effect of time averaging of a process such as z^2 is to filter out the high frequency components associated with the fundamental fluctuating process x and reveal the nature of the modulation function y. Figures V.6 and V.7 show actual examples of two point intermittent temperature fluctuations, ΔT_{12}, their absolute magnitude, $|\Delta T_{12}|$ (which behaves similarly to their square, $(\Delta T_{12})^2$) and the effect of time averaging. In figure V.6, the time averaging is a digital RC filter which tends to smooth out the sharp boundaries between regions of different levels of turbulent activity. Figure V.7 shows the same fluctuations now averaged using a 'boxcar' or 'tophat' averaging scheme. This involves simply an unweighted average of a sequential sample of data. This method, at least visually, yields a better example of the intermittent envelope process. The probability density function of samples of this boxcar averaged data are shown in Figure V.8. In the case of averaging for 500 milliseconds, the distribution function has a tendency toward a double humped appearance, but is not a simple two level function as discussed above.

V.5. Quantitative View of Intermittent Turbulence

In Table 10 are tabulated a number of statistical properties of two probe differential temperature fluctuations observed under different conditions. After the mean wind speed, we see the normalized standard deviation in short time measurements of $(C_n^2)_\tau$

$$R = \frac{\text{St. Dev. } (C_n^2)_\tau}{\overline{C_n^2}}$$

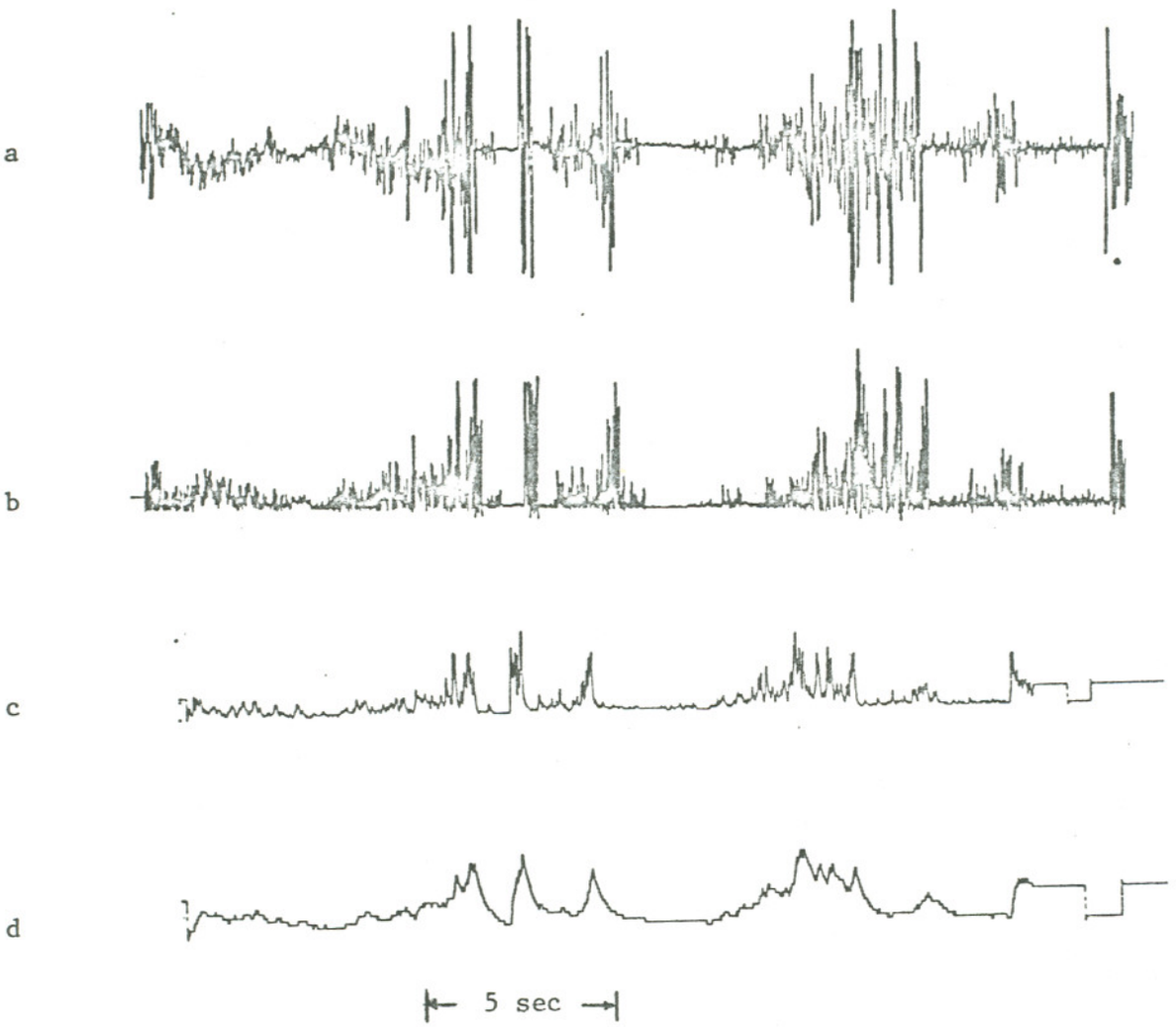

Figure V.6. Intermittent turbulence with time averaging: RC filtering.

a, $\tau = 0$
b, $\tau = 5$ ms
c, $\tau = 50$ ms
d, $\tau = 500$ ms

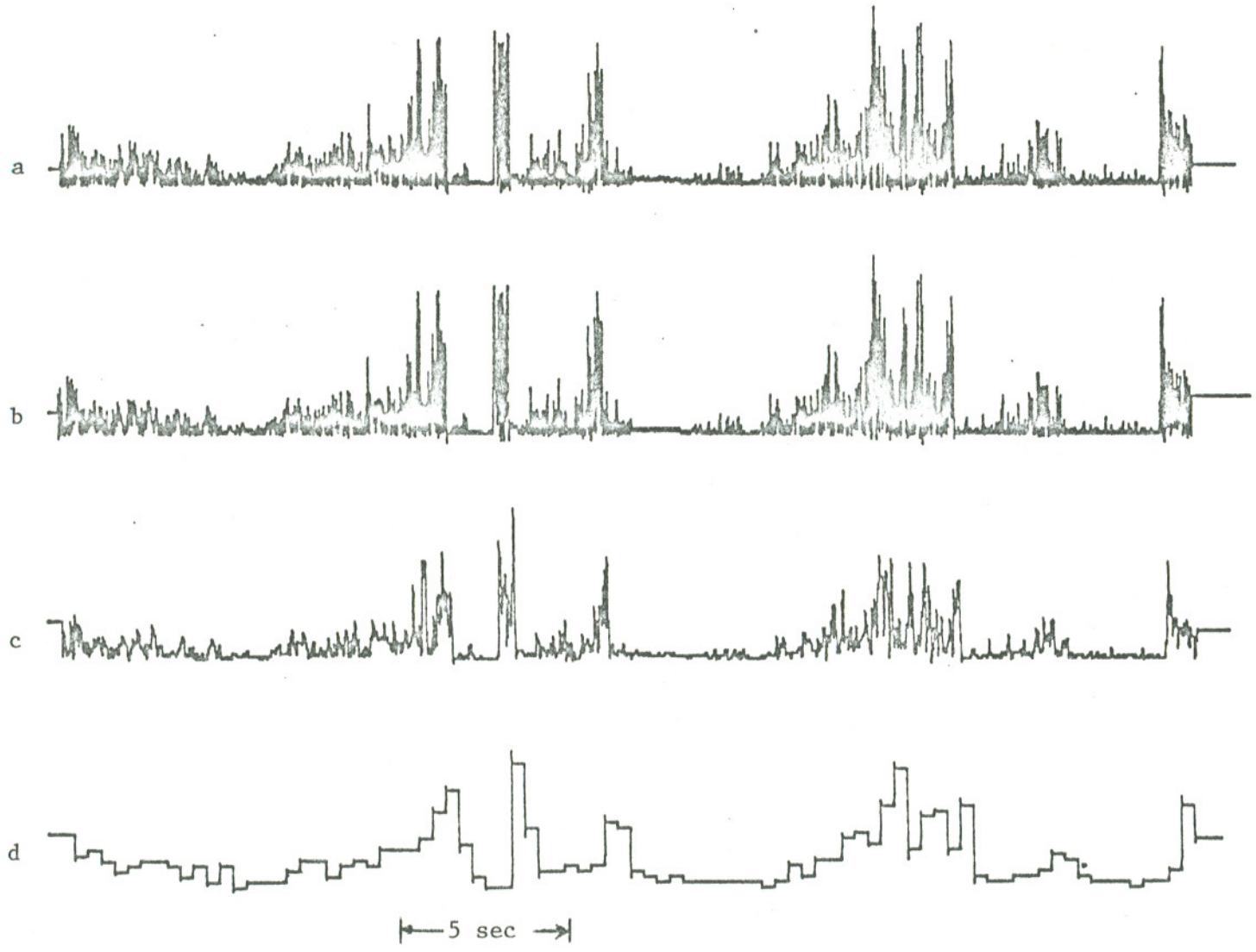

Figure V.7. Intermittent turbulence with time averaging: boxcar filter. a, $\tau = 0$; b, $\tau = 5$ ms; c, $\tau = 50$ ms; d, $\tau = 500$ ms.

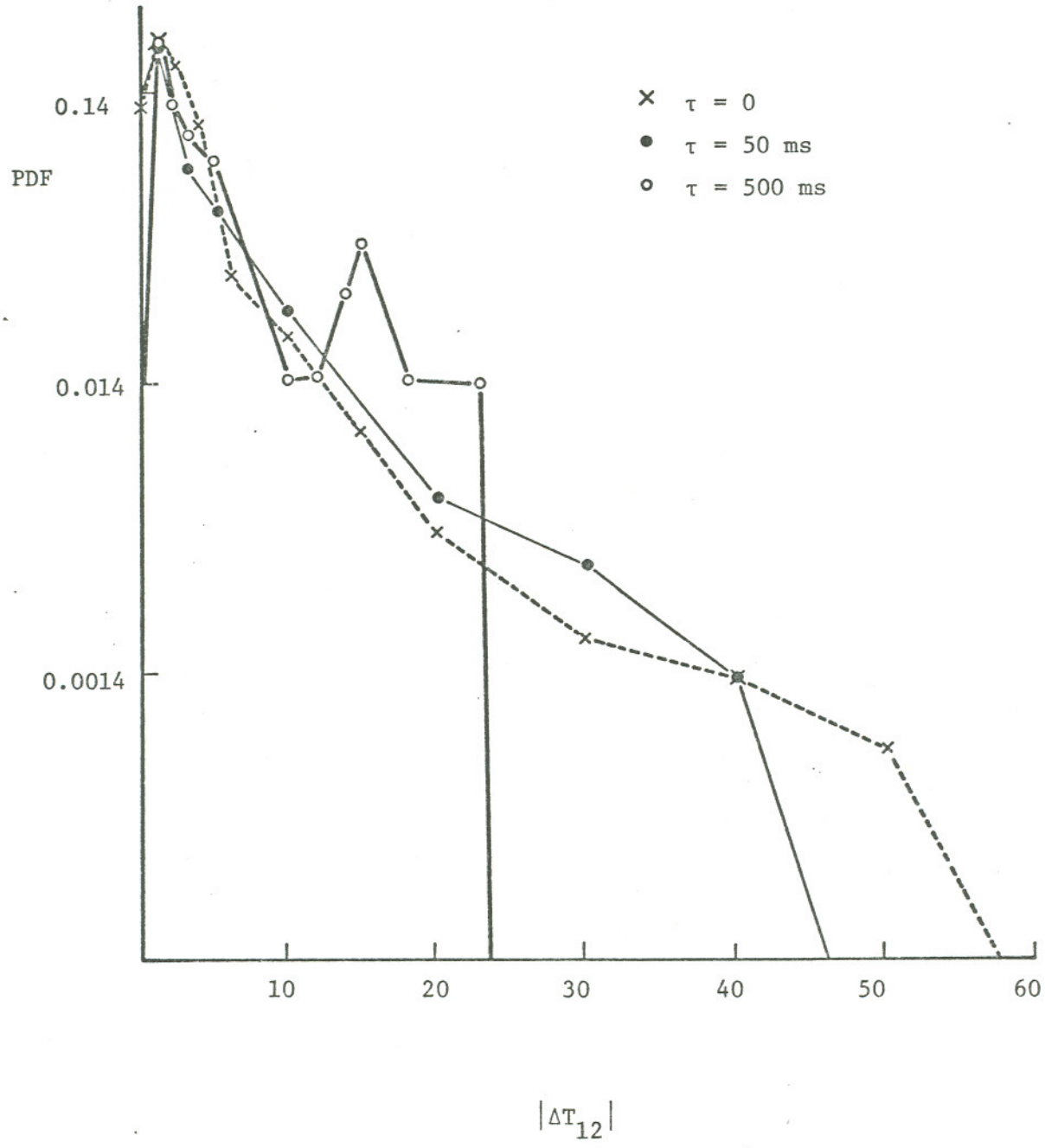

Figure V.8. Probability density function of intermittent temperature fluctuations for various averaging times.

for τ = 10 seconds. This is again the definition of finite time data spread as seen in Figure IV.2 and has served as the operational measure of turbulent intermittency. There is negative correlation between wind speed and intermittency level (the more pronounced the intermittency, the larger the relative standard deviation in $(C_n^2)_\tau$ for a given averaging time). As discussed above, the integral scale of the square of an intermittent process should be larger than in the equivalent non-intermittent case due to increased spectral density in the low frequency region of the spectrum. This is evident in the table. Also shown is the kurtosis measured from the distribution function of the unaveraged temperature fluctuations, $K_{\Delta T_{12}}$. This shows a strong tendency to increase with increasing intermittency as discussed above.

V.6. Conclusion

Finally, a comment on the effects of intermittent turbulence on the optical propagation problem, particularly amplitude scintillation. Experimentally, at least for the case of spherical wave propagation, there have been no anomolous effects due to the intermittent nature of the turbulence. There is no evidence that intermittency causes saturation effects or the observed probability distribution functions of the optical amplitude fluctuations. Intermittency will play a strong role in determining data spread in both the atmospheric and optical measurements, through Eq. (IV.10). For spherical wave propagation over long paths, the problems of intermittency will however be relatively minor in the optical measurements because of the broad path weighting function. In the case of focused beam propagation or other schemes where the path weighting function may be more strongly localized, and thus the effective number of 'turbulent slabs' (see Chapter IV) is small, strong intermittency may cause large fluctuations in the observed scintillation level.

Table 10

Mean Wind Speed $\bar{u}$ (m/sec)	St.Dev.$(C_n^2)_\tau$ / $\overline{C_n^2}$ τ = 10 sec.	$I_{\Delta T}^2$ τ = 1 sec. (sec)	Corr.Length $\bar{u} \cdot I_{\Delta T}^2$ (m)	$K_{\Delta T_{12}}$
9	.270	0.8	7.2	5.5
5.5	.261	1.38	7.6	8.35
4.5	.457	1.47	6.6	11.15
3.8	.468	1.49	5.7	13.4
1.5	.767	3.48	5.2	12.3

CHAPTER VI.

Summary

A detailed inquiry has been presented into the short time averaged statistical properties of certain random processes associated with the propagation of light through the turbulent atmosphere. The random processes of concern are the small scale temperature fluctuations, which relate to the index of refraction structure parameter C_n^2, and fluctuations in the log amplitude of the received optical signal. One of the primary goals of this work has been to investigate the accuracy of short time averaging on measurements of the moments of these random processes, specifically the variance. This problem was approached by considering the normalized variance (or standard deviation) of the short time variance measurements, referred to above as the data spread. Eq. II.13 describes the predicted averaging time dependence of this normalized variance. In practical terms, Eq. II.13 describes the expected statistical error in short time averaged measurements of the variance of a given stationary process. It depends on certain fundamental statistical properties of the basic random process: the kurtosis or normalized fourth moment and the integral scale, a measure of the extent of significant correlation of the process.

In Chapters II and III, we have compiled results of the statistical analysis of the random processes characterizing the atmospheric temperature fluctuations and the optical amplitude fluctuations. These results included the probability distribution function and associated moments, of long time averaged measurements and power spectral densities and autocorrelation functions under a variety of homogeneous atmospheric conditions. From these analyses have been derived specific results useful in predicting time averaging effects and general properties of the random processes ΔT and log amplitude fluctuations χ under varied atmospheric conditions.

The temperature difference fluctuations, even under the most well developed turbulence conditions were observed to be significantly non-Gaussian by virtue of the high flatness factors associated with their probability distribution functions. This in itself suggests the possibility of large data spreads in short time averaged variance measurements from

Eq. II.13. In addition, the possibility of large integral scales, T_2, (see Eq. II.14) due to large scale spatial correlation which can also lead to large data spreads have been demonstrated. Finally with regard to temperature fluctuations, the probability distribution function of $(\Delta T_{12})^2$ was shown to be essentially lognormal in agreement with the theory presented by Gurvich and Yaglom over a range of short averaging times. Under conditions of poorly developed turbulence, stable light winds and intermittency, deviations from lognormality have been observed.

The log amplitude fluctuations of the received optical signal were the subject of Chapter III. These fluctuations were seen to be normally distributed under most atmospheric conditions with some slight deviations from normality in the tails of the distribution under the highest turbulent conditions observed. These observations and the measurements of the power spectra of the log amplitude fluctuations are in agreement with previous observations and theories. Additionally the autocorrelation functions of these fluctuations have been calculated. The decorrelation time was seen to be more dependent on the wind speed, as expected in low turbulence than on the turbulence level, which should dominate under very high turbulence conditions. Finally in Chapter III an investigation of the two point joint probability distribution function of the log amplitude fluctuations was presented. As pointed out in Chapter III, knowledge of these functions would aid in the design of certain types of communication systems. Measurement of conditional distribution functions was described. The results indicate that under low turbulence conditions, log amplitude fluctuations are at least two-dimensional Gaussian. Thus the literature on Gaussian processes is directly applicable and could yield useful results in areas such as fading statistics, level crossing, and conditional sampling.

The actual effects of short time averaging on the variance measurements described above were investigated experimentally. Figures IV.1 and IV.2 show the results of long time averaging ($\sim$ 10 minutes) and short time averaging (10 seconds) respectively on measurements of σ_τ^2 ($\propto C_n^2$) and σ_m^2. With long time averaging there was excellent agreement between theory and experiment below the saturation value while in the short time averaged case there are large fluctuations in C_n^2. These fluctuations indicate large probable

errors in single short time averaged measurements and this data spread must be recognized in the design of atmospheric propagation experiments. The dependence of the data spread on wind speed and averaging time was demonstrated to be as expected. In the next section the relationship between the normalized variance (data spread) of the short time measurements of σ_χ^2 and C_n^2 has been described. The variance of $(\sigma_\chi^2)_\tau$ was seen to be equal to the variance of $(C_n^2)_\tau$ times a factor (less than unity) dependent of the spatial structure of $(C_n^2)_\tau$ and the propagation path weighting function. Experimental test of this dependence was made both with the assumption of a discrete, uncorrelated slab model of the turbulence along the path and without this assumption by directly measuring the large scale spatial correlation function of $(C_n^2)_\tau$. While some of the derived relationships were verified, measurements, particularly under low wind speed, intermittent conditions showed large deviations from the analytical results. This intermittency was considered in Chapter V.

Intermittency in a practical sense, was defined here as the existence of a slow modulation of varying envelope function on the observed atmospheric fluctuations as seen in Figure V.1. Intermittent atmospheric turbulence has been observed under a variety of conditions but it is most extreme in light wind conditions. The causes of intermittency include 'bursting' generation of the turbulence and thermal 'structures' in the flow. One form of these structures is a thermal convective plume. Examples of these plumes were shown indicating how they may account for the observed intermittency. Of more direct interest, however, is the effect of such intermittency on short time averaged measurements of C_n^2 and σ_χ^2. The increase in data spread due to increased intermittency will depend on the parameters of Eq. II.13 and mechanisms for both large integral scales and large kurtoses with intermittent turbulence were derived. These results are supported by experimental observations. Finally, it is observed that the primary effect of intermittency of the optical propagation measurements is the increase in the data spread in short time measurements of σ_χ^2 through Eq. IV.10.

Bibliography

Barakat, R. G. and Blackman, E. S., 1974, Fundamental Limitations on Image Restoration, RADC-TR-74-C-0176.

Batchelor, G. K. and Townsend, A. A., 1947, Proc. Royal Soc. of London, A190, 534-440.

Bendat, J. S. and Piersol, A. G., 1971, Random Data: Analysis and Measurement Procedures, Wiley, New York.

Blake, I. F. and Lindsey, W. C., 1973, Level Crossing Problems for Random Processes, IEEE Trans. on Info. Theory, Vol. IT-19, No. 3, 295.

Boston, N. E. J., 1971, Some Features of Temperature Fluctuations in the Atmospheric Boundary Layer, APS Annual Meeting, San Diego, California.

Brigham, E., 1974, The Fast Fourier Transform, Prentice Hall, N.J.

Chen, W. Y., 1971, Lognormality of Small Scale Structure of Turbulence, Phys. of Fluids, 14, No. 8, 1639.

Clifford, S. F., 1971, Temporal Frequency Spectra for a Spherical Wave Propagating Through Atmospheric Turbulence, JOSA, 61, No. 10, 1285.

Collins, S. A., 1971, Investigation of Laser Propagation Phenomena, RADC-TR-71-0132.

deWolf, D. A., 1973a, Strong Irradiance Fluctuations in Turbulent Air, JOSA, 63, No. 2, 171.

deWolf, D. A., 1973b, Effects of Turbulent Instabilities on Laser Propagation, RADC-TR-72-C-0486.

Doob, J. L., 1953, Stochastic Processes, Wiley and Sons, Canada.

Fried, D. L., 1967, Propagation of a Spherical Wave in a Turbulent Medium, JOSA, 57, 175.

Fried, D. L., Mevers, G. E., Keister, M. P., 1967, Measurements of Laser-Beam Scintillation in the Atmosphere, JOSA, 57, 787.

Friehe, C. A., Gibson, C. H., and Dreyer, G., 1972, Effects of Temperature and Humidity on Refractive Index Fluctuations over the Open Ocean, JOSA, 62, 1340.

Friehe, C. A. and Larue, J. C., 1973, Effect of Humidity and Temperature on Optical Refractive Index Fluctuations, JOSA, 63, 1327.

Friehe, C. A. and LaRue, J. C., 1974, Dependence of Optical Refractive Index on Humidity and Temperature, OSA Meeting on Optical Propagation Through Turbulence, Boulder, Colorado.

Gibson, C. H. and Masiello, P. J., 1972, Observation of Variability of Dissipation Rates of Turbulent Velocity and Temperature Fields, Statistical Models and Turbulence, Springer-Verlag, Heidelberg.

Gibson, C. H., Stegen, G. R., and Williams, R. B., 1970, Statistics of the Fine Structure of Turbulent Velocity and Temperature Fields Measured at High Reynolds Numbers, Journal of Fluid Mechanics, 41, 153.

Gurvich, A. S., 1967, Probability Distribution of the Square of the Temperature Difference Between Two Points of a Turbulent Flow, Soviet Physics-Doklady, 12, 17.

Gurvich, A. S. and Yaglom, A. M., 1967, Breakdown of Eddies and Probability Distributions for Small Scale Turbulence, Physics of Fluids, Supplement, 559.

Hinze, J. O., 1959, Turbulence, McGraw Hill, New York.

Kaimal, J. C., 1974, Translation Speed of Convective Plumes in the Atmospheric Surface Layer, Quarterly Journal of the Royal Meteorological Society, 100, No. 423, 46.

Kaimal, J. C. and Businger, J. A., 1970, Case Studies of a Convective Plume and a Dust Devil, Journal of Applied Meteorology, 9, 612.

Kerr, J. R., 1972, Experiments on Turbulence Characteristics and Multiwavelength Scintillation Phenomena, JOSA, 62, No. 9, 1040.

Kerr, J. R., 1973, Propagation of Multiwavelength Laser Radiation Through Atmospheric Turbulence, RADC-TR-73-54.

Kerr, J. R., Elliott, R. A., Pincus, P. A., and Lee, M. H., 1974, Propagation of Multiwavelength Laser Radiation Through Atmospheric Turbulence, RADC-TR-74-0082.

Kolmogorov, A. N., 1962, A Refinement of Previous Hypotheses Concerning the Local Structure of Turbulence in a Viscous Incompressible Fluid at Low Reynolds Number, Journal of Fluid Mechanics, 13, 82.

Kruspe, G., 1974, Measurements of Fluctuation of Vertical Wind Velocity, Temperature, and Radio Refractive Index Above the Sea, Boundary Layer Meteorology, 6, 257.

Kuo, A. Y. and Corrsin, S., 1971, Experiments on Internal Intermittency and Fine Structure Distribution Functions in Fully Developed Turbulent Fields, Journal of Fluid Mechanics, 50, Pt. 2, 285.

Landau, L. O. and Lifshitz, E. M., 1959, Fluid Mechanics, Pergamon Press, Inc., London.

Lauffer, J. and Narayanan, M. A. B., 1971, Mean Period of the Turbulent Production Mechanism in a Boundary Layer, Physics of Fluids, 14, No. 1, 182.

Lawrence, R. S., Ochs, G. R., and Clifford, S. F., 1970, Measurements of Atmospheric Turbulence Relevant to Optical Propagation, JOSA, 60, 826.

Lawrence, R. S. and Strohbehn, J. W., 1970, A Survey of Clear Air Propagation Effects Relevant to Optical Communications, Proceedings of the IEEE, 48, 1523.

Lu, S. S. and Willmarch, W. W., 1973, Measurement of the Mean Period Between Bursts, Physics of Fluids, 16, 2012.

Lumley, J. L., 1970, Stochastic Tools in Turbulence, Academic Press, N. Y.

Mitchell, R. L., 1968, Permanence of the Lognormal Distribution, JOSA 58, No. 9, 1267.

Mollo-Christensen, E., 1971, Physics of Turbulent Flow, AIAA Journal, 9, No. 7, 1217.

Mollo-Christensen, E., 1973, Intermittency in Large Scale Turbulent Flows, Annual Review of Fluid Mechanics, 5, 101.

Oboukhov, A. M., 162, Some Specific Features of Atmospheric Turbulence, Journal of Fluid Mechanics, 13, 77.

Ogura, Y., 1957, The Influence of Finite Observation Intervals on the Measurement of Turbulence Diffusion Parameters, Journal of Meteorology, 14, 176.

Orszag, S. A., 1970, Indeterminacy of the Moment Problem for Intermittent Turbulence, Physics of Fluids, 13, 2211.

Rice, S. O., 1954, Mathematical Analysis of Random Noise, in Selected Papers of Noise and Stochastic Processes, Ed. Wax, Dover, N. Y.

Silversides, R. H., 1974, An Empirical Method for Demonstrating the Influence of Heat Flux on the Shape of Temperature Spectra, Boundary Layer Meteorology, 6, 381.

Stewart, R. W., Wilson, J. R., and Burling, R. N., 1970, Some Statistical Properties of Small Scale Turbulence in an Atmospheric Boundary Layer, Journal of Fluid Mechanics, 41, 141.

Strickland, J. A. and Simpson, J. L., 1975, Bursting Frequencies Obtained from Wall Shear Stress Fluctuations in a Turbulent Boundary Layer, Physics of Fluids, 18, No. 3, 306.

Strohbehn, J. W., 1968, Line of Sight Wave Propagation Through the Turbulent Atmosphere, Proceedings of the IEEE, 56, 1301.

Strohbehn, J. W., Wang, T. I., and Speck, J. P., 1975, On the Probability Distribution of Line of Sight Fluctuations of Optical Signals, Radio Science, 10, 59.

Tatarskii, V. I., 1971, Effects of Turbulent Atmosphere on Wave Propagation, NTIS, Springfield, Virginia.

Taylor, G. I., 1938, Proceedings of the Royal Society, A164, 476.

Tennekes, H. and Wyngaard, J. C., 1972, Intermittent Small Scale Structure of Turbulence, Journal of Fluid Mechanics, 55, 93.

Van Atta, C. W., 1971, Influence of Fluctuation in Local Dissipation Rates on Turbulent Scalar Characteristics in the Inertial Subrange, Physics of Fluids, 14, 1803.

Wang, T. I., and Strohbehn, J. W., 1974a, Log-Normal Paradox in Atmospheric Scintillations, JOSA, 64, 583.

Wang, T. I., and Strohbehn, J. W., 1974b, Perturbed Log-Normal Distribution of Irradiance Fluctuations, JOSA, 64, 994.

APPENDIX I

Digital computer processing of data of a random nature now permits fast reliable calculation of statistical properties from large data bases. With the computing power available, care must be exercised to avoid processing beyond fundamental limits set by the characteristics of the data, such as signal-to-noise ratio, resolution of digitizing procedure, and bandwidth. The general procedures for statistical time series analysis are discussed in Bendat and Piersol (1971), and many other references dealing with specific topics and problems of analysis. One in particular, Tennekes and Wyngaard (1972) deals specifically with hazards of data processing related to signals with characteristics seen in the small scale atmospheric turbulent fluctuations. We outline the basic methods used in the processing of the data presented in the previous chapters.

All digital processing was performed on a PDP-11/20 computer with programs specifically written for this project in machine language. Analog data was introduced onto the computer through a 12 bit A/D converter at a computer controlled rate and either processed directly or recorded on 9 track digital tape for later processing. The sampling rate of the data should be dependent on the bandwidth of the signal (for accurate spectral representation without aliasing, the sampling rate must be at least twice the highest frequency at which there is significant energy in the signal.) Sampling rates of one and four kilohertz were employed depending on the signal and the particular processing to be performed.

A fast fourier transform algorithm described by Cooley and Tukey (see Brigham 1974 for a description of the method and further references) was used in the calculation of all spectra and correlation functions reported here. The power spectra were obtained by calculating the complex fourier transform of a block of data representing the signal. This yields the real and imaginary fourier components from which the power spectrum is derived by summing the squares of the real and imaginary parts at each frequency. The standard block size used was 1024 points. Spectra of long records of data were calculated by repeating this procedure for successive data blocks and then averaging the resultant spectra from each block.

Additionally, the final spectra were smoothed over a small frequency interval. (The effects of frequency smoothing and segment averaging are discussed in Bendat and Piersol (1971)p329.) For a sampling rate of f(hertz) and N points in the transform, this procedure results in spectral estimates over the frequency range f/N (hertz) to f/2 (hertz). To extend the low frequency cutoff, with a given block size, the sampling rate must be decreased. This may be accomplished without aliasing by low pass filtering the signal before it is sampled. A simple first order recursive digital filter was constructed for this purpose. Thus with an appropriate filter time constant, the low frequency cutoff of the spectra was limited only by the total length of the data sample.

The autocorrelation functions were calculated directly from the power spectral estimates through the use of the fast fourier transform again. Direct application of the FFT, calculating the cosine transform, yields however a 'circular correlation function' which is particularly contaminated for large lag times, rather than the desired correlation function (Bendat and Piersol 1971, 313). This problem may be avoided by adjusting the original data from which the power spectral density estimates were made. This procedure which involves appending a number of zeros to each original data block, was made a routine part of the processing.

Numerical probability density function measurements are particularly adaptable to digital processing. If the digitization procedure yields signal values between -L and +L, and the total number of samples is N, then the probability density estimate P(I) for a signal level I is

$$P(I) = N(I)/N$$

where N(I) is the number of samples of the data equal to I. The cumulative probability distribution function is then

$$CP(I) = \sum_{J=-L}^{L} P(J)$$

and the m^{th} moment of the distribution is

$$\mu'_m = \sum_{J=-L}^{L} P(J)*J^m \quad .$$

The central moments μ_m may be calculated from

$$\mu_m = \sum_{J=-L}^{L} P(J)*(J-\mu)^m$$

where μ is the mean, or directly from the μ'_m. The flatness factor and the skewness then are defined as

$$K = \frac{\mu_4}{(\mu_2)^2} \quad , \qquad S = \frac{\mu_3}{(\mu_2)^{3/2}} \quad .$$

APPENDIX II

We show here that for a process with nonzero integral scale, the integral scale of the correlation function of the process averaged over a time τ approaches $1/2\ \tau$ as the averaging time becomes much greater than the integral scale of the original process. Consider a process $f(t)$, with zero mean, variance σ_X^2, autocorrelation function $\rho(t)$, and integral scale I defined as

$$I = \int_0^\infty \rho(t)\, dt$$

Defining an averaged processed $g_\tau(t)$ as

$$g_\tau(t) = \frac{1}{\tau} \int_{-\tau/2}^{\tau/2} f(t+t')dt'$$

we investigate the integral scale of $g(t)$. The correlation function of $g_\tau(t)$ is

$$\rho_g(t') = \frac{\langle g_\tau(t)\ g_\tau(t+t')\rangle}{\langle g_\tau^2\rangle}$$

where

$$\langle g_\tau(t)\ g_\tau(t+t')\rangle = \left\langle \frac{1}{\tau^2} \int_{-\tau/2}^{\tau/2} f(t+t''')dt''' \int_{-\tau/2}^{\tau/2} f(t+t'+t'')dt'' \right\rangle$$

Interchanging the ensemble and time averaging yields

$$\langle g_\tau(t)\ g_\tau(t+t')\rangle = \frac{1}{\tau^2} \int_{-\tau/2}^{\tau/2} \int_{\tau/2}^{\tau/2} dt''dt'''\langle f(t+t''')f(t+t'+t'')\rangle$$

$$= \frac{\sigma^2}{\tau^2} \int_{-\tau/2}^{\tau/2} \int_{-\tau/2}^{\tau/2} dt''dt'''\rho(t'+t''+t''')$$

$$= \frac{\sigma^2}{\tau^2} \int_{-\tau/2}^{\tau/2} dt \int_{-\tau/2-t}^{\tau/2+t} dt'' \rho(t'+t'') \quad .$$

Integrating by parts,

$$\langle g_\tau(t)\, g_\tau(t+t')\rangle = \frac{\sigma^2}{\tau} \int_0^\tau (1-t/\tau)[\rho(t'+t) + \rho(t'-t)]dt$$

Setting $t' = 0$, yields the variance of $g_\tau(t)$

$$\langle g_\tau^2\rangle = \frac{2\sigma^2}{\tau} \int_0^\tau (1-t/\tau)\rho(t)\, dt \quad .$$

Thus the correlation function of g(t) is

$$\rho_g(t') = \frac{\frac{\sigma^2}{\tau} \int_0^\tau (1-t/\tau)[\rho(t'+t) + \rho(t'-t)]dt}{\frac{2\sigma^2}{\tau} \int_0^\tau (1-t/\tau)\rho(t)dt}$$

Calculating the integral scale by integrating over t' gives

$$I_{g_\tau} = \frac{\frac{2\sigma^2 I}{\tau} \int_0^\tau (1-t/\tau)dt}{\frac{2\sigma^2}{\tau} \int_0^\tau (1-t/\tau)\rho(t)dt}$$

$$= \frac{\tau I}{2 \int_0^{\tau} (1-t/\tau)\rho(t)dt}$$

If τ is very large compared to the integral scale, I, of f(t), then the integral in the denominator reduces to I and

$$I_{g_\tau} = \tau/2$$

as stated.